SITUATION-ORIENTED INTEGRATION OF HUMANS AND AUTOMATION FOR THE OPERATION OF REGENERATIVE LIFE SUPPORT SYSTEMS

A Dissertation
Presented to
The Academic Faculty

by

Gregorio E. Drayer Andrade

In Partial Fulfillment
of the Requirements for the Degree
Doctor of Philosophy in the
School of Electrical and Computer Engineering

Georgia Institute of Technology
December 2013

SITUATION-ORIENTED INTEGRATION OF HUMANS AND AUTOMATION FOR THE OPERATION OF REGENERATIVE LIFE SUPPORT SYSTEMS

Approved by:

Professor Patricio Vela,
Committee Chair
School of Electrical and Computer Engineering
Georgia Institute of Technology

Professor Arthur Koblasz
School of Electrical and Computer Engineering
Georgia Institute of Technology

Professor Ayanna M. Howard, Advisor
School of Electrical and Computer Engineering
Georgia Institute of Technology

Professor Karen Feigh
School of Aerospace Engineering
Georgia Institute of Technology

Professor George Vachtsevanos
School of Electrical and Computer Engineering
Georgia Institute of Technology

Date Approved: October 24, 2013

To my wife Tracie, without whom I would

have hardly finished this manuscript on time;

to all my family, for their love and support

from the distance;

and for the coming offspring that will bring us

joy and brighten all our lives.

ACKNOWLEDGEMENTS

I would like to thank my advisor, Dr. Ayanna Howard, for her invaluable support and patience during my years as member of the Human-Automation Systems Lab and to my lab- and class-mates who made my experience at Georgia Tech the source of many memories that I will cherish for many years to come. I would also like to thank my doctoral committee for the recommendations and discussions aimed at improving this manuscript. I would also like to thank Mr. Vincent Pickett, to all the team of the International Fulbright Science and Technology Program at the Bureau of Educational and Cultural Affairs of the United States Department of State and to the corresponding members of the Institute of International Education; among these I thank very especially Ms. Anna Rendon and Ms. Sarah Boeving. I want to thank the Cultural Office of the United States Embassy in Caracas, in particular I would like to highlight the support and trust offered to me by Ms. Sally Hodgson, Mr. Angel Garcia, Ms. Elena Broszkowski and Ms. Tatiana Escobar since before my application to the prestigious Fulbright scholarship that allowed me to conduct my doctorate at Georgia Tech. I want to thank my entire family, which increased greatly in size during these years. In particular, I want to thank my parents, whose support made the difference in various challenging moments these four years. I would also like to thank Dr. Russell Kerschmann for his support, mentorship and friendship since his visit to Caracas in 2007. Finally, but very importantly, I want to thank my wife Tracie, who over these years also became my editor, reviewing multiple manuscripts for conferences, journals, and for deliverables of the academic program. All of them had a very special role to play during my studies at Georgia Tech, and I am sure they will continue to do so in the years ahead.

TABLE OF CONTENTS

LIST OF TABLES

LIST OF FIGURES

GLOSSARY

BLSS Bioregenerative life support system, p. 33.

CAES Closed aquatic ecosystem, p. 35.

CD Carbon dioxide, p. 41.

CEBAS Closed equilibrated biological aquatic system, p. 35.

CM Command module, p. 25.

CRA Carbon dioxide reduction assembly, p. 28.

DMSD dimethylsilanediol, p. 3.

DO Dissolved oxygen, p. 36.

ECLSS Environmental control and life support system, p. 25.

EID Ecological interface design, p. 15.

FAM Fuzzy associative memory, p. 5.

GPS Global positioning system, p. 138.

HC Human computation, p. 136.

HCI Human-computer interaction, p. 136.

HDS Heterogeneous dynamic system, p. 1.

ICT Information and communication technologies, p. 137.

IPPD Integrated product and process development, p. 13.

ISS International space station, p. 3.

JAXA Japanese Aerospace Exploration Agency, p. 35.

JSC Johnson Space Center, p. 29.

kH Carbonate hardness, p. 37.

LCP Light compensation point, p. 43.

LED Light-emitting diode, p. 36.

LEO Low Earth orbit, p. 34.

LM Lunar module, p. 25.

LOA Levels of automation, p. 11.

LOC Loss of crew, p. 23.

LOM Loss of mission, p. 23.

LSS Life support system, p. 23.

LSSIF Life support system integration facility, p. 34.

MABA-MABA Men-are-better-at machines-are-better-at, p. 19.

NASA National Aeronautics and Space Administration, p. 23.

OGS Oxygen generating system, p. 28.

PI Proportional-integral controller, p. 48.

PSO Particle swarm optimization, p. 67.

RLSS Regenerative life support system, p. xvi.

SKB Situation knowledge base, p. xvi.

SpaceX Space Exploration Technologies, Inc., p. 27.

TOCA Total Organic Carbon Analyzer, p. 28.

UAV Unmanned aerial vehicle, p. 22.

WPA Water processing assembly, p. 3.

WRS Water recovery system, p. 3.

SUMMARY

The objective of the proposed research is to study the integration of humans and automation for the operation of regenerative life support systems (RLSS). RLSS combine physico-chemical and biological processes with the purpose of increasing the autonomy of space habitats and the life quality of their living organisms by properly reusing byproducts and regenerating consumable resources. However, these processes require energy and time to transform chemical compounds and organic wastes into nutrients, consumables, and edible products. Consequently, the maintenance of RLSS imposes a considerable workload on human operators. In addition, the uncertainties introduced by unintended chemical reactions promoted by material loop closure may create unexpected situations that, if unattended, could translate into performance deterioration, human errors, and failures. The availability of novel chemical and biological sensors together with computational resources enable the development of monitoring and automation systems to alleviate human workload, help avoid human error, and increase the overall reliability of these systems.

This research aggregates sensor data and human-expert situation assessments to create a representation of their situation knowledge base (SKB). The representation is used in a switched control approach to the automation of RLSS, for decision support, and human-automation coordination. The aggregation method consists of an optimization process based on particle swarms. The purpose of this work is to contribute to the methodological development of situation-oriented and user-centered design approaches to human-automation systems. Experiments and simulations are supported on the process of respiration in an aquatic habitat acting as a RLSS.

CHAPTER I

INTRODUCTION

1.1 Origin and History of the Problem

Since the invention of the first automated systems during the Industrial Revolution, advances in sensor technology [14, 15, 16, 17, 18], computing power [19, 20, 21, 22], and communications [23, 24, 25, 26, 27] have dramatically increased the opportunities to incorporate devices and equipment into ever more complex systems. These innovations have helped entire industries to evolve and new business models to emerge in domains such as energy [28, 29], transportation [30, 31, 32], health [33, 34, 35], security [36, 37, 38], and entertainment [39, 40]. Many of these solutions are what today make up power systems, water supplies, and digital communication networks, among others. However, automation has also played an important role in undesired events and fatal accidents. Such is the case of the Air France flight 447 that intended to transport 216 passengers and its 12-person crew from Rio de Janeiro to Paris on June 1, 2009 [41]. In this accident, the Airbus A330-200 crashed into the Atlantic Ocean after the aircraft entered an aerodynamic stall caused by erroneous readings from the airspeed sensors. These readings triggered a sequence of events that resulted in the disengagement of the autopilot, which left the control of the aircraft to the crew. At that moment, the crew had insufficient awareness of the situation to react properly to the flight condition.

In the commissioning and life-cycle of heterogeneous dynamic systems (HDS), composed of humans, physical systems, and computer agents, accidents are not just a consequence of the failure of a particular device or the collapse of an automation system. Humans, as well, play a role in most of these accidents, with human error

being responsible for 60%-90%, of the accidents reported in domains such as process control, aviation, and health care [3, 42, 43]. In particular, a review of military aviation mishaps [44] and a study of accidents in major air carriers found that 88% were caused by human error resulting from a lack of situation awareness [45]. As this example highlights, beyond purely technology-based problems, a number of issues exist in the integration of humans and automation technology [2, 8], with a lack of situation awareness being an important cause of human errors.

This work does not intend to overcome the causes of the Airbus accident in Air France flight 447; in general, issues with human-automation systems are complex and dependent on their specific application domain. However, this research aims to make a contribution by informing tools of decision making with methods of computational intelligence and principles in cognitive engineering for the safe operation and automation of HDS. The theoretical objective is to provide a methodology for the integration of human-automation systems that generates a representation of the situation knowledge base (SKB) of human-experts in order to assist other operators, who may not necessarily be experts, in the operation and supervision of such systems. These efforts may result in user interfaces that provide operators with additional information in support of real-time decision making.

1.1.1 Life Support Systems and Their Challenges

One HDS of particular interest is regenerative life support systems (RLSS). These systems grow in importance with the development of long-duration human space exploration systems. The capability of habitation systems to regenerate life support consumables, such as oxygen, is one of the challenges of long-duration human space flight [46]. Such capability would reduce the frequency of resupply missions and presumably also reduce their operation cost. An example of such efforts is the

commissioning of the Water Recovery System (WRS) in the U.S. segment of the International Space Station (ISS), which recycles waste liquids, including urine, back into potable water [47, 11, 48]. Indeed, on April 10th 2010, at the Kennedy Space Center, President Barack Obama pronounced his "Remarks on Space Exploration in the 21st Century," and in his speech he included life support systems as a key technology to be developed for future long-duration space flight missions:

> "*And we will extend the life of the International Space Station likely by more than five years, while actually using it for its intended purpose: conducting advanced research that can help improve the daily lives of people here on Earth, as well as testing and improving upon our capabilities in space. This includes technologies like more efficient life support systems that will help reduce the cost of future missions.*"

RLSS combine physico-chemical and biological processes to transform metabolic byproducts back into consumables. Their purpose is to increase the autonomy of the space habitat and to maintain an acceptable quality of life for its living organisms by properly reusing byproducts and regenerating consumables. But these processes require energy and time to transform byproducts and nutrients into consumables and edible products. Consequently, their maintenance imposes considerable workload to operators. In particular, their monitoring and automation poses a challenge: material loop closure may promote unintended interactions between chemical species within the habitat, potentially leading to the accumulation of unexpected chemical compounds that may affect individual life-support processes or even crew health. An example of such unintended chemical interactions is found in the 2010 WRS anomaly, caused by the accumulation of dimethylsilanediol (DMSD) in the Water Processing Assembly (WPA) of ISS [11]. This anomaly served as a good example of the disconnect that in some cases may be apparent between humans and automation, thus

becoming a potential cause for conflicts that may be addressed if considered as an issue between humans and automation.

We can address this problem of disconnect by detecting such anomalies early enough and using measurements to present sensor information that improves the observability of these errors in monitoring and automation systems to the human operator. By addressing this problem, we seek to minimize human errors while increasing system reliability.

1.1.2 Situation-Oriented Automation of RLSS

The availability of new chemical and biological sensors, together with computational resources, enables the development of automation systems aimed to alleviate human workload, avoid human error, and increase overall reliability of RLSS. Beyond methods in robust [49] and adaptive control [50, 51], paradigms in switched control [52, 53, 54, 55] offer advantages for the management of the uncertainty caused by material loop closure. Switched control introduces attributes of flexibility and modularity to the control system [55]. These attributes may be used to allow for different control actions depending on the *operational condition* of the physical system and its *situation* in a given context. The *situation* can be understood as the subjective state of a system in relation to its context, which can be in itself defined by the environment and active goals.

The combination of abundant sensor information creates a *sensing space* in which these situations may be defined, which when detected may be used to influence the operation of the system toward a specific goal. Furthermore, the ability to detect known situations in the sensing space may also open opportunities to detect unknown situations, in which case the automation system may alert and request a human expert to perform observations, collect data, or intervene. In this case, the human expert would contribute his/her knowledge to the situation, *i.e.* his/her situation awareness,

defined as the "perception of the elements in [his/her] environment within a volume of time and space, the comprehension of their meaning, and the projection of their status into the near future" [56, 57].

This work proposes a situation-oriented approach to the switched control paradigm that performs a quantization of the sensing space to allow the automation system to actively probe for information [54]. It employs a granular decomposition [58, 59] of the measured or estimated variables, with each granule defining a *situation* in which a specific control objective governs the RLSS. The granular decomposition is made consistent with the SKB of a human-expert through an adaptation process that enables the automation system to "learn" the human perception of each situation, or the concept of a particular situation, from sensor readings, measurements, and inputs from an human expert. An advantage of the consistency between the granular decomposition and the human perceptions of situations is the capacity it provides to the system for the development of coordination strategies between the human and automation, *i.e.* the *human-automation system*.

In particular, this dissertation makes use of a reactive agent architecture based on fuzzy associative memories (FAM), or FAM-based agents, composed of n-dimensional non-interactive fuzzy sets [60, 61]. The methodology aggregates sensor information and a set of human-expert situation assessments to obtain a parametric representation of their SKB. Data sets collected by human experts are a raw and uncompressed representation of their knowledge about the system. These data sets can be obtained from individual human experts or crowdsourced to a group of them.

1.1.3 Summary

The overall goal of this work aims to contribute to the methodological development of situation-oriented and user-centered design approaches for the integration of humans and automated RLSS. Despite the fact that many of the processes involved in RLSS

can be automated, these systems still require humans-in-the-loop for monitoring and intervention. Furthermore, because not all their functions may be fully operationalized, RLSS needs the ability and involvement of the human operators. The approach used in this work consists of collecting data from experts and implementing control policies suitable for human-system interaction. As such, this work makes five main contributions:

1. The design, modeling, and simulation of a ground-based platform for research in RLSS (Chapter 3). This ground-based platform provides a testbed for validation.

2. The development of a a granular approach to the automation of regenerative life support systems (Chapter 4) to enable the management of control policies based on situation.

3. The development of an aggregation algorithm to obtain situation knowledge bases from human experts (Chapter 4) that is used to automate system processes.

4. The characterization and validation of the aggregation algorithm employing data sets from simulation and human participants (Chapters 5 and 6). It provides observations and recommendations on data set requirements based on ideal conditions and offers validation making use of data sets produced by human participants.

5. The exploration of data-set combination techniques based on granular computing to obtain crowdsourced situation knowledge bases (Chapter 7). It demonstrates the advantage of employing techniques that operate on the situation knowledge base of individuals after these have been aggregated with the algorithm instead of combining them as raw data sets.

CHAPTER II

LITERATURE REVIEW

2.1 Human-automation Systems

2.1.1 Human Factors and Automation

The field of human factors consists of "the study of human beings and their interaction with products, environments and equipment in performing tasks and activities" [3]. Among the objectives of this field is to maximize system efficiency and human health, comfort, safety, and quality of life [62]. From a research perspective, this field studies the capabilities and limitations of humans and how these factors may determine design methods used to build anything from the simplest manual hand tool to complex interactive automated systems. From the application perspective, this field offers the opportunity to apply such methods to the design, evaluation, and commissioning of engineered systems [63].

Because the study of human factors focuses on how the human element affects the performance of a system within its goals and environment, this field draws from perspectives in systems theory. Aristotle refers to systems in his *Metaphysics* as "*all things which have several parts and in which the totality is not, as it were, a mere heap, but the whole is something beside the parts*" [64], i.e. the whole is more than the sum of its parts. In the case of human factors, the performance of the system is evaluated in terms of the context of the human-machine system, defined as "a system in which an interaction occurs between people and other system components, such as hardware, software, tasks, environments, and work structures "[3]. A familiar case of a human-machine system composed of a human user and a personal computer is shown in Figure 1. The characteristics of the human being and computer are used

to describe the interaction taking place between them. The description includes the sensory, cognitive, and motor characteristics of the human, which may be influenced by age, gender, and training. The computer description shows sensors and transducers as inputs; processor and memory as a counterpart to "thinking;" and visual, auditory, and tactile devices as outputs. The interaction, as described in Figure 1, is an interplay between the actuation of the computer system and the actions of the human.

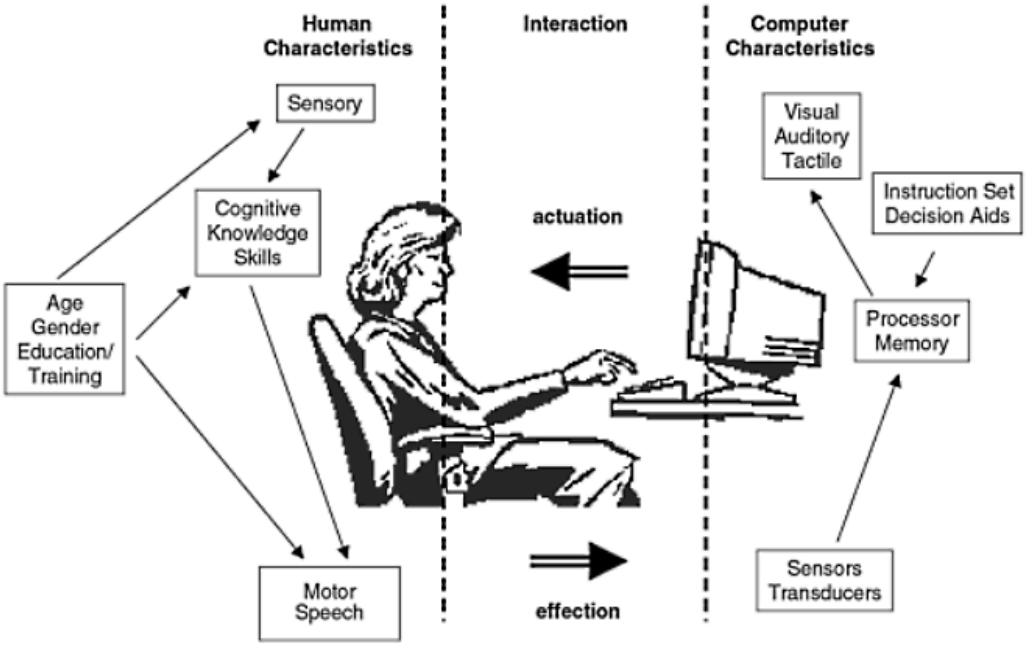

Figure 1: Example of a human-machine system [3].

The development of systems in engineering has been traditionally guided by the *reductionist* approach inspired by René Descartes in his *Discourses* [65], whereby instead of studying the behavior of a system as a whole, he rather proposes to focus on the analysis of its components in isolation. The field of human factors aims to complement the reductionist approach by bringing into consideration ideas from systems theory by concerning itself with both the behavioral/system-oriented approach as well as the constitutive/reductionist view of the system. Thus, human factors aims to make use of systems theory as a unifying framework for these two complementary

perspectives [66].

The adoption of the systems approach began during World War II, when the complexity of military systems became a problem for their successful operation. The early stage of human-automation systems has been described in three phases, as shown in Figure 2 [2].

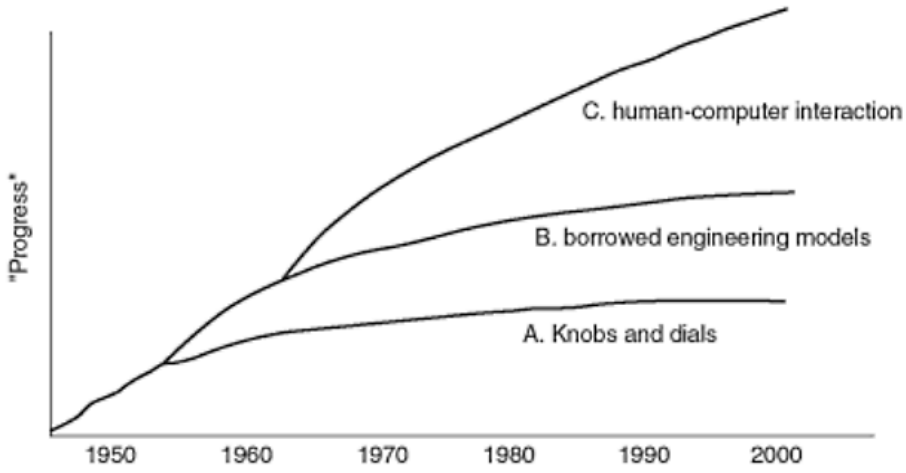

Figure 2: History of human-machine systems engineering [2].

The initial use of the human-machine systems concept is represented by Phase A. During this time, special attention was given to the field of civilian and military aviation and weapon systems. The concept also found application in the automotive and communication industries. The period in which the human factors field began to borrow models from systems in engineering to describe human performance, *e.g.*, concepts from control systems theory were used to propose models to describe and predict the performance of human operators, is reflected in Phase B. Finally, a so-called "human-computer interaction" period is referenced by Phase C [2], characterized by the use of computing power and automation. This phase dramatically changed the way in which humans and machines interacted. Such advances posed new challenges to both designers and operators. On one hand, operators would perform less physical work, while having more cognitive-intensive interactions with automated systems.

On the other hand, designers would have to consider how automated systems would help operators perceive, detect, think, and make decisions in real time [67, 68]. In consequence, human factors professionals needed to know more about the attributes of information processing and cognition in humans to integrate these considerations into their designs, leading to the emergence of cognitive engineering [69].

Cognitive engineering focuses on "complex, cognitive thinking, and knowledge-related aspects of human performance, whether carried out by humans or by machine agents" [70] and overlaps with the fields of cognitive science and artificial intelligence [3]. The relationship of the latter with cognitive engineering is illustrated in Figure 3 [2].

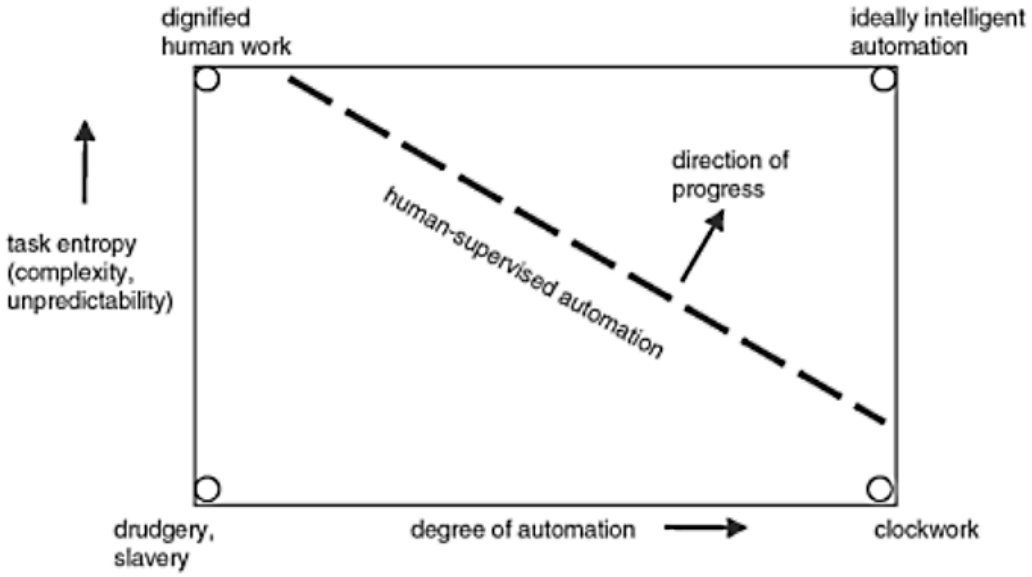

Figure 3: The trend of progress in human-supervised automation [3].

Artificial intelligence is described from the perspective of supervisory control in Figure 3 as the upper-right corner of the chart [8]. In this case, the automation is ideally intelligent, *e.g.* a robot with a high level of intelligence, able to operate in unstructured environments and follow various goals, where the role of the human would be that of an observer, an assisted subject, or a peer. However, most systems require human supervision for their operation, as expressed by the spectrum of *degrees*

of automation. Also called levels of automation (LOA), these go from the completely manual to the fully automatic extremes, and for various job complexities. Cognitive engineering finds its work domain in the intermediate range of this chart, *i.e.* in the combination of humans and machines operating at increasing degrees of automation. Two different levels of automation are shown in Figure 4: (a) Robonaut, a teleoperated robotic system [4]; and (b) RobuBOX-Kompai, an autonomous system that finds application in health care and assistive robotics [5].

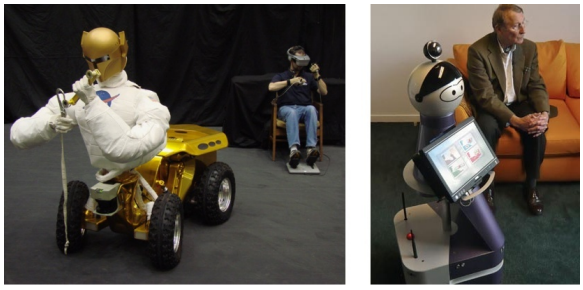

(a) (b)

Figure 4: (a) Robonaut [4]; (b) RobuBOX-Kompai [5].

Another way to represent the notion of LOA is shown in Figure 5 [6, 8]. Six types of supervisory control architectures are compared in Figure 5: Type 1 represents the purely manual control, while Type 6 shows a fully autonomous control. The intermediate architectures of supervisory control are characterized both in a strict formal sense (Types 3-5) and in a broader sense (Type 2) [8]. The strict formal sense of supervisory control implies that human operators may intermittently interact with the computerized system, configuring operating conditions and adjusting settings in an interface. In a broader sense of supervisory control, the interface between the human and the machine produces an integrated display of data becoming a telerobotic/teleoperated system.

The elements common to all supervisory control architectures are the tasks to be considered and the human operator. The questions are: to what LOA should human-automation systems be developed? and more specifically, how will automation

technology complement and enhance humans in conducting their tasks and directing their goals? How are the goals defined in each case? Depending on whether the tasks are performed by humans or machines, a wide variety of problems may arise. Such problems may be due to hardware/software design, variations in human performance, or the interaction between the human and the automation components.

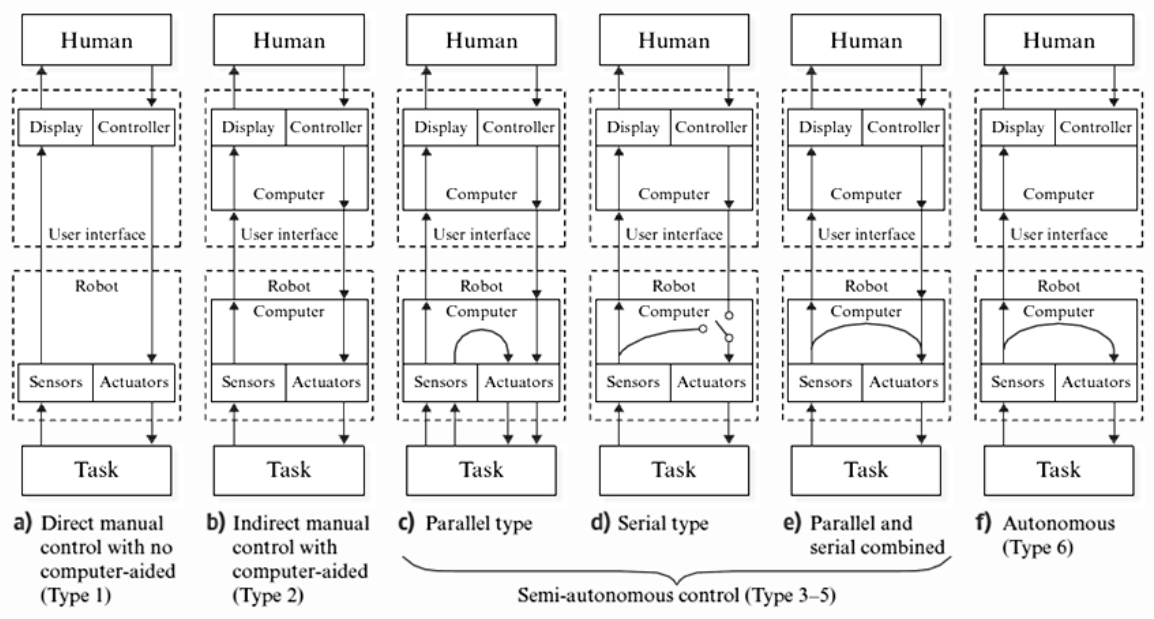

Figure 5: Supervisory control in human-robot interaction [6].

Some variations in human performance may be attributed to human information-processing functions, such as perception, attention, working memory, or long-term memory, among others. These considerations and those related to interaction issues pose challenges that will be addressed in Subsection 2.1.3.

2.1.2 Approaches to Human-automation System Design

Traditional models of system design propose sequential unit processes that transform inputs into outputs that serve posterior stages, transitioning from the conceptual stage of design, to detailed engineering, implementation, integration, testing, validation and verification. The traditional approach to systems engineering follows the reductionist approach [65] mentioned in Subsection 2.1.1, where separate components of the system

are designed in isolation and then integrated. An example of this is the Georgia Tech Integrated Product and Process Development (IPPD) Methodology [71], which in Figure 6 has been integrated with the Vee diagram commonly used by the United States Department of Defense.

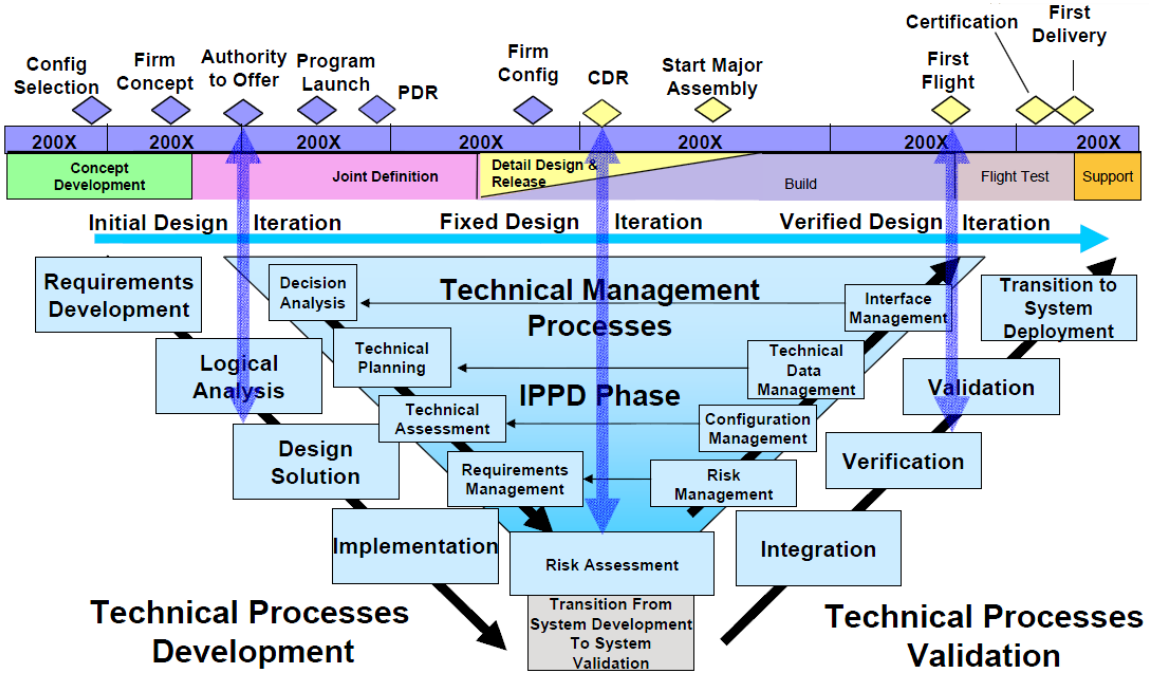

Figure 6: Department of Defense Systems Engineering Process Model [7].

The deployment of ever more complex systems and the failures reported in some cases have demonstrated the need for additional tools that may account for the human component in these systems [3]. As previously discussed, one aim of the field of human factors is to *complement* the reductionist approach by enhancing system concepts. The literature acknowledges four design approaches that incorporate human factors into system design [3]: (1) sociotechnical systems, (2) participatory ergonomics, (3) ecological interface design, and (4) user-centered design.

2.1.2.1 Sociotechnical Systems Approach

The sociotechnical systems approach consists of processes and methods used to analyze, design, and implement systems composed of social, technical, and environmental

components. It is viewed as a macroergonomic approach to system design given that it considers aspects of the human, organization, machine, and environment components. In contrast, microergonomics only focuses on the human-machine interface. Although the design objective of this approach is the optimization of the social and technical components of the system [72], the literature reports drawbacks by the overemphasis it makes on the social component [3].

2.1.2.2 Participatory Ergonomics Approach

Participatory ergonomics makes use of the knowledge of users to incorporate their requirements and concerns into the design process. It employs techniques that enhance user participation, such as focus groups, quality circles, and inventories. It is mostly used for workplace, job, and product design. It is not considered as a design process, but only a perspective for the design of individual components. It advocates that user participation should be an essential component of system design, and that its importance should not be underestimated.

2.1.2.3 Ecological Interface Design (EID) Approach

This approach enables the design of human-system interfaces for complex sociotechnical systems [68, 73]. It supports the cognitive abilities of users by focusing on their adaptation to changes in system demands. It leads to the design of human-system interfaces that enable controls and displays that mimic the dynamics between the system and its environment, hiding away the detailed behavior of individual system components [74]. It proposes the analysis of the work domain through a means-ends analysis that results in an abstraction hierarchy [75]. It also makes use of the skills-rules-knowledge taxomony [76] as a tool to describe how the information should be displayed. One of the purposes of this approach is to effectively support human operators in all situations: familiar, unfamiliar, and unanticipated. This approach has been successfully applied to a wide range of domains, including aviation, process

control, and medicine. Among its current challenges are the difficulties in analyzing work domains, interfaces, and the integration of EID to system components.

2.1.2.4 User-Centered Design Approach

User-centered design proposes that the system should maximize the involvement of users at the task level, leaving the control of the system to the human operator. In this case the technical component of the system is designed to cooperate with the user. This approach considers user requirements, goals, and tasks from the conceptual stages of design, when changes made to the technical component of the system may translate into lower costs and faster commissioning. The literature refers to a detailed process [77] for user-centered design that conceives system design as evolutionary, developing the system in an incremental fashion. Tools in user-centered design include task analysis, checklists, interviews, and focus groups. Two different views exist toward the nature of user involvement within this approach: one emphasizes that participation should be encouraged along the design process because those involved are a fair representation of end-users; the other one considers users as sources of data and, as a result, a greater effort is given to translating user knowledge into useful tools [3].

2.1.3 Issues between Humans and Automation

Automation for the sake of automation, or just because it is possible, can be entertaining and become a curious academic exercise, but may not always be a good idea in practice. It is meant to support human work and activities, and not vice versa. Furthermore, it should maximize the extent to which energy may be utilized toward this purpose. The field of human-automation systems brings about issues that, together with advances in automation technology, have evolved over time but nevertheless persist due to the presence of the human element [2]. The following paragraphs describe some of these issues.

2.1.3.1 Complexity: Emerging Behaviors

Automation is composed of sensors, decision elements, and actuators. These may form intricate networks from predetermined relationships established intentionally by engineers and designers. In this case, *complexity* refers to emerging relationships and behaviors that result from the interaction of these elements given a particular context. Such relationships tend to be unanticipated and studied only after the behavior has been expressed during tests. This is especially true for large-scale systems, like power grids, which are said to be highly dynamic in terms of (a) pace of change, (b) scale of operations, (c) integration of operations, (d) aggressive competitions between elements, and (e) deregulation by government [78]. Furthermore, the distributed nature of these automated systems may lead to conflicting decision elements, each of which may pursue a different goal at the same time. This is known as the *mixed-initiative problem* which, when involving humans as decision elements, is called the *mixed human and computer initiative problem* [2]. One approach to this particular problem is the use of a "human-machine overseer" or a "meta-supervisor," which aims to coordinate behaviors and goals. One example of such approach, drawn from artificial intelligence, is called the subsumption architecture [79, 80, 81], which inspired the FAM-based agent architecture [60, 82] introduced in Subsection 1.1.2. Additionally, the human may be unable to develop a mental model of how the system works, degrading human performance by limiting the extent to which operators comprehend the situation of the system and how its behavior may evolve over time [57].

2.1.3.2 Monitoring: A Burden to Humans

One result of applying automation in the workplace is the changing role of the human. Instead of manually conducting his/her work, the human trains to take on the role of supervisor. Ideally, supervision involves some form of interaction that would maintain cognitive engagement by the human. However, in many cases automation is designed

to conduct repetitive tasks in a monotone manner, becoming a source of boredom for the human supervisor [2]. This can be counterproductive for two reasons [57]: (1) if the system operates continuously and without anomalies, the human may divert his/her attention to other sources of information, perhaps even tunneling his/her attention to signals that will not help to maintain situation awareness; and (2) it may mistakenly take the human out-of-the-loop, putting the system in risk of failure by human error in the event of an anomaly. In such case, it would be challenging for the human to regain control of the system due to his/her slow response in comparison to automation. In fact, it is said that the human nervous system is limited to a range of bandwidths that is far slower than that of automation: "At the low frequencies humans fail statistically, and at high frequencies, above 1Hz, they fail reliably" [2].

2.1.3.3 Decision Support: Undertrust and Overtrust

Due to the supervisory role undertaken by humans, one artifact that becomes apparently convenient as part of the human interface is a decision aid or decision support system. The issues of providing decision support originate from: (1) the inability of the engineer/developer to obtain a complete model of the controlled process, and (2) the non-existence of a design objective for the decision aid. The engineer/developer would ideally need a complete model of the dynamic system and an objective function in order to design and evaluate the decision support system. However, if these were available, the decision aid would not be necessary, because the system could then be fully automated. This is known as the *Rosenborough Dilemma* [83], which concludes that "in any system requiring a human operator, the objective validity of a specific decision aid can never be established." Another author, however, offers a way out from this dilemma by validating the decision aid in situations in which the human may make mistakes, demonstrating the motivation for using decision support. Even in use, there is no guarantee: the human operator may always decide whether or not

to use the information offered by the decision aid depending on how suitable he/she finds it in any given situation [2]. This may lead to *undertrust* of the decision support system by the human operator, which may especially be the case if the decision aid frequently gives false alarms, i.e. becomes a *nuisance*, resulting in the *crywolf syndrome*. At the other extreme, routinely relying on decision aids may cause the human operator to develop a dependence on what the decision aid recommends, partially or totally abandoning his responsibilities and thus, through human error, potentially causing system failure.

2.1.3.4 Levels of Automation

As discussed in Subsection 2.1.1 with Figure 3, there is a range of degrees for the development of automated systems, from the completely manual to the fully autonomous. Most people, however, believe that systems can only be controlled either manually or automatically, and discard the possibility of having humans work with automation at various degrees. Such is the case in the domain of space exploration: most people take extreme sides and consider fully robotic missions versus manned ones, and do not highlight the advantages of having humans and automation collaborate in a shared mission [2]. This polarization is most probably due to the lower costs of conducting purely robotic missions. The question becomes: to what degree should a system be automated? The so-called *technological imperative* [8] has driven the trend to automate the easiest processes, leaving the remaining tasks, and often times more difficult tasks, to the human. Such trends may lead to situations in which humans find themselves executing tasks that are counterintuitive, or that are not directly related, producing other kinds of vulnerabilities in human performance. Such incoherences are said to result in the degradation of the overall human-automation system performance, and lead to certain contradictions or "ironies" in the uses of automation

[84, 85]. One way to discern what tasks are to be assigned to humans or to automation is to perform a function allocation, which can be guided by the MABA-MABA list [1], shown in Table 1, named from "Men-Are-Better-At Machines-Are-Better-At."

Table 1: The Fitts MABA-MABA list [1].

Humans are better at	Machines are better at
- Detecting small quantities of visual, auditory, or chemical energy - Perceiving patterns of light or sound - Improvising and using flexible procedures - Storing information for long periods of time - Inductive reasoning - Exercising judgment	- Responding quickly to control signals - Applying great force, smoothly and precisely - Storing information briefly - Deductive reasoning

Other researchers have preferred to decompose the human-automation system in sequential stages, *i.e.* information acquisition, analysis, action decision, and implementation, each of which can be automated to a certain degree [86]. Researchers following this perspective observe comparable degrees of automation along these various stages [8].

2.1.3.5 User-Centered Automation

During the 1990's, user-centered design gained wide popularity as the most appropriate way to integrate humans and machines in various domains [87, 88, 89]. The main issue has been defining what is user-centered design. The research community has debated on its meaning according to their fields of application. What they have agreed upon, as shown in Table 2, are some of the characteristics found in user-centered designs and objections to each.

Other authors have approached the definition of user-centered design by specifying what it is not [57]. For these authors, user-centered design does not mean: (1) asking users what they want and providing it, (2) only presenting supposedly needed information to users, (3) providing a system that makes decisions for the user, nor (4) doing at anytime everything for the user. Instead, the objective of the system is to:

(1) organize technology around the goals, tasks, and abilities of the user; (2) support human information processes and how operators make decisions; and (3) maintain the user in the control loop with awareness of the state of the system. This approach makes use of *situation awareness* as a driver in the design of user-centered automation systems, and uses *human error* as the dependent variable to be minimized.

Table 2: Characteristics of user-centered design and their objections [2]

Characteristics	Objections
- Allocate tasks to humans or machines as appropiate	- There is no consensus
- The human remains in the control loop	- Human has low bandwidth
- The operator is the final authority	- Humans are poor supervisors
- Make the human job more enjoyable	- Leaves out system performance
- Empower human operators at maximum	- May generate human conflicts
- Encourage trust in the operator	- Leads to overtrust on automation
- Provides decision support	- May overload the operator
- Reduce error and response variability	- Limits human flexibility
- Human supervises the automation	- Manual control may be better
- Optimizes combined human and automatic control	- Objective function does not exist

2.1.3.6 Model of the Human Component: A Limit to System Design

Initially motivated by computer science, the field of cognitive psychology has made efforts to model the human mind such that the interaction of *information processing* functions in the human mind is analogous to computer systems [90, 91, 92]. These functions focus mainly on describing how humans make use of perceptions, how they transform these perceptions to aid decision making, and to finally perform an action [93]. However, these models do not take into account the interaction of the human with his/her environment, thus limiting their use for the design of human-automation systems. In contrast, models used in *ecological interface design* (EID) take the environment into consideration by looking more into the flow of information between the environment and the human and less into the details of the internal processing sequences [94, 95]. One outcome of the EID approach is the development of interfaces

that bring control elements and displays to the reach of the human operator, mimicking dynamic relationships present in the environment and certain characteristics of how humans perceive them [74]. In contrast to the perspectives of cognitive psychology and EID, cognitive engineering presents a top-down approach [67]; it draws knowledge from these two bottom-up approaches and combines ideas in control theory and engineering in order to enable design methods that consider the overall system goals and constraints. Instead of focusing primarily on the interaction of the human with a physical system, cognitive engineering centers its analysis on knowledge structures both in the machine and inside the human mind [93]. The main challenges in human modeling consist of achieving a description of the mental models created by humans in different situations, defining the relationship between these models and the decisions aids, and coping with the flexibility inherent in the human capacity to adapt and learn.

2.1.4 Uses of Automation and Domains of Application

The commissioning of automated systems has historically been led by its application to industries in a business-to-business fashion, i.e. a firm that specializes in equipment, procurement, and training offers their products and services to industrial and corporate customers. With advancements in automation technology, the availability of these systems has progressively found ground in the consumer market, including assistive robots for individuals with disabilities or ailments [96, 97, 98], home automation [99, 100], robotic kits [101, 102], and entertainment and toys [103, 104]. It is evident that automation technology will continue finding applications in evermore aspects of human activity, although the nature of the interaction between the human and the system may change.

The more traditional fields of application include process control, manufacturing, aviation and air traffic control, trains, ships, spacecrafts, robotic vehicles, healthcare

systems, battlefield command and control, office systems, and education [2]. All of these fields employ automation to varying degrees, and are found in different areas of Figure 3. As an example, some application domains are distributed in different areas in relation to more familiar references, as illustrated with Figure 7.

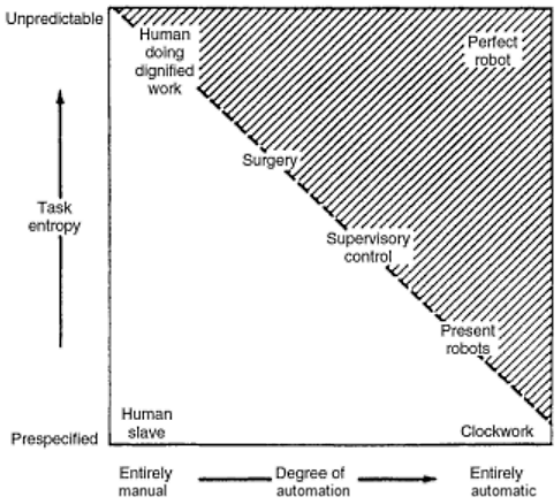

Figure 7: Human-automation system examples [8]

Figure 7 shows, for example, that prespecified tasks can be fully automated by present robots and replace human workers, as shown in the lower-right corner. These robots can be found in motor-vehicle assembly lines and other production lines. Others, more complex, such as in surgery, may employ automation but to a limited degree. An example of such system in healthcare is the *da Vinci* robot [105, 106, 107], which is increasingly used to perform critical tasks that require precision and minimal invasion of the patient's body for a faster recovery. A still more recent and debated application of automation and robotics is found in unmanned aerial vehicles (UAV) for military applications [108, 109, 110]. Questions arise about the human roles in the operation of UAV, if the human should always be in-the-loop for the deployment of weapons and how mechanisms in adjustable autonomy may enable such capability in an ethical way.

Still, other applications of human-automation systems are yet to be explored. Such

is the case in the interaction of crowds with computer systems to enable functionalities or capacities not feasible by other means. These systems make use of crowds as sources of information and intelligence, *i.e. crowdsourcing*. One application of crowdsourcing is widely spread in CAPTCHA systems, in which computers implement what is called an inverse Turing test, to detect when a human is interacting with the system or not. Others include swarming dynamics to generate recommendations in social networks, such as Amazon, YouTube, MySpace, and Facebook [111]. Scientists, as well, are developing crowdsourcing tools to take advantage of the computational power latent in entire populations, implementing what is being called "citizen science" [112].

2.2 The Domain of Spaceflight Life Support Systems

A case mentioned in Section 2.1.3.4 as an issue in human-automation systems referred to the debate in the space community of whether to support either purely robotic or manned missions for space exploration – the main argument in support of the former being that they are less expensive.

The cost of both robotic and manned missions is determined by requirements in mass, volume, and power [113]. Manned missions differ from robotic ones in that, in addition to science instruments, they also need to support the physiological demands and quality of life of a human crew [46, 114]. The subsystems that keep the crew alive while contributing to mission success are called *life support systems* (LSS). These subsystems add mass and volume to mission elements, resulting in the need for greater launch capacities, which as a consequence increase their overall cost [115]. In addition, the presence of a human crew has traditionally created the need for expensive management structures to minimize the risk of loss-of-mission (LOM) and loss-of-crew (LOC) events. For example, the Space Shuttle program management at the National Aeronautics and Space Administration (NASA) used to absorb 69% of the total budget allocated to generic operations and infrastructure functions [116].

Recent innovations in commercial spaceflight aim to considerably reduce costs while increasing autonomy of operations [117].

Besides mission requirements, mission duration also increases the cost of manned missions. If the LSS operates in *open loop*, *i.e.* byproducts are not recycled on board the spacecraft, the total mass of consumables must be launched, stored, and consumed throughout the duration of the mission. In consequence, the mass of consumables, as well as byproducts, increase with mission duration. Although early space exploration systems were able to revitalize air, they were unable to recycle water from urine nor to produce food, thus limiting the autonomy of the spacecraft to only 14 days [46].

One way to cope with this problem is to regenerate consumables by recycling byproducts. The components that provide these capabilities are called *regenerative* LSS; they include a suite of technologies based on physico-chemical and biological processes aimed to transform wastes and byproducts back into consumables. Regenerative LSS are meant to be autonomous and to help maximize crew time dedicated to mission objectives. However, their operation is not trivial: regenerative LSS processes require considerable effort and time, and they constitute complex mass and energy transfer networks subject to the behaviors of their unit processes and to crew demands. As a consequence, they pose novel challenges for their integration and operation.

This section introduces spaceflight LSS as a domain of research and application for human-automation systems. It provides background on life support technologies used in the past and those considered for future manned missions. It describes the Water Recovery System (WRS) currently commissioned on the International Space Station (ISS) and lessons learned from an anomaly occurring during Expeditions 23 through 26. Finally, it presents the challenges in this domain for their integration, automation, and safe operation.

2.2.1 Background

During the Space Race, a total of 34 astronauts rode three different spacecrafts in the Mercury, Gemini, and Apollo Programs [118]. Twelve of them were enabled to walk and explore the Moon during this period. The aim of these programs was to test and determine how NASA would send a crew to the Moon, ensure they accomplish mission objectives, and guarantee their safe return to Earth. The Moon landings were conducted according to a mission profile similar to Figure 8.

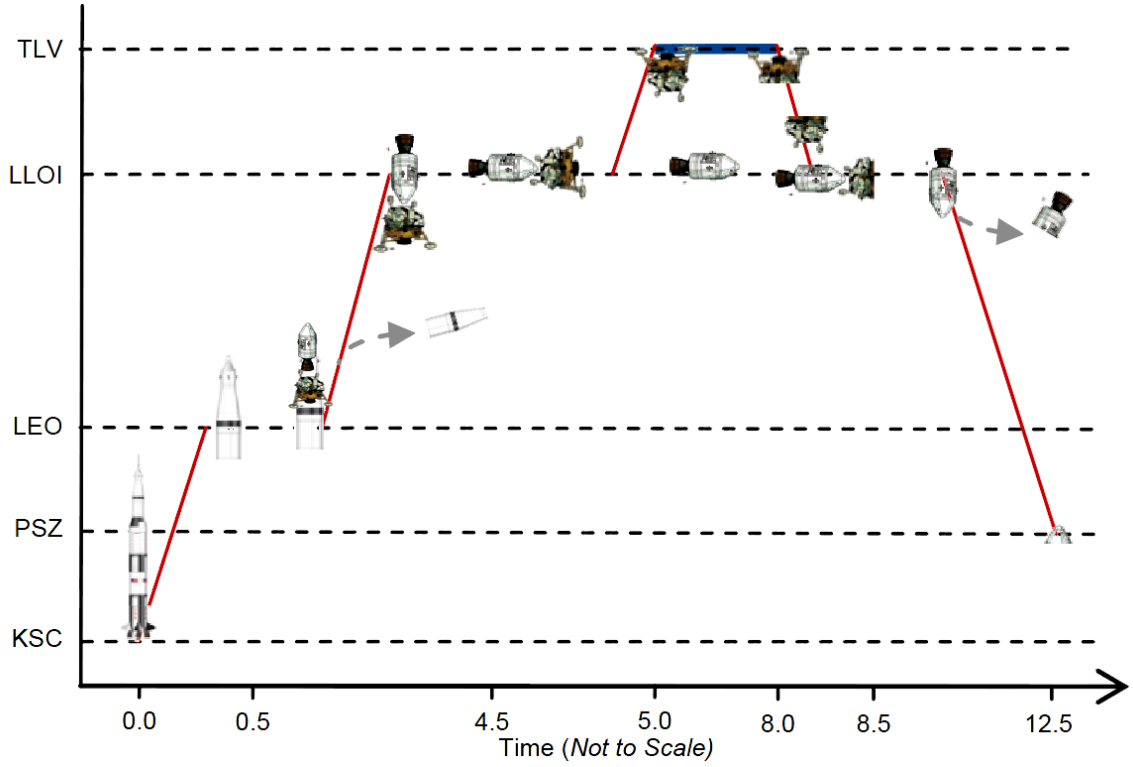

Figure 8: Bat chart of the Apollo 17 moon landing mission [9].

The spacecraft that enabled the six landings on the Moon was composed of two modules with independent LSS [46]: the Command Module (CM), and the Lunar Module (LM). Figures 9 and 10, respectively, show the diagrams of their environmental control and life support systems (ECLSS). As Figure 9 shows, the liquid and solid byproducts of the physiological processes of the crew operated in an open cycle (bottom left), *i.e.* liquid wastes were dumped into space and the solids were stored

on board. In addition, the power subsystem, shown as the fuel cell in the top right of Figure 9 produced water while generating electricity.

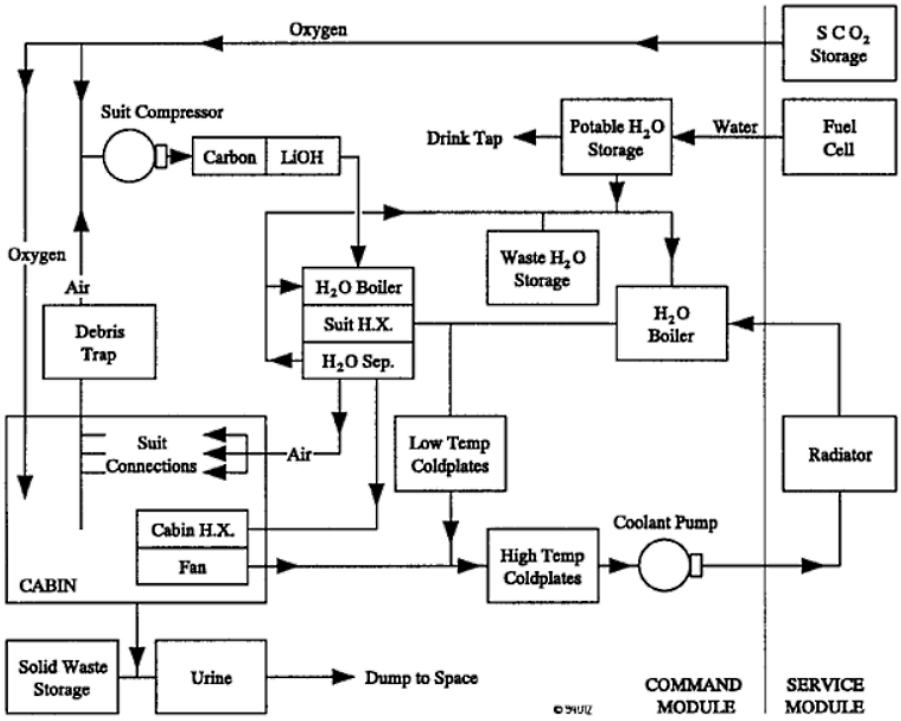

Figure 9: ECLSS of the Apollo Command Module [10]

Here, fuel cells converted chemical energy from hydrogen and oxygen into electricity, while also generating water for the crew. In contrast, the byproduct from gaseous processes, i.e. respiration and transpiration, was processed in a closed cycle. In this case, air containing humidity was extracted from the cabin atmosphere by an air revitalization process that included a carbon and a lithium hydroxide filters. The regenerated air flowed back into the cabin through space suit connections. These LSS processes enabled humans to explore the Moon. Since then, no other nation has undertaken space exploration missions. While one problem is, of course, their apparent cost-benefit, another is the autonomy of human exploration systems. The question is: How can spacecrafts be made more sustainable?

Yet another question can be raised from Figure 10. The water subsystem of the LM was composed of a number of valves that had to be manually operated. Such

tasks imposed additional workload on the crew that, if automated, could have freed crew time for other mission tasks. It is important to note that this still was an open cycle subsystem; future technologies may operate in closed cycle, increasing system complexity and further justifying the need for automation. The question is then: How specifically may automation enable the deployment and proper operation of increasingly complex LSS?

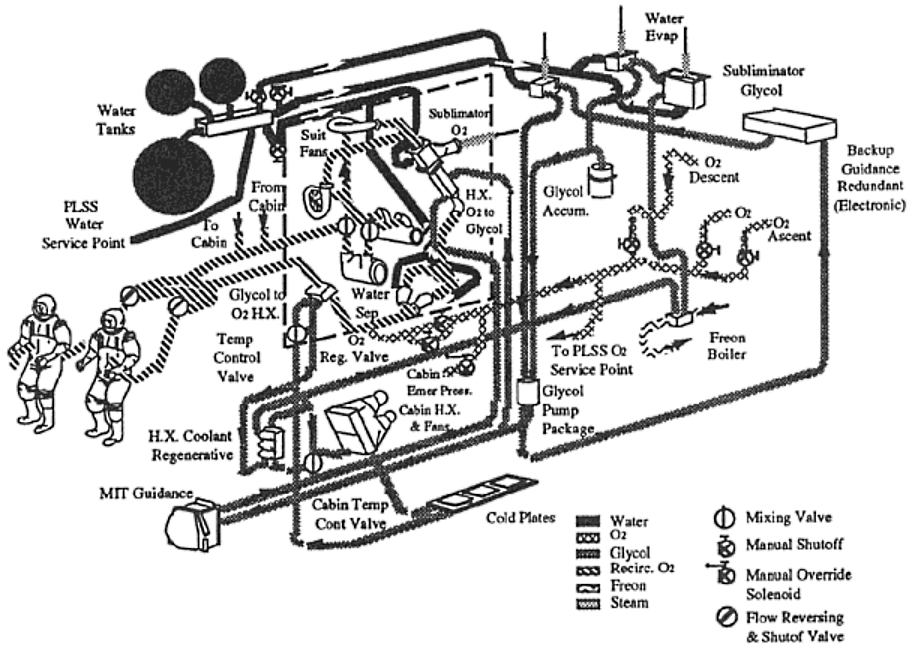

Figure 10: ECLSS of the Apollo Lunar Module [10]

During the span of more than 60 years, various space agencies have studied regenerative technologies to increase spacecraft autonomy [46, 119]. Some regenerative technologies have been successfully demonstrated in ground-based experiments [120]. A few technologies have already started to mature in current hardware on the International Space Station (ISS). The ISS is today the platform used for the development of LSS technologies to enable future exploration missions to the Moon and to other destinations in the solar system. Private companies, such as Space Exploration Technologies (SpaceX) and Bigelow Aerospace, are expected to build capacities and destinations to join in these efforts.

The ISS is also the primary space-based ECLSS research platform. Among its purposes is to test, incorporate, and mature technologies to reduce the need for resupply missions and to enable long-term manned space flight beyond low earth orbit [121]. Its three key components are the Water Recovery System (WRS), the Oxygen Generating System (OGS), and the Carbon Dioxide Reduction Assembly (CRA) [122]. These processes are entirely physico-chemical and help to close the water and atmosphere regeneration cycles.

2.2.2 A Challenge in Monitoring and Automation

The integration of various subsystems into a single life support system is a critical aspect of their design [46]. It primarily involves defining subsystem interfaces and determining the dynamics of mass and energy flows in, within, and out of the system. Although investigations continue to evaluate various single physico-chemical and biological technologies to increase loop closure, the challenges for their integration are still to be fully understood [46].

One challenge is the increasing complexity of their mass and energy flow networks. As discussed in Subsection 2.1.3.1, such complexity refers to unanticipated relationships that are said to "emerge" from the dynamic interaction of subsystems. In the case of LSS, these not only refer to mass and energy flows, but may also include unexpected chemical reactions taking place within the system. These emerging dynamics are usually discovered during test runs or during operation.

An example of such situations may be illustrated by an anomaly associated with the WPA and TOC measurements that occurred between June and November of 2010 on ISS [11, 48, 47]. TOC is a non-selective technique that provides a measure of the overall organic compounds contained in water samples; on ISS it is detected by manual measurements conducted with the Total Organic Carbon Analyzer (TOCA) [123].

The NASA Toxicology Group at Johnson Space Center (JSC) and the National Research Council established the maximum TOC concentration for ISS at 3000 [ppb]. By May 2009, after NASA had verified flight rules and procedures to regenerate water, the WRS was commissioned to recycle urine distillate and humidity condensate, allowing ISS to support a crew of six. During more than a year, TOC levels remained sufficiently stable, below 500 [ppb], such that stakeholders began wondering if the number of tasks related to the TOCA could be reduced. But on June 15, 2010, TOCA started to detect an unexpected and monotone increase of TOC in WPA-recycled water, as shown in Figure 11.

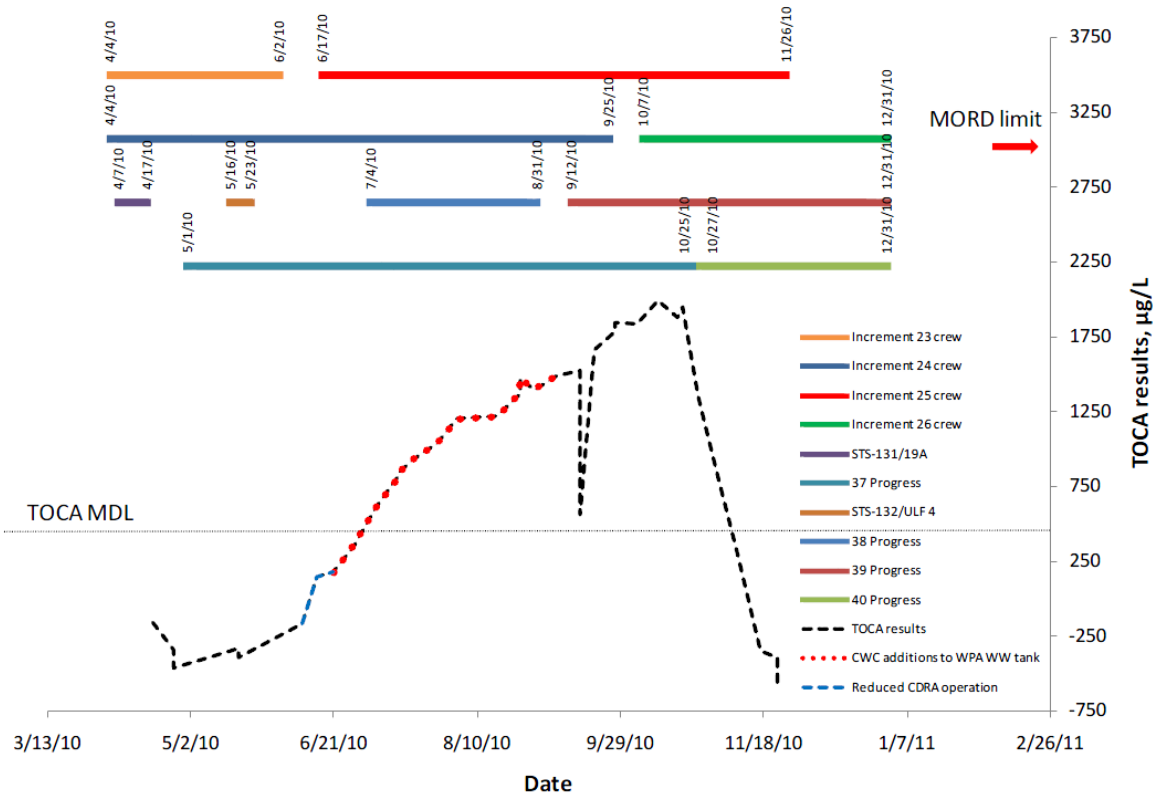

Figure 11: TOC increase in measurements of WPA water from ISS [11].

Only after Soyuz 22 brought back archived water samples in late September, 2010, teams at JSC and MSFC began analyzing the identity of the compound that produced such increase. For months, the crew on ISS and flight controllers on ground

remained uncertain about how to proceed if TOC levels reached the 3000 [ppb] health-based limit. The crew and mission control attempted potential solutions, such as changing out critical multifiltration systems and adjusting the temperature of the WPA catalytic reactor. However, nothing improved the TOC situation. Meanwhile, teams analyzing water samples identified the organic compound as dimethylsilanediol (DMSD)[11], a silicon-organic compound often obtained from the degradation of other silicon-based organic compounds. These are found in hygiene products, medications, sealants, lubricant oils, and a myriad of items also present on ISS. Although toxicologists determined that a 8000 [ppb] DMSD concentration (out of a 25,000 [ppb] maximum exposure limit) posed no risk to the crew, the source of DMSD remained unidentified. Finally on October 2010, DMSD concentration began a sudden drop toward nominal values without an apparent reason.

The case of the DMSD anomaly helps to illustrate the emergence of unknown situations in the operation of increasingly closed life support systems. Some of the lessons learned from the experience are:

1. *Uninterrupted monitoring is recommended*

   Even without apparent extraordinary findings, monitoring provides insight into operations under nominal conditions. It also offers *context* that helps build human-operator situation awareness, which may influence their intervention during off-nominal conditions.

2. *Archive samples complement in-flight monitoring*

   Despite having monitoring instruments on-board, not all chemical analyses will be possible in-flight. Archive samples provide a *screening* capability to identify unknown compounds and to perform forensic investigations to help determine the causes of unexpected situations.

3. *Allowing for margin is critical*

In-flight monitoring allows for operational margin during transitions to off-nominal conditions, given that it provides *time* to attempt troubleshooting, isolate and mitigate anomalies, analyze diagnostic archive samples, refine health-based standards, and develop operational plans.

4. *Unknown situations are to be expected*

   Although human-rated flight hardware undergoes extensive ground testing and an on-orbit-checkout period prior to crew utilization, unexpected events may develop even after two years of nominal on-orbit operations: "[Even with NASA having] the best intentions, the most comprehensive plans, the clearest fault trees, and the most logical hypothesis, the unexpected still happens" [11]. This lesson calls to incorporate redundancy in designs, to plan for failures that may never occur, and to expand perspectives on how to manage these complexities.

Some other challenges that NASA has posed as critical toward the integration of closed-loop LSS include [46]: (1) determination of health and safety requirements for waste treatment, (2) achievement of safe and reliable overall system operation, (3) investigation of control systems response to instabilities and anomalies, and (4) the capability to correct instabilities and anomalies by chaos and fuzzy logic.

2.2.3 Remarks

The field of human-automation systems is inherently multidisciplinary and finds its application in diverse domains. Some of the challenges between humans and automation are posed by issues that continue to evolve as new technologies and computational methods become available. The domain of life support system is not an exception. Given their slow time responses, the interaction between humans and automation pose specific issues relevant to situation awareness. Fortunately, innovation in sensing technologies allows measurements of multiple environmental variables to assess the state of life support systems. However, such challenges require the development

of methods to fuse their data, produce relevant information, and enable real-time decision making minimizing human errors. This research aims to offer an approach to this challenge by developing a solution in the domain of life support systems. Toward this purpose, the first question to be addressed was to develop a research platform that would allow experiments relevant to regenerative life support system. Chapter 3 presents the development of a small-scale and ground-based bioregenerative life support system as a response to this question.

CHAPTER III

BIOREGENERATIVE LIFE SUPPORT PLATFORM

On April 10th 2010, at the Kennedy Space Center, President Barack Obama pronounced his "Remarks on Space Exploration in the 21st Century." The President included closed-loop life support systems (LSS) as a technology that "can help improve daily lives of people here on Earth, as well as testing and improving upon capabilities in space." Researchers continue to develop and test *regenerative* life support technologies that may help reduce the frequency of resupply missions and presumably also reduce the cost of such space habitats in terms of logistics. An example is the commissioning of the Water Processing Assembly (WPA) in the U.S. segment of the International Space Station, which recycles waste liquids, including urine, back into potable water. One subset of regenerative technologies considered are *bioregenerative* life support systems (BLSS), which make use of biological processes to transform biological by-products back into consumables [46]. An example of such research employs aquatic habitats as small-scale platforms for BLSS research [124]. Aquatic habitats involve biological processes, such as photosynthesis, that regenerate life support resources, such as oxygen. Their reuse of a limited volume of water, their opportunity for isolation from the atmosphere, and their capacity to support life forms make them a candidate for the study of closed-loop life support systems (LSS).

3.1 Background

Larger-scale proof of concept projects have been undertaken by public and private organizations to study the sustainability problems and issues that arise from integrating human participants within a variety of life support processes. The main challenge has been the development of subsystems and their integration in a single ecosystem.

While some projects have tested single regenerative processes to recycle byproduct into consumables, others have established entire biomes and attempted their integration. Such is the case of the project *Biosphere 2* in which, with a volume of 204,000 [m^3], attempted to integrate six biomes and a human habitat for a crew of seven or eight participants. A series of experiments were performed in Biosphere 2 during 1991-1994 [46]. Figure 12 shows some of the facilities that have been built for this purpose, including Biosphere 2.

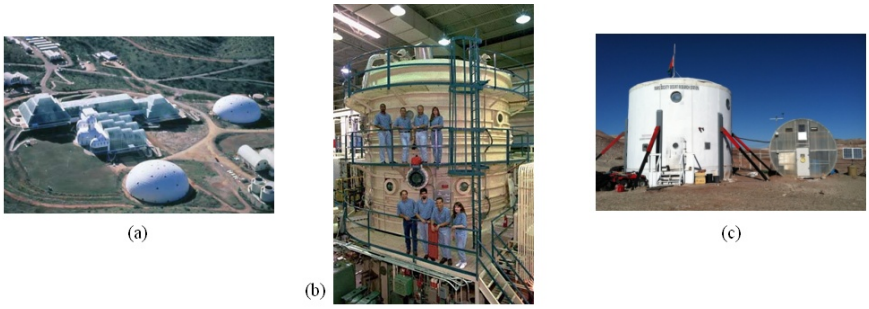

Figure 12: (a) Biosphere 2, (b) Life Support Systems Integration Facility, and (c) Mars Desert Research Station.

These facilities vary in scale and in the reach of the activities they support. The Life Support Systems Integration Facility (LSSIF), displayed in Figure 12(b), contained a volume of 226.5 [m^3] in which it was able to support crews of four participants [120]. This facility performed various experiments during 1995-1997 in support of what has come to be known as BIOPlex at Johnson Space Center in Houston, Texas. Volunteer-driven organizations have also pursued initiatives in this direction. Figure 12(C) shows the Mars Desert Research Station operated in Utah by the Mars Society. Although these facilities were effective, there are alternatives to the use of large-scale facilities for closed-loop LSS research. Such alternatives have made use of aquatic habitats for experiments in zoology and physiology in low Earth orbit (LEO) [125, 126, 13, 127, 128], and for ecotoxicological studies in ground-based hardware [129, 130]. Results obtained with the *Closed Equilibrated Biological Aquatic System*

(CEBAS) minimodule in Space Shuttle missions STS-89 and STS-90 show that microgravity does not affect aquatic habitats considerably for exposure periods of up to 16 days [126]. This module also flew in STS-107 [127], but no results were reported due to the accident of the Space Shuttle Columbia. Researchers from the Chinese Academy of Sciences have employed a *Closed Aquatic Ecosystem* [131, 132] (CAES) as well for experiments relevant to ecophysiology, a discipline that "seeks to clarify the role and importance of physiological processes in ecological relations of species [133]." A recent initiative by the Japanese Aerospace Exploration Agency (JAXA) plans to include an aquatic habitat in their International Space Station module, Kibo [134]. Beyond these efforts, very little has been done to make use of aquatic habitats for research on RLSS control and automation.

Contribution 1: Given the high costs and difficulties of performing experiments in large-scale RLSS, the first contribution of this work is the use of an aquatic habitat, or aquarium, for experiments relevant to RLSS [61, 135]. The idea builds on the use of aquatic habitats as small-scale platforms for Earth-based and spaceflight LSS research [46] and applications [129]. Their reuse of a limited volume of water and their capacity to support life forms, such as aquatic animals and plants, make them a candidate for the study of sustainability attributes of larger-scale environmental systems. Aquaria may involve biological processes, such as photosynthesis, that regenerate life support resources, such as oxygen. This further makes them attractive as an option for RLSS research. This particular research platform enables experiments that focus on the process of respiration. Other biological processes take place in the habitat, some of which help to balance the ecosystem by decomposing toxic compounds, like ammonia. The use of this aquatic habitat provides a learning tool to comprehend the challenges and limitations of automation technology in the operation of RLSS and other bioengineering systems. However, the temporal response of life support

variables in the habitat is very slow. Therefore, another aspect of this contribution is the mathematical modeling, description, and simulation of the aquatic habitat. The model serves as a numerical testbed for both RLSS and human-automation integration research [136].

3.2 Preliminary Description

One of the questions addressed by studying RLSS are the mass balances that ensure the correct operation of closed-loop systems in such a way that they may be sustainable over time. Mass balances can focus on a particular consumable or a byproduct associated to a metabolic process of a biological component. Experiments with the aquatic habitat focus on the process of respiration, in which O_2 is consumed by 15 snails of the genus *Pomacea* while exhaling CO_2 as a byproduct. Plants of the species *Bacopa Monnieri* regulate the concentration of CO_2 through photosynthesis, enabled by a 6-LED lamp of 300 [lm] and 90° view angle, producing the oxygen needed by snails and bacteria while aiming to maintain acceptable concentration levels in the habitat. Water serves as the medium in which these quantities are stored (dissolved), and through which they are exchanged between the organisms. The habitat consists of a 10-gallon tank divided in four compartments by three separators, as shown in Figure 13; the first two with an opening area of 12.60 [cm^2] and the third with 48.00 [cm^2]. Further details about the design and construction of the habitat have been discussed in previous work [136].

The first and second compartments contain animals (consumers) and plants (producers), respectively. Snails are fed regularly with sinking algae tablets. The third compartment contains Bio-Fill^{TM}, active carbon, and water filtration foam as the media serving the purpose of biological, chemical and mechanical filtration. The fourth compartment allows access for sensors and the water pump. The sensors used include dissolved oxygen (DO), pH and ORP. The water circulates through the four

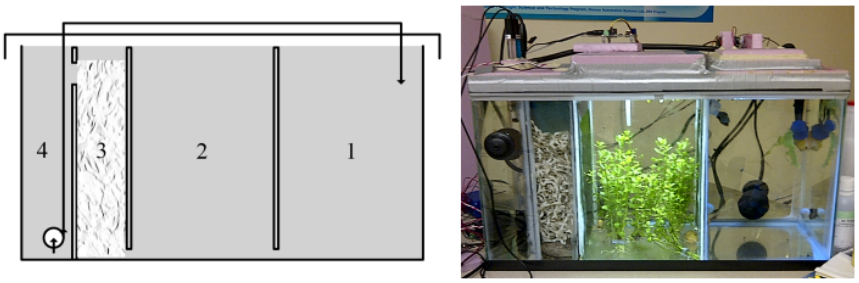

(a) (b)

Figure 13: (a) Recirculation diagram of the habitat; (b) Physical realization of the habitat.

compartments. The first compartment has a motorized hatch of 10cm×10cm and an aerator that allow for reconfigurability, making the system open (volatile) or closed (non-volatile) if necessary; this mechanism is triggered as a fail-safe mechanism when the DO levels reach a minimum of 2.0 [mg/L]. The second compartment holds the LED-lamp and gives access to a dosifier pump that provides a sodium bicarbonate solution to increase the carbonate hardness (kH) of the water; the changes in kH are monitored through variations of the pH readings. Measurements from the sensors are processed by a computer/controller operating under LabVIEW®. The controller delivers the control signals that regulate the LED-lamp power via a pulse-width modulation (PWM) board, and also controls the hatch, and the air and dosifier pumps. The control signals can be generated by control laws or driven manually through a graphical user interface (GUI).

3.3 Physico-Chemical Model of the Aquatic Habitat

The physico-chemical description of the aquatic habitat [136] makes use of a control volume for each compartment. The assumptions made in the formulation of the general mathematical model are as follows: (a) recirculation flow is assumed laminar; (b) water density is constant; (c) the recirculation flow is the same for all compartments; (d) liquid solutions are perfectly well-mixed in all compartments; (e) output concentrations are those inside each compartment; (f) the water level of all compartments

is the same and constant; (g) the volume of the compartments is constant.

3.3.1 Mass Balance in Recirculating Systems

For a substance x the mass balance equation is written as:

$$V\dot{[x]} = F_{in}[x]_{in} - F_{out}[x]_{out}$$

where V is the control volume defined for the mass balance, $[x]$ is the concentration of the substance x inside the control volume in milligrams per liter [mg/L] or parts per million [ppm], F_{in} and F_{out} are the incoming and outgoing flow rates in [L/h], and $[x]_{in}$ and $[x]_{out}$ are the concentrations of those flows, respectively. The rate of change of the concentration $\dot{[x]}$ multiplied by the control volume V defines the rate of accumulation of x in [mg/h]. For a recirculating system, the incoming and outgoing flow rates are the same. If the flow-rate is time dependent, the model is a non-linear system. Therefore, for a recirculating system with n compartments and a variable flow $F(t) > 0$ the general mass balance is expressed as:

$$A_i h\dot{[x]}_i = F(t)\left([x]_j - [x]_i\right); \quad \forall\{1 \leq i \leq n\} \in \aleph; \quad j = \begin{cases} n & i = 1 \\ i-1 & \forall i \neq 1 \end{cases} \tag{1}$$

where A_i is the surface area of each compartment and h is the height of the water level for all comparments.

3.3.1.1 Diffusion at Reduced Recirculation Flow Rates

Diffusion becomes dominant when $F \approx 0$ and a description for the gradient concentration between adjacent compartments becomes necessary. With Fick's law of diffusion [137], the transfer between the two compartments is proportional to the following factors: (1) the concentration difference between them, (2) the equivalent cross-sectional area A_s through the separators, and (3) a constant D. The complete general equation for a closed recirculating system of n compartments with $[x]_l \leq [x]_i \leq [x]_k$ is:

$$A_i h\dot{[x]}_i = f_{r,i} \equiv F(t)\left([x]_j - [x]_i\right) + DA_{s_{k,i}}\left([x]_k - [x]_i\right) + DA_{s_{i,l}}\left([x]_i - [x]_l\right) \qquad (2)$$

$$k = \begin{cases} i+1 & i \neq n \\ i & i = n \end{cases}; \quad l = \begin{cases} i & i = 1 \\ i-1 & i \neq 1 \end{cases}$$

Parameters $A_{s_{k,i}}$ and $A_{s_{i,l}}$ are the equivalent cross sectional areas between the compartment i and the adjacent compartments k and l, respectively. Note that, with the definitions of k and l, one of the diffusion terms is zero for the first and last compartments given that they only have one adjacent compartment.

3.3.2 Reconfiguration into an Open System

The model can be reconfigured into an open (volatile) system by allowing the transfer of gases between the water and the atmosphere.. The expression used to model the mass transfer (i.e. oxygen and carbon dioxide) between the water and the atmosphere is based on Henry's law of gas solubility and Fick's first law of diffusion [137, 138]. The transfer is proportional to the contact surface area A_i between gas and liquid phases, the concentration difference between the liquid phase $[x]_i$ and the equivalent concentration of the gas phase $[x]_{atm}$, and a constant k_v. The equation for a reconfigurable recirculating system is:

$$\dot{[x]}_i = \frac{1}{h}\left(\frac{f_{r,i}}{A_i} + k_{v,i}\left([x]_{atm} - [x]_i\right)u_\sigma\right) \qquad (3)$$

$$\forall\{1 \leq i \leq n\} \in \aleph; \quad u_\sigma = \begin{cases} 0 & \text{non-volatile} \\ 1 & \text{volatile} \end{cases}$$

where u_σ is a switching signal that activates only one of the configurations at a time.

3.3.3 Design of a Four Compartment, Switching System

The simulations presented in this chapter are prepared for a 10-gallon tank with $n = 4$. Its reconfigurability is made possible by an aerator in the first compartment: $k_{v,1} = k_v \neq 0$; $k_{v,2} = k_{v,3} = k_{v,4} = 0$. The system has $n - 1$ separators with cross sectional areas A_{s_a} for the first two, and A_{s_b} for the third. The model of the habitat is described by the switching system in Eq. 4. It considers that consumers are contained in the first compartment, producers in the second and a biofilter in the third. The fourth compartments is left for sensors and water pumps.

$$\frac{d}{dt}[\vec{x}] = \begin{cases} [A]_{cr}\,[\vec{x}] + [B]\,\vec{x} & \text{non-volatile; recirculating} \\ [A]_{cd}\,[\vec{x}] + [B]\,\vec{x} & \text{non-volatile; diffusive} \\ [A]_{or}\,[\vec{x}] + [B]\,\vec{x} + \vec{r}_g & \text{volatile; recirculating} \\ [A]_{od}\,[\vec{x}] + [B]\,\vec{x} + \vec{r}_g & \text{volatile; diffusive} \end{cases} \tag{4}$$

Matrices and vectors for Eq. 4 are:

$$[A]_{cr} = \begin{bmatrix} -\frac{F}{A_1 h} & 0 & 0 & \frac{F}{A_1 h} \\ \frac{F}{A_2 h} & -\frac{F}{A_2 h} & 0 & 0 \\ 0 & \frac{F}{A_3 h} & -\frac{F}{A_3 h} & 0 \\ 0 & 0 & \frac{F}{A_4 h} & -\frac{F}{A_4 h} \end{bmatrix}$$

$$[A]_{cd} = \begin{bmatrix} -\frac{DA_{s_a}}{A_1 h} & \frac{DA_{s_a}}{A_1 h} & 0 & 0 \\ -\frac{DA_{s_a}}{A_2 h} & 0 & \frac{DA_{s_a}}{A_2 h} & 0 \\ 0 & -\frac{DA_{s_a}}{A_3 h} & -\frac{D}{A_3 h}\left(A_{s_a} - A_{s_b}\right) & \frac{DA_{s_b}}{A_3 h} \\ 0 & 0 & -\frac{DA_{s_b}}{A_4 h} & \frac{DA_{s_b}}{A_4 h} \end{bmatrix}$$

$$[A]_{or} = \begin{bmatrix} -\frac{1}{h}\left(\frac{F}{A_1} + k_v\right) & 0 & 0 & \frac{F}{A_1 h} \\ \frac{F}{A_2 h} & -\frac{F}{A_2 h} & 0 & 0 \\ 0 & \frac{F}{A_3 h} & -\frac{F}{A_3 h} & 0 \\ 0 & 0 & \frac{F}{A_4 h} & -\frac{F}{A_4 h} \end{bmatrix}$$

$$[A]_{od} = \begin{bmatrix} -\frac{\left(\frac{DA_{s_a}}{A_1}+k_v\right)}{h} & \frac{DA_{s_a}}{A_1 h} & 0 & 0 \\ -\frac{DA_{s_a}}{A_2 h} & 0 & \frac{DA_{s_a}}{A_2 h} & 0 \\ 0 & -\frac{DA_{s_a}}{A_3 h} & \frac{D\left(A_{s_b}-A_{s_a}\right)}{A_3 h} & \frac{DA_{s_b}}{A_3 h} \\ 0 & 0 & -\frac{DA_{s_b}}{A_4 h} & \frac{DA_{s_b}}{A_4 h} \end{bmatrix}$$

$$[B] = \begin{bmatrix} \frac{1}{A_1 h} & 0 & 0 & 0 \\ 0 & \frac{1}{A_2 h} & 0 & 0 \\ 0 & 0 & \frac{1}{A_3 h} & 0 \\ 0 & 0 & 0 & \frac{1}{A_4 h} \end{bmatrix}$$

$$[\vec{x}] = \begin{bmatrix} [x]_1 & [x]_2 & [x]_3 & [x]_4 \end{bmatrix}^T$$

$$\vec{x} = \begin{bmatrix} x_1 & x_2 & x_3 & x_4 \end{bmatrix}^T$$

$$\vec{r}_g = \begin{bmatrix} \frac{k_v [x]_g}{h} & 0 & 0 & 0 \end{bmatrix}$$

The substances x considered are dissolved oxygen (DO), carbon dioxide (CD) and carbonate hardness (kH). The output equation is $y = [[DO]_4 \; pH_4 \; [kH]_4]^T$, where the conversion from $[CD]_4$ into pH is given by[139] $pH_4 = 6.3 - log\left([CD]_4/[kH]_4\right)$. This transformation is valid within a 5-10% accuracy for $6.5 \leq pH \leq 9.5$. The vector $\vec{r}_g$ establishes the equivalent concentration of gases in the atmosphere (an infinite buffer) as a reference value for the volatile configuration of the system. The model is implemented making use of the parameters listed in Table 3.

3.4 Biological Processes and Ecophysiological Phenomena

Biological processes affect Equation 3 by adding a term x_i to $f_{r,i}$ to account for the rate of production or consumption of the substance x in the compartment i in [mg/h].

$$\dot{[x]}_i = \frac{1}{h}\left(\frac{1}{A_i}\left(f_{r,i} + x_i\right) + k_{v,i}\left([x]_{atm} - [x]_i\right)u_\sigma\right) \tag{5}$$

Table 3: Initial parameters of the reconfigurable aquatic habitat.

Parameter	Value	Units	Description
h	26.28	cm	Height of the water level in the habitat
$A_1 = A_2$	533.40	cm^2	Surface area of the first and second compartments
$A_3 = A_4$	186.69	cm^2	Surface area of the third and fourth compartments
A_{s_a}	12.60	cm^2	Cross-section flow area in the separators type "a"
A_{s_b}	48.00	cm^2	Cross-section flow area in the separators type "b"
F	390	l/h	Flow rate of the recirculation pump
$[DO]_g$	8.40	mg/l	Dissolved oxygen saturation concentration
$[CD]_g$	0.69	mg/l	Dissolved carbon dioxide saturation concentration
D	1500	cm/h	Liquid phase diffusion constant
k_v	200	cm/h	Gas transfer diffusion constant, for DO and CD only

Such rates represent a measure of how chemical substances are produced or consumed in a given compartment. This research makes use of this term in Equation 5 to introduce ecophysiological phenomena in the mathematical description of the aquatic habitat. In particular, this term is used to describe (1) animal and (2) botanical elements. Snails are modeled through their rate of consumption, treated as a random variable to account for changes in metabolic rates and aestivation. Aestivation consists in brief periods of torpor of the metabolism of the snails (similar to hibernation) in which oxygen consumption is considerably reduced. The plants, instead, are modeled through their rate of CO_2 assimilation as a function of irradiance. The following subsections present these two models. Because this research focuses on respiration, the life support compounds considered are dissolved oxygen (DO), carbon dioxide (CD), carbonate hardness (kH).

3.4.1 Animal Component: Population of *Pomacea* Snails

The rate of O_2 consumption, DO, and CO_2 production, CD, by the respiration of a population of snails are modeled by differential equations with time constant τ and a random number of Gaussian distribution with mean $\mu \geq 0$, variance σ^2, and sample time T:

$$\frac{d}{dt}DO(t) = -\frac{1}{\tau}\left[DO(t) + rand\left(\mu, \sigma^2, T\right)\right] \tag{6}$$

$$\frac{d}{dt}CD(t) = \frac{1}{\tau}\left[CD(t) + rand\left(\mu, \sigma^2, T\right)\right] \tag{7}$$

The models in Eqs. 6 and 7 are proposed from observations in the validation of the temporal response of the model with Blüm-type experiments [127, 13, 126].

3.4.2 Botanical Component: *Bacopa Monnieri* Plants

Photosynthesis is proportional to irradiant energy up to a limit in which plants reach their capacity to assimilate carbon dioxide [140, 12]. This phenomena is due to light saturation in chloroplasts as described by the light-response curve of Figure 14 and approximated by Equation 8 as a non-rectangular hyperbola [12]. In Equation 8, A represents the assimilation rate in [μmol/m^2/s], I is the irradiance in [μmol/m^2/s], ϕ is the slope or the light-limited region, Θ determines the point of saturation by carboxylation, A_{max} is the upper boundary of assimilation, and R_d is the dark respiration of the plant. The light compensation point (LCP) in Figure 14 represents the irradiance value in which photosynthesis and dark respiration have equal magnitudes and result in a zero net assimilation of CO_2.

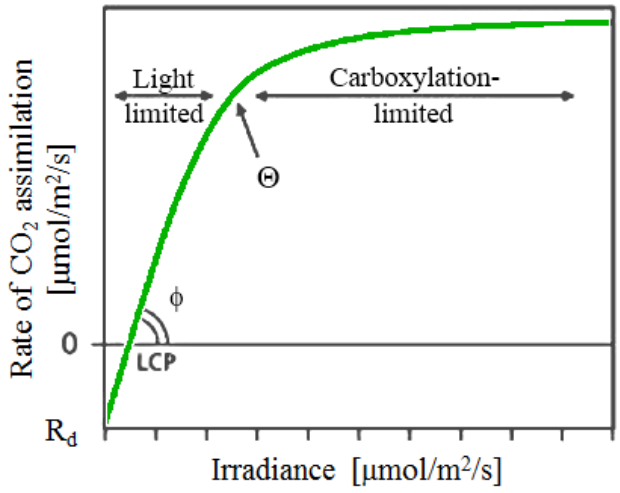

Figure 14: Light-response curve of photosynthesis to irradiance [12].

$$A = \frac{\phi \cdot I + A_{max} - \sqrt{(\phi \cdot I + A_{max})^2 - 4 \cdot \Theta \cdot \phi \cdot I \cdot A_{max}}}{2 \cdot \Theta} - R_d \qquad (8)$$

3.5 Simulations and Validation

This paper presents four experiments. They are based on simulations implemented in MATLAB Simulink, run with a stiff Mod. Rosenbrock numeric method [141] with maximum step of 0.01. The first simulation is meant to produce results comparable to those obtained with CEBAS [13]; because that project was led by Professor Volker Blüm, this paper refers to it as "Blüm-type experiment." The second experiment provides insights into the role of feedback for the equilibrium of closed-loop systems; it compares two simulations that exhibit a similar on/off duty-cycle of the lamp, with and without feedback. The third experiment addresses the study fail-safe/fail-operational mechanisms for this system; it makes use of a failure in the water pump to compare the performance of two fail-safe/fail-operational mechanisms. This experiment makes use of the reconfigurability of the system to allow the exchange of gases with the atmosphere. The fourth experiment makes use of the results obtained in the first one and elaborates on observations of the performance of biological components in the aquatic habitat. It validates the model of the animal component and employs the ecophysiological model presented in Subsection 3.4.2 to observe the robustness of a continuous-time controller that regulates DO concentration and takes into consideration the dark cycle of the botanical component. The following subsections provide additional details about each experiment.

3.5.1 Blüm-type Experiments

This experiment implements a closed-loop on/off control of the DO concentration via photoregulation (by photosynthesis). In this case, a simple controller turns on and off the lamp of the second compartment when the DO concentration in the fourth reaches 4.0 [mg/l] and 6.5 [mg/l], respectively. The simulation time is seven days

and its initial conditions are in equilibrium with the equivalent concentration of the atmosphere at 22 °C at sea level. The production and consumption rates presented in Table 4 are selected to achieve an on/off lamp duty cycle similar to results obtained with CEBAS [13].

Table 4: Production and consumption rates for $\vec{x}$ in [mg/h]

	DO_1	CD_1	DO_2	CD_2	DO_3	CD_3	kH_3
Values	-40.0	40.0	90.0	-90.0	-5.0	5.0	-3.5

Subscripts in DO, CD, and kH denote their associated compartment. The variable $[DO]_4$ represents the concentration of dissolved oxygen in the fourth comparment. During validation, new rates of consumption and production are obtained and presented in Subsection 3.6.1. The new parameters are used in a new simulation and its performance is contrasted with the response obtained from a seven-day experiment conducted on hardware at the laboratory. During validation, DO concentration is regulated through photosynthesis between 6 and 7 [mg/L] with an on/off controller driving the LED lamp. Initial conditions are $[DO] = 6.106$ [mg/L], $[CD] = 6$ [mg/L], and $[kH] = 95$ [mg/L].

3.5.2 Insight to Closed Systems

The second experiment implements an illumination duty cycle similar to the first experiment, i.e. with a period of 6 hours. In addition, a small disequilibrium is added by changing the rates of consumption in the biofilter to $DO_3 = -6.0$[mg/h] and $CD_3 = 6.0$ [mg/h], to simulate a mortality and its decomposition in the system. The simulation time is also seven days. The discussion about this experiment centers on showing need for feedback mechanisms to procure the balance of small-scale and closed-loop environmental systems.

3.5.3 Fail-safe/Fail-operational Mechanisms

The third experiment simulates the failure and replacement of the water pump. The pump fails at 48 hours into the simulation and is fixed within six hours after 24 hours from the fault. The system returns to regular operation at 76 hours. In this experiment two cases are considered: (a) the oxygen levels are regulated via photoregulation (b) the system is switched to a volatile configuration during the fault until it resumes normal operation. Both cases consider measurements of DO concentration in the first and fourth compartments. In this case, the discussion highlights the need for additional resources or reconfigurability to sustain and overcome contingencies in these systems.

3.5.4 Performance of Biological Components

The simulations prepared incorporate the biological models presented in Section 3.4 of this paper. Two simulations are presented: (1) introduction of a model for the animal component to approximate results from the validation and (2) the addition of the model of botanical elements to compare system performance under three light-response curves.

3.5.4.1 Simulation of Consumer Model

For the simulation of the consumer model and, as mentioned in Section 3.4.1, models in Equations 6 and 7 are proposed from observations in the Blüm-type Experiment. The simulation compares the steepness of the DO signal in the Blüm-type validation for a consumer/produce model with parameters $1/\tau = 5$ [rad/s], $\sigma^2 = 10$ [mg/h], and $T = 1$ [h]. The mean value μ of the Gaussian distribution are DO_1 and CD_1 from Table 4. These parameters were obtained by testing and comparing various other values, which were not included in Subsection 3.6.4.1 for clarity.

$$DO_1 = -\frac{1/\tau}{s+1/\tau} rand\left(\mu, \sigma^2, T\right) \tag{9}$$

$$CD_1 = \frac{1/\tau}{s+1/\tau} rand\left(\mu, \sigma^2, T\right) \tag{10}$$

3.5.4.2 Simulation of Botanical Elements

For the simulation of botanical elements, Equation 8 approximates the mole to mole relationship of CO_2 assimilation in higher plants as a function of irradiance. Such relationship is adapted here to address the consumption of CO_2 as a function of the percent lamp power, $P_l[\%]$. As such, A_{max} is replaced by CD_{max} to account for the upper bound of CO_2 consumption. Equation 11 presents the modified light-response relationship and Figure 15 shows three curves for different values of ϕ. Additional parameters are $CD_{max} = 23$ and $\Theta = 0.95$. All other parameters are similar to Section 3.4.2. This paper does not consider the dark cycle of respiration in the plants, *i.e.* $R_d = 0$.

$$\begin{aligned} CD_2 &= -DO_1 = \\ &= \frac{\phi \cdot P_l[\%] + CD_{max} - \sqrt{(\phi \cdot P_l[\%] + CD_{max})^2 - 4 \cdot \Theta \cdot \phi \cdot P_l[\%] \cdot CD_{max}}}{2 \cdot \Theta} \end{aligned} \tag{11}$$

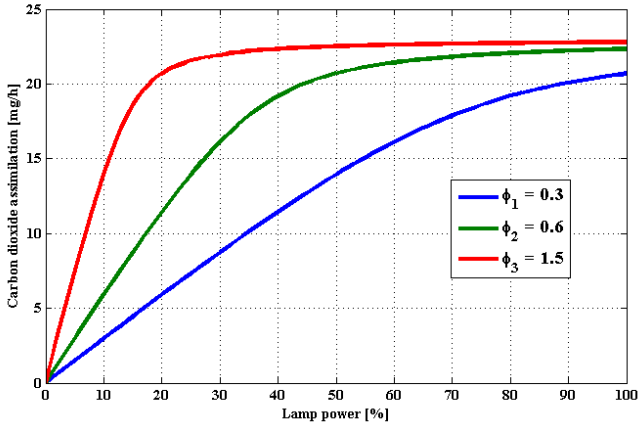

Figure 15: Light-response curves used in simulation

This simulation makes use of a proportional-integral (PI) controller that regulates the DO concentration in the fourth compartment, with a reference signal with a duty cycle of 18 hours for every 24. Such duty cycle helps to account for the physiological requirements of the botanical elements. The PI controller uses $P = 200$ and $I = 50$. The reference alternates between 6.75 and 6.25 [mg/L].

3.6 Results and Discussion

3.6.1 Blüm type Experiments

Figure 16 presents the on/off control of the DO level for a balanced system, varying between 4 [mg/l] and 6.5 [mg/l] in the fourth compartment; the consumption and production rates of the compartment containing plants is turned on and off depending on these limit values, respectively.

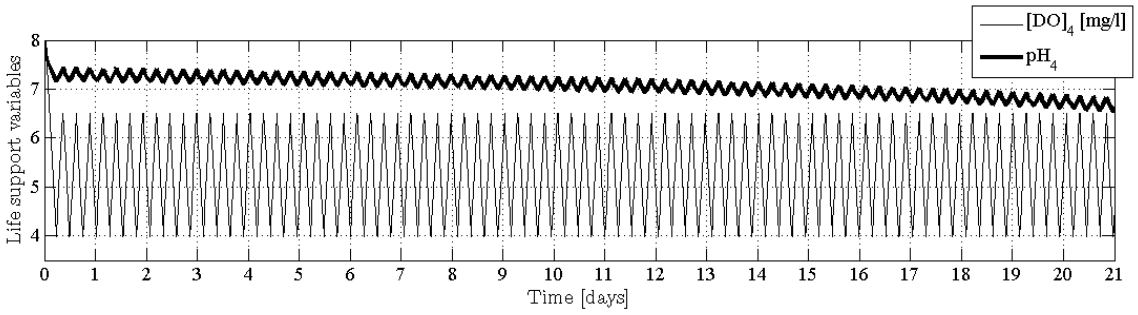

Figure 16: Dissolved oxygen and pH for conditions comparable to CEBAS experiments [13].

The result is similar to results reported in the past [13], which also show the deterioration of the pH level, most probably due to consumption of equivalent carbonate hardness (kH) by the bacteria in the biofilter. The rates of consumption and production used (Table 4) result in a lightning duty cycle of ∼6 hours. Such on/off control does not account for the physiological requirements of the biological elements. Therefore, other control strategies [61] need to be developed to operate bioregenerative life support systems. Given the results obtained for a 10-gallon (37.85 [l]) tank, estimations can be made for experiments performed with the CEBAS-minimodule: with a

volume ∼8.8 [l], and assuming that the system was perfectly balanced, the biological oxygen demand (BOD) should have been nearly half of the oxygen generation rate, or ∼1.2 [mg/h/l]. Hence, its oxygen production rate results in ∼2.4 [mg/h/l]. Values reported [13] show that the system was apparently producing somewhere between "3.5 and 7.5 mg/l" per hour, which is a comparable value. The authors[13] also report about the "steepness" of the oxygen production, which in this research is obtained by taking the first derivative of the DO concentration of the fourth compartment – see Fig. 17.

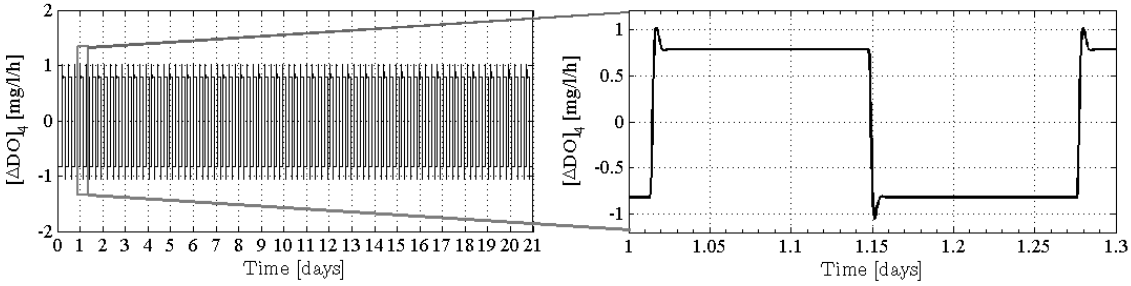

Figure 17: Observation on steepness of oxygen production.

It shows that the maximum steepness achieved is 1.0 [mg/l/h] with stabilization values of 0.8 [mg/l/h]. These values are comparable to the results obtained with CEBAS[13], which show a "steepness" also centered in zero and taking values between ±1 [mg/l/h]. Despite differences in volume, this simplified model is able to reproduce values similar to CEBAS, which at the same time serve to validate the quantities and parameters used therein, and provides a tool to perform forensic analysis.

Figures 18 and 19 show the validation of the mathematical model [135, 136] of the aquatic habitat for the parameters presented in Table 5. Signals in color are from the hardware, while black ones are from simulations. Figure 18 shows the DO and pH values, while Figure 19 shows the "steepness"[13] of the DO signal, *i.e.* its derivative.

Results from the Blüm-type simulation validate the model of the aquatic habitat

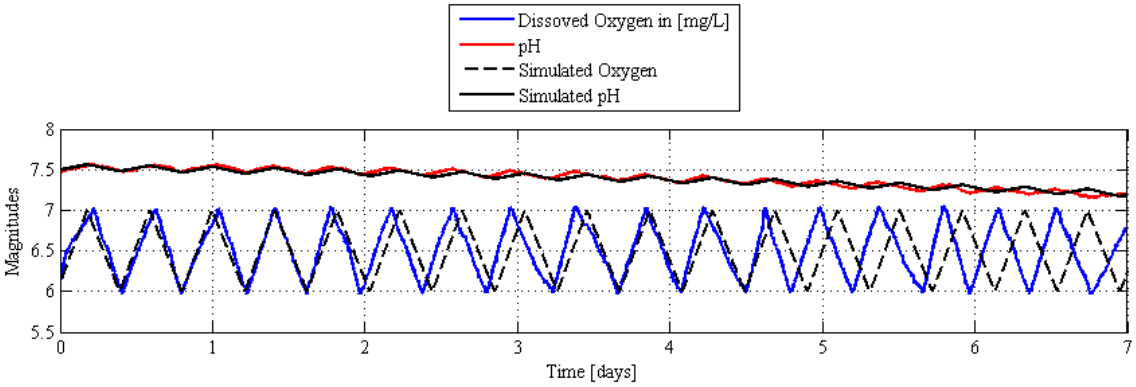

Figure 18: Validation of Blüm-type experiments.

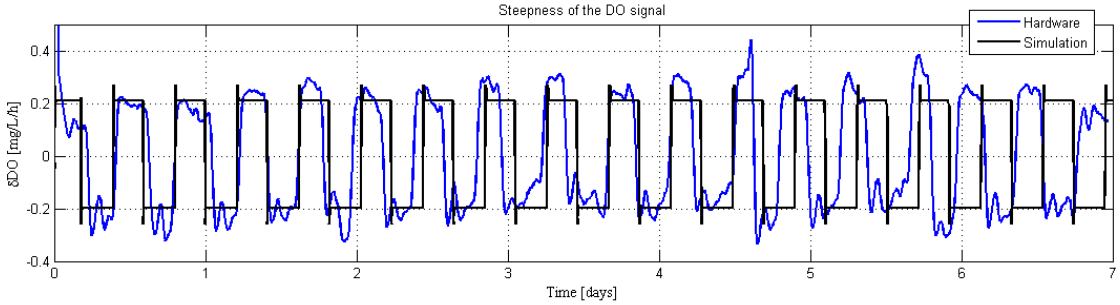

Figure 19: Validation of Blüm-type experiments.

Table 5: Production and consumption rates in [mg/h]

	DO_1	CD_1	DO_2	CD_2	DO_3	CD_3	kH_3
Values	-4	4	23.0	-23.0	-7.0	7.0	-17

and the design proposed in previous work [136]. Especially, the combination of measurements from hardware and validation of the simulation enable forensic analyses of the system to obtain the initial value of carbonate hardness, at 95 [mg/L], and its rate of consumption, at 17 [mg/h]. Figure 18 highlights the comparison between the DO and pH signals, for simulation and hardware. Although there are periods of time, up to days, in which the signals overlap well, there are others that show lack of synchronism. This is due to the on/off control used (like a thermostat) and the disturbances introduced by the population of snails (consumers). Until this validation, it was not expected that the behavior of snails would considerably disturb the

time response of life support variables, i.e. these were assumed to be approximately constant and without disturbances. However, the Blüm-type validation allowed the discovery of the aestivation or metabolic depression [142] that snails may undergo. This is particularly evident in Figure 19, which shows the rates of accumulation and depletion of oxygen in the habitat. While for a balanced system the steepness of the simulation respectively predicts a square signal between -0.2 and 0.2 [mg/L/h] of depletion and accumulation, the response obtained from hardware shows apparently random variations around those same values. This is why Section 3.5 proposes Equations 6 and 7 as the models for the animal component of the system, which is compared with the steepness signal of the validation in Figure 22.

3.6.2 Insight to Closed Systems

The result of the second simulation is reported in Fig. 20. It shows the difference of using an open-loop versus closed-loop control; a small unbalance of just 1 [mg/h] results in a progressive deterioration of dissolved oxygen levels in an open-loop duty-cycle, which potentially would harm the consumers contained therein. In contrast, the use of feedback and a regulation mechanism as simple as an on/off control is sufficient to balance the system. These observations highlight the importance of feedback control mechanisms to bring a simple closed environmental system to balance, and (2) may help understand and raise questions about the effects of unattended unbalances in larger-scale environmental systems like the Earth, for which climate change increasingly becomes a concern. Furthermore, other questions and experiments [61] may contribute to better understand the reach and limitations of the so-called Gaia hypothesis, which states that biological processes alone and their interaction will compensate for environmental unbalances in Earth's biosphere [46].

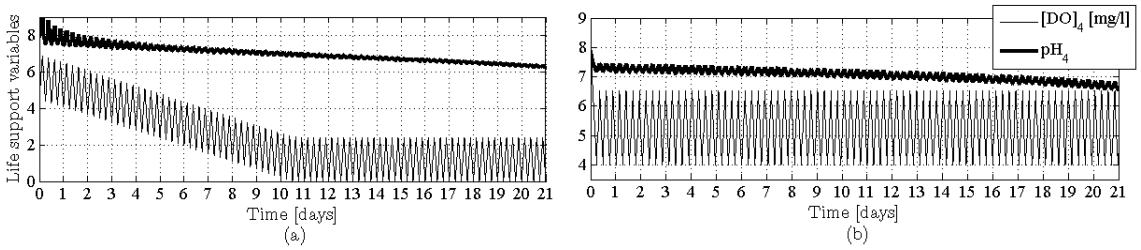

Figure 20: Response of an unbalanced system driven by (a) a fixed open-loop duty cycle, and (b) an on/off closed loop control.

3.6.3 Fail-safe/Fail-operational Mechanisms

Figure 21 presents the simulation of the failure and replacement of the recirculation water pump. The time responses presented in this case show two different approaches to handle the contingency. Figure 21 (a) allows the system to automatically regulate the oxygen concentration via photosynthesis and diffusion, and shows the dissolved oxygen concentrations for compartments 1 and 4. If the consumer species contained in the first compartment are not able to withstand concentration levels below 2 [mg/l], then this approach may not be the preferred one. Instead, a different "fail-safe" mechanism may be necessary, e.g. an aerator, which in Figure 21 (b) becomes more appropiate to guarantee acceptable levels of dissolved oxygen in the system. This result also shows that experiments with small-scale reconfigurable environmental systems may serve not only test control laws, but also to combine them with other automated safety mechanisms that may prove critical during contingencies.

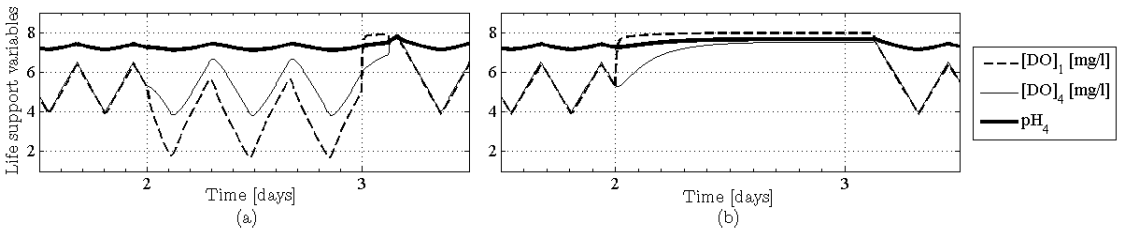

Figure 21: Result of two different "fail-safe" contingency policies upon a fault in the recirculation pump.

3.6.4 Performance of Biological Components

3.6.4.1 Consumer Model

Given the changes in rates of consumption of O_2 and production of CO_2 by the snails, Figure 22 compares the first two days of data. The intention is to have a measure of the variance of the steepness in DO, allowing the model to account for metabolic variations in the animal component of the system (consumers).

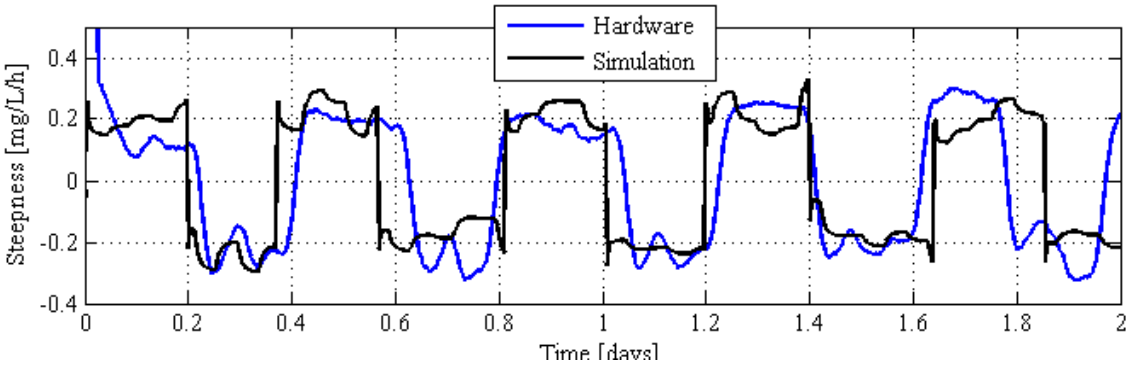

Figure 22: Validation of Blüm-type experiments.

The result of using a random variable with a first order filter seems to be a fair first approximation to the behavior and disturbances introduced by the consumers. These simulations have to be limited to two days, because the disturbances trigger the on/off control at different times and encourages loss of synchronism, and further distorts the ability to compare the signals. However, the intention of such comparison is to achieve an approximate value for the variance σ^2, $1/\tau$, and T which in this case have been set to 10 [mg/h], 5 [rad/h], and 1 [h], respectively. The meaning of these values is: the rate of consumption is 4 [mg/h], but may change randomly every $T = 1$ [h] with a dispersion $\sigma^2 = 10$ [mg/h] and a time constant $\tau = 0.2$ [h].

3.6.4.2 Botanical Model

Figure 23 presents the temporal response of the habitat, including DO, pH, and lamp power signals for $\phi = \{0.3, 0.6, 1.5\}$. The main observation in this case refers to the

similarity in DO and pH responses versus the different behaviors obtained for the lamp power signal.

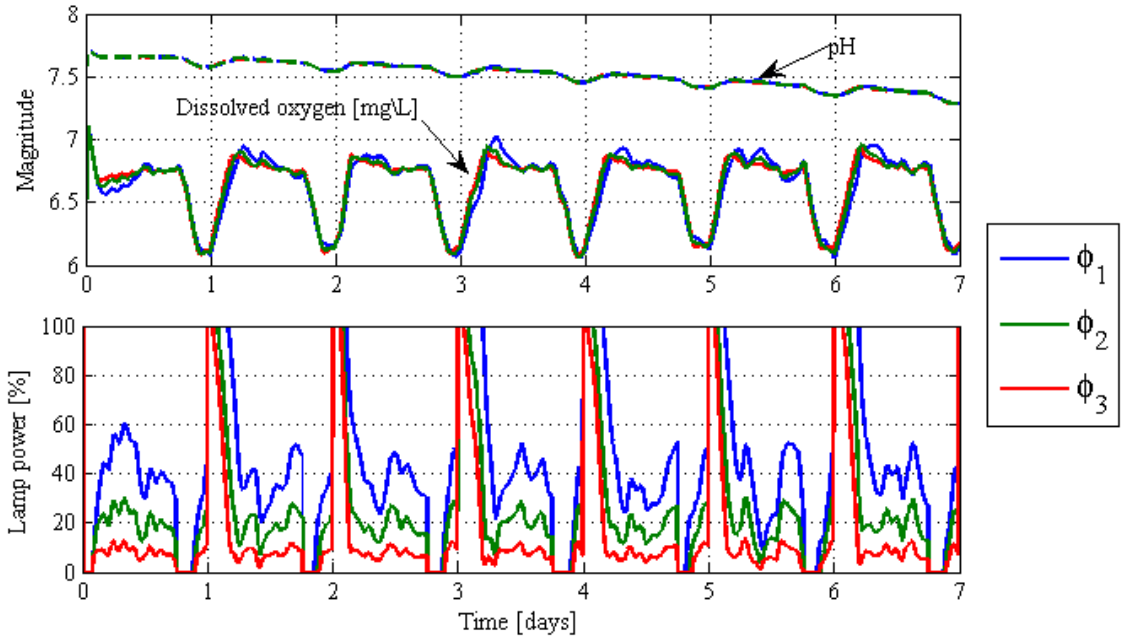

Figure 23: Comparison of three light-responses in simulations including animal component.

In contrast to the on/off control used in the second simulation, Figure 23 makes use of setpoint control and photoregulation, and studies three light-response curves and their effects on simulations. Even though these simulations make use of the disturbances proposed for the consumer model, very small differences are noticeable in the time response of life support variables, DO and pH. This is especially true in the temporal response of pH, for which the three signals overlap. Another observation is found in the time response of the lamp power: the robustness apparent in the temporal response of the life support signals for a PI controller is product of the changes that occur in the lamp power signal. These show periodic steady-state values between 10 and 40 [%], for different values of ϕ. This distribution is expected from Figure 15. The curve with smaller ϕ will require more lamp power to achieve similar values of CO_2 assimilation.

3.7 Summary

This chapter presented the modeling, design and simulation of a reconfigurable aquatic habitat intended for experiments in RLSS, control, and automation. It presented the model of an aquatic habitat for experiments relevant to closed-loop LSS and as an option for small-scale and ground-based BLSS research focusing on the process of respiration, and expanded the description of biological processes by introducing models of ecophysiological phenomena for consumers and producers. It elaborated on the modeling, design and simulation of a reconfigurable aquatic habitat intended for experiments in life support control research. The model focuses on the process of respiration and produces results comparable to those reported in ground-based and spaceflight experiments. The model is general enough to enable the design and simulation of other systems of the same nature. Results obtained and reported in this chapter highlight the importance of feedback control in combination with fail-operational/fail-safe mechanisms to balance and support life in closed environmental systems. This chapter supports the use of small-scale aquatic habitats to explore concepts that may be difficult to test in larger-scale systems. The model of the plants includes a description of the rate of CO_2 assimilation as a function of irradiance. The snails instead are modeled through their the rate of consumption, treated as a combination of a constant and a random variable to account for changes in metabolic rates and aestivation. Simulations and validation runs with hardware show how these phenomena may act as disturbances and introduce non-linearities. Other research opportunities with the aquatic habitat include enabling time-varying parameters in the botanical model to account for their growth, and to enable exploration of robust-adaptive approaches to regulate oxygen production.

CHAPTER IV

GRANULAR APPROACH TO BLSS AUTOMATION

Contribution 2: Regenerative life support systems (RLSS) offer various options to recycle metabolic byproducts, such as urine, and to achieve an incremental closure of gaseous and liquid material cycles. Such *material loop closure* increases the autonomy of space habitats and helps reduce the frequency of resupply missions and their overall cost. But as researchers continue their efforts to integrate regenerative technologies and to achieve system closure, new challenges arise from unintended interactions between chemical species in the closed-loop system. Material loop closure not only makes possible the interconnection of complex material networks, but may also promote unintended interactions between chemical species within the habitat. Such interactions may lead to the accumulation of unexpected chemical compounds that could affect individual life-support processes or crew health. Such uncertainty is to be expected, and its effects may be discovered as *anomalies* during operation [2]. An example of such phenomena is found in the 2010 WRS anomaly caused by the accumulation of dimethylsilanediol (DMSD) [11] presented in Subsection 2.2.2.

Beyond methods in robust [49] and adaptive control [50, 51], paradigms in switched control [52, 53, 54, 55] offer advantages for the management of the uncertainty caused by material loop closure. The contribution discussed in this chapter makes use of a perception-based approach to a switched control paradigm. Switched control introduces attributes of flexibility and modularity to the control system [55]. These attributes may be used to allow for different control actions depending on the *operational condition* of the physical system and its *situation* in a given context. In other words, these changes may depend on the internal state of the physical system and on

external factors defined by its environment and active goals.

The increasing availability of sensor information and measurements motivates the granular approach of this contribution. The combination of such sensor information creates a *sensing space* in which the operational conditions of the system may be found. This granular approach takes advantage of the opportunity to define perceptual elements or granules within the sensing space, in which each granule represents a specific situation. In particular, this work employs intelligent agents based on FAM made of granular structures composed of n-dimensional non-interactive fuzzy sets [143, 60, 82, 61]. Granular structures [58, 144, 145, 59] define the situations in which each control action governs the system, thus implementing a switched control paradigm to their automation. Situation-rich signals serve as the switching mechanism and provide observability of the operational condition and context of the system, or *situation observability*. This contribution is presented in Section 4.1.

The invention of methods to measure environmental variables by means of microsystems or optical devices tends to reduce the unit cost of novel sensor technology and opens opportunities for engineers to integrate evermore complex systems. Such innovations allow individual human operators to perform more complex tasks (as is the case with single pilots flying fleets of UAV's) and to assist humans to do their jobs (or even replace them) through automation. Towards this purpose, Subsection 4.1 presents the FAM-based agent architecture as a framework that enables a granular approach to automation and control. Such an approach is conceived as a switching control paradigm with attributes of flexibility and modularity. However, Subsection 4.3 poses the question of how to make this granular approach practical for systems composed of a greater number of sensors. The difficulty of manually defining fuzzy sets for each individual condition makes such techniques impractical. Therefore, the main contribution of our work proposes to exploit the interaction of human experts

with the system to collect situation-rich data useful to represent their situation knowledge base (SKB). The SKB is then used in the perception function of the FAM-based agents to generate the switching signals that combine control laws into an integrated control signal. Those switching signals contain information about the situation of the system and may also be used in user-interfaces for human-automation coordination. This general contribution is composed of four specific steps: (A) data collection, (B) aggregation algorithm, (C) coherence operation, and (D) implementation. The steps are represented in Figure 24 as blocks in the diagram and described in Subsection 4.2.1, with a numerical example in Subsection 4.2.2.

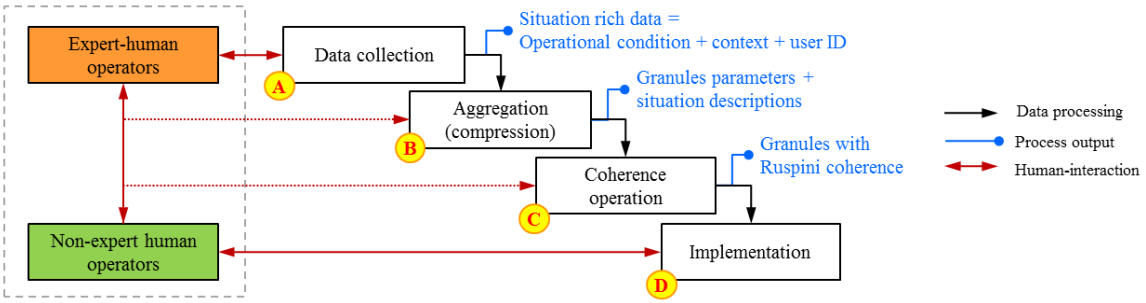

Figure 24: Granular multi-sensor fusion method.

4.1 Granular Approach to the Automation of the Habitat

This section introduces the use of agents based on fuzzy associative memories (FAM) [82, 60, 143] to develop granular structures composed of n-dimensional non-interactive fuzzy sets, used to define operation conditions and the control law that governs an action in each situation. The objectives are the following: (1) to implement a switched control strategy on the dynamic model of a reconfigurable aquatic habitat, introducing flexibility into the dynamics of the system; and (2) to explore how the granular structure of FAM-based agents may generate useful information to enhance situation observability and thus potentially provide human operators with resources for real-time decision making. Such exploration is oriented toward the development of methods in user-centered design that take into account situation awareness to inform

better ecological interfaces [57], [2]. Although results presented herein are based on simulations, hardware of the system described is used to identify model parameters.

4.1.1 The FAM-based Agent Architecture

The FAM-based agent architecture has found motivation in the monitoring and automation of LSS [135] and implements a switched control approach [54] that assigns a control action to each situation in which the system may operate in the form of (Situation, Controller). The switching capability introduces flexibility in the behavior of the system and enables its development in a modular and incremental fashion. The architecture is characterized by a perception function, a set of controllers, and a correspondence function. The latter associates a controller to each situation defined in the perception function and combines them into an integrated control signal. Figure 25 shows a diagram of a single FAM-based agent with a user interface manipulating a single variable in a small-scale aquatic habitat. The diagram describes the components of the FAM-based agent with the following blocks: (A) Perception, (B) Control Signals, and (C) Correspondence Function. Some advantages of this approach have been shown in previous work [135].

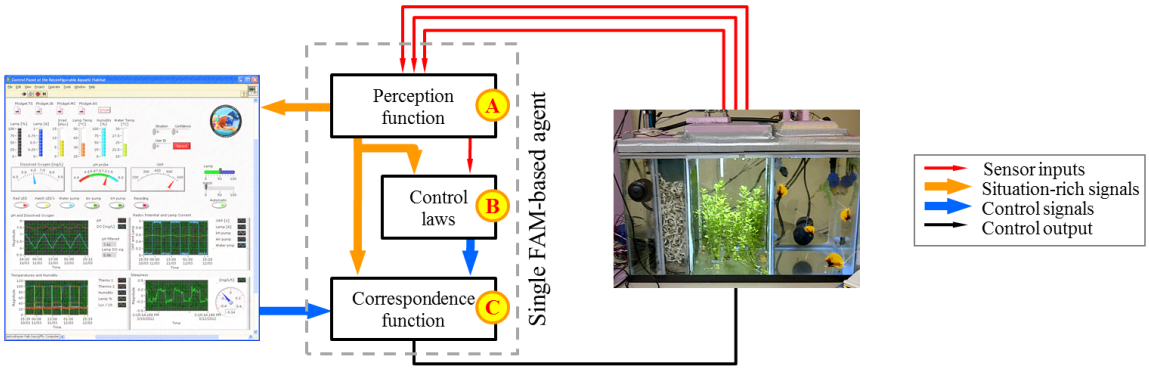

Figure 25: Diagram of the FAM-based agent and its components.

4.1.1.1 Perception Function and Granular Structure (A)

The perception function assumes the availability of n measurable variables x_i for $i = 1, 2, \ldots, n$ from sensors and their universes of discourse X_i so that $x_i \in X_i \subseteq \Re$; the variables are non-redundant and non-interactive: $X_i \neq X_j$; $j = 1, 2, \ldots, n$; $i \neq j$. Each universe X_i is partitioned in k_i subsets, each of which is denoted as $X_i^\alpha \subset X_i$, $\alpha = 1, 2, \ldots, k_i$. Continuous membership functions describe each one of the subsets as $\mu_{X_i^\alpha}(x_i)$, which are normal and convex [146]. Such partitions are *coherent* when complying with the Ruspini condition [147]:

$$\sum_{\alpha=1}^{k_i} \mu_{X_i^\alpha}(x_i) = 1 \quad \forall i = 1, 2, \ldots, n \tag{12}$$

This condition becomes of importance in automation systems because of its capacity to ensure that there will not be regions in X for which a control policy is not assigned or with conflicts between controllers. As a result, a number of l possible situations or operating conditions are defined as non-interactive fuzzy sets $\tilde{A}_j$, for $j = 1, 2, \ldots, l$. The l situations are the Cartesian product of the combination of the subsets X_i^α in X_i. The Cartesian product is implemented with the *minimum* operator as in Equation 13, for $l = \prod_{i=1}^{n} = k_i = k_1 \cdot k_2 \cdot \cdots \cdot k_n$.

$$\tilde{A}_j\left(x_1, \ldots, x_n\right) = \min_{\substack{i=1,\ldots,n \\ \alpha=1,2,\ldots,k_i}} \left(\mu_{X_i^\alpha}\left(x_i\right)\right) \tag{13}$$

The set $\tilde{A} = \{\tilde{A}_j\}$ represents the granular structure in which each granule $\tilde{A}_j$ describes a different situation and a percept of the FAM-based agent.

4.1.1.2 Control Signals (B)

In the same fashion, the set of control signals $U = \{u_j\}$ are obtained from up to l different control laws. Controllers generate signals u_j that correspond to each condition $\tilde{A}_j$. These signals may be treated modularly to form the set $U = \{u_1, u_2, \ldots, u_l\}$,

with the maximum number of different control signals limited by l. The control signals can be generated by model-based methods or techniques in soft-computing and computational intelligence. The error modulation solution [82] or a similar technique is required for controllers with integral control action (poles in zero). Considerations on switched control [54, 55] should be included in this component of the FAM-based agent and in the correspondence function Ω described in the next subsection.

4.1.1.3 Correspondence Function and Integrated Control Signal (C)

With the sets $\tilde{A}$ and U defined, the correspondence function Ω can be expressed as a rule-base or in pairs (Situation, Control Signal) as in Equation 14.

$$\begin{aligned} &\Omega : \tilde{A} \rightarrow U \\ &\Omega = \{\Omega_j\} = \left\{ \left(\tilde{A}_j \left(x_1, \ldots, x_n \right), u_j(t) \right) \right\} \end{aligned} \tag{14}$$

The resulting FAM is defuzzified with the weighted average technique to obtain an integrated control signal u_I. This signal drives a single actuator in the system. Thus, each actuator and its controller in a physical system may be conceived as an agent, constituting a FAM-based multi-agent system. The weights used in Equation 15 are the membership values of each corresponding situation, and the weighted arguments are their corresponding control signals.

$$u_I \left(x_1, \ldots, x_n, t \right) = \frac{\sum_{i=1}^{l} \mu_{\tilde{A}_i} \left(x_1, \ldots, x_n \right) \cdot u_i(t)}{\sum_{i=1}^{l} \mu_{\tilde{A}_i} \left(x_1, \ldots, x_n \right)} \tag{15}$$

4.1.2 Application to the Model of the Habitat

This subsection presents the application of the FAM-based agent architecture to the control of the DO levels in the model of the aquatic habitat presented in Chapter 3 and which regenerative cycles and variables are shown in Figure 26. It defines (1) the

operating range of the life support variables considered; (2) the operational conditions that result from the combination of the operating ranges, and their corresponding control actions; and (3) the simulation performed on the habitat for this subsection.

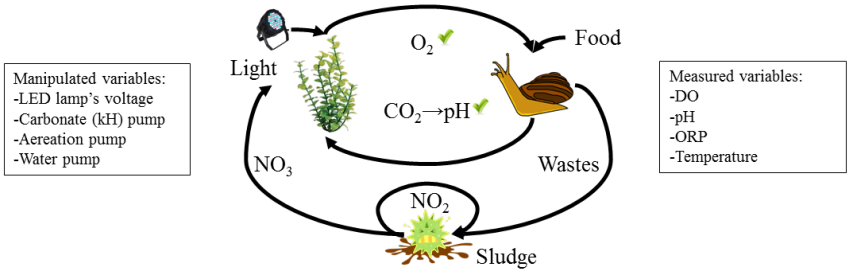

Figure 26: Regenerative cycle of the aquatic habitat

4.1.2.1 Life Support Signals and their Operating Ranges

The life support variables are the DO and pH in the fourth compartment. Their operating ranges and fuzzy membership functions are shown in Figure 27.

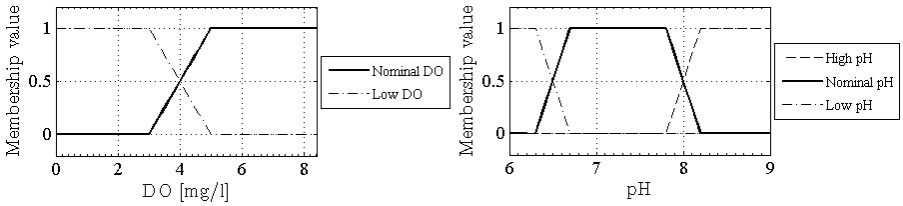

Figure 27: Fuzzy partitions of the DO and pH variables.

These ranges are defined considering the minimum DO concentration allowed for fresh water animals (2 [mg/l]), and the pH values in which most aquatic organisms may live with low stress [139]. There are two conditions for the DO concentrations: nominal and low. The pH has three ranges: nominal, high and low.

4.1.2.2 Control Laws and their Operating Conditions

Two control actions are used to drive the power level of the LED-lamp: (1) power on and constant at 100% and (2) a proportional-integral (PI) controller that may dim the lamp in the 0-100% range. The PI controller is used in most of the operating

conditions, with $P = 200$ and $I = 50$. The differences of the PI controllers for each operating condition is in the controlled variable and its reference. A representation of the operating conditions and the control actions for each case is shown in Table 6.

Table 6: Control actions for different operating conditions.

	Low pH	Nominal pH	High pH
Nominal DO	$pH_{ref} = 6.3$	Nominal	$pH_{ref} = 8.0$
Low DO	Lamp on	$DO_{ref} = 3$	DO_{min}

These operating conditions result from the combination of the operating ranges of each variable, according to Subsection 4.1.1.1. To ensure that the system works correctly, note that the PI controller uses the error modulation technique presented in [82]. The nominal and DO_{min} controllers make use of a reference signal with a duty cycle of 18 hours for every 24. This duty cycle helps to account for the physiological requirements of the botanical elements. For the nominal condition, the reference alternates between 6.0 [mg/l] and 5.0 [mg/l], while for the DO_{min} the reference switches between 4.5 [mg/l] and 4.0 [mg/l].

4.1.2.3 Simulation Performed on the Habitat Model

The simulation presented in this subsection explores the transitions between operational conditions triggered by the depletion of kH and the lack of supply from the dosifier pump in the second compartment. This substance is consumed by the bacteria of the biofilter during the process of nitrification. The source of kH is inhibited until day 14; on day 14 the kH source is restored. The purpose of this simulation is to explore the operating condition transitions of the FAM-based agent and the time response of the life support variables considered. In addition, the simulation also shows the evolution of the membership values of the life support variables in each of the operating conditions, making the system observable from this perspective at

any given time. The simulations are implemented with a stiff Mod. Rosenbrock numeric method with maximum step of 0.01. Initial conditions are $[DO] = 8.4$ [mg/l], [CD]=0.69 [mg/l], and [kH]=20 [mg/l]. The simulation time is 21 days and its initial conditions are in equilibrium with the equivalent concentration of the atmosphere at 22 °C at sea level.

4.1.3 Results from the Granular Approach

The depletion of the kH in the system deteriorates the pH below nominal values, triggering a operating condition transition as shown during day 12 in Figures 28, 29 and 30. Between days 12 and 15 the system continues to transition into different situations and recovers its nominal condition thereafter, when the kH supply is re-enabled. These results show the dynamics of the transitions from three perspectives: (1) the evolution of life support variables, DO and pH, is shown in Figure 28; (2) the behavior of the LED-lamp is presented in Figure 29; and (3) the membership value of the operational condition of the system over time is shown in Figure 30. The system remains "fail-op/fail-safe" within the conditions defined in Table 6. From day 5 to about day 11, the system shows consistent and mostly periodic temporal responses as evidenced in Figures 28 and 29.

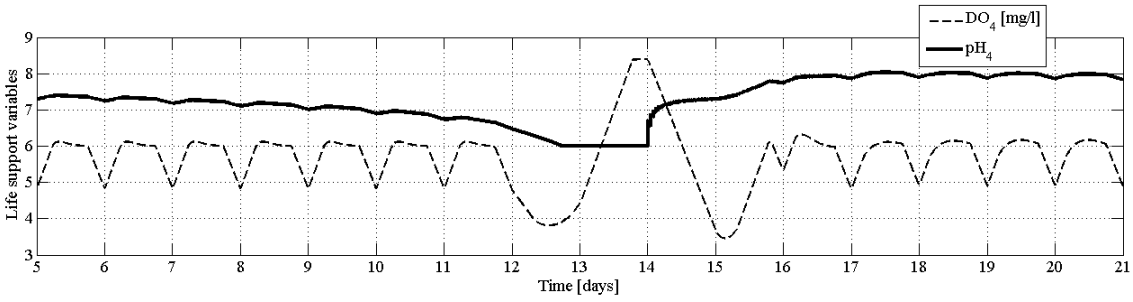

Figure 28: Evolution of the life support variables during the simulation

During this period of time and, without looking at Figure 30, it can be said that the system remains within a single operating condition, in this case in the "nominal" condition, and seems to be performing well. However, once the first transition enters

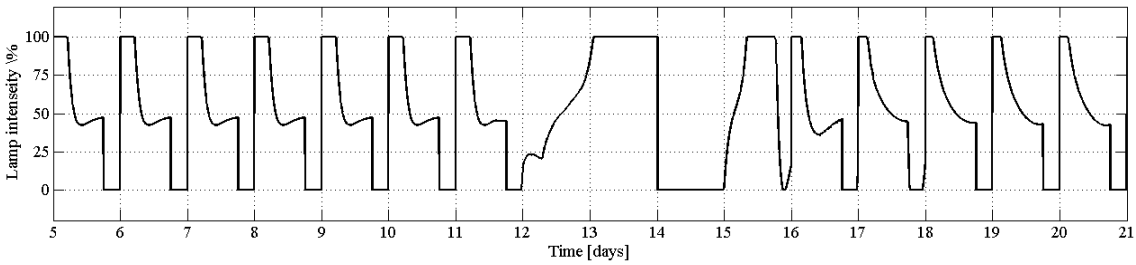

Figure 29: Lamp intensity for the simulation

into effect at around day 12, it becomes harder to assess in which situation the system is in until it goes back into "nominal" on day 15. The lack of *situation observability* evident for only two or three signals in this case, is more so true for large-scale socio technical systems composed of many more sensors and signals. Hence, having a granular structure that allows the system to identify its mode of operation becomes helpful not only to allow for automation strategies that adapt the system to various situations, but also to generate new signals that better describe their evolution. This is what Figure 30 presents in the signals (a) through (f); it shows the history of the situation of the system. In these figures, membership values are shown for the conditions defined in Table 6 as follows: (a) Nominal-DO/High-pH; (b) all nominal; (c) nominal-DO/low-pH; (d) low-DO/high-pH; (e) low-DO/nominal-pH; (f) low-DO/low-pH.

These signals allow us to understand not only the situation in a real-time scenario, but also to perform forensic analysis on Figures 28 and 29. For example, between days 12 and a slightly after day 15, the system transits between three different operating conditions before going back to "nominal." These conditions are (not in chronological order): nominal-DO/low-pH, low-DO/nominal-pH, and low-DO/low-pH. The last of these conditions to enter into effect before the system is dominantly back at "nomimal" is low-DO/nominal-pH. Under this condition and according to Table 6, the system sets the dissolved oxygen reference value to 3 [mg/l]. Thus, it can be seen in Figure 28 that the oxygen goes from being in saturation at 8.4 [mg/l] down to

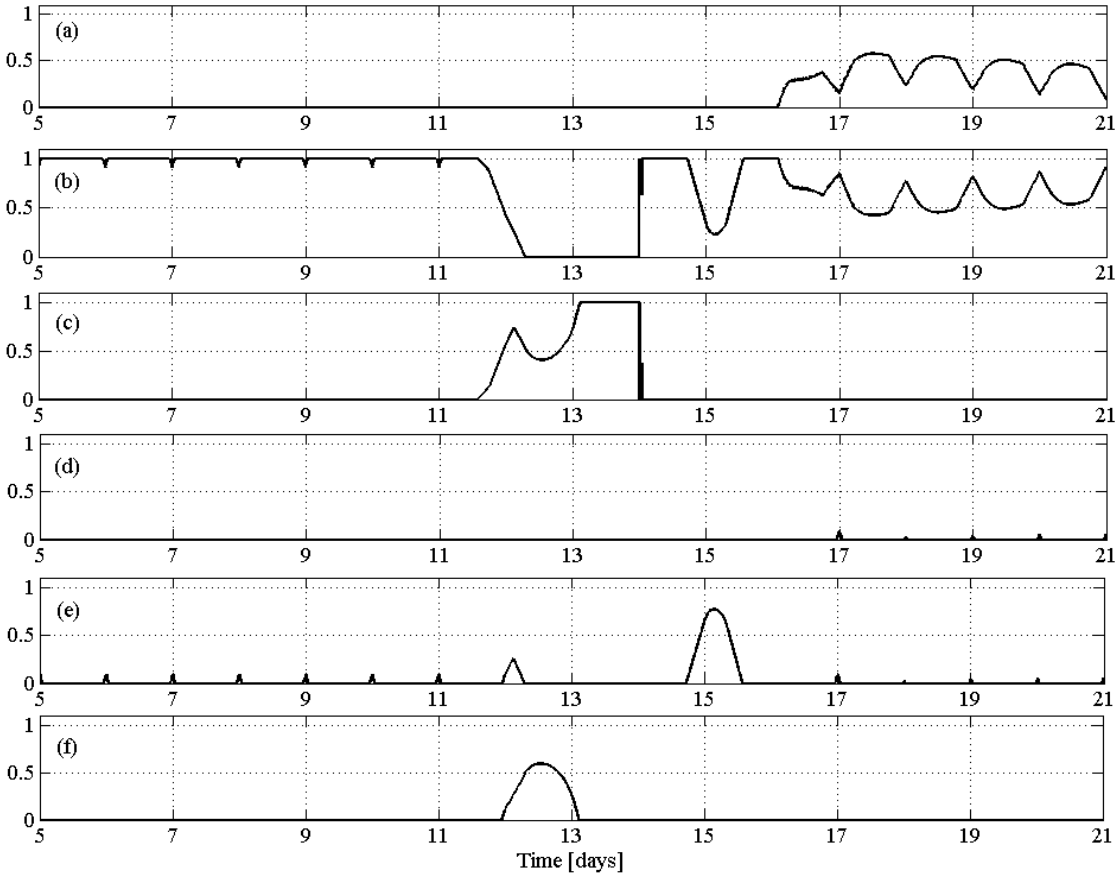

Figure 30: Membership values of the conditions defined in Table 6.

about 3.5 [mg/l], just before the last transition back to "nominal" comes into effect. Note also, that in order to bring down the oxygen level from 8.4 [mg/l] to about 3.5 [mg/l], the LED-lamp has to be at 0% (turned off) in Figure 29 to prevent the plants from generating oxygen and allowing other organisms to consume it. After this transition the system alternates between "nominal" and Nominal-DO/High-pH, which then again, according to Table 6, alternates the controlled variable between the pH level at 8.0 and the dissolved oxygen concentration following the LED-lamp duty cycle. The forensic analysis of Figures 28 and 29 described above is possible to most observers because of the information provided by Figure 30. Such information could be displayed in ecological interfaces to support human operators in real-time

decision making tasks. The signals generated by the FAM could also be used to assess the evolution of systems in the future, looking at further applications in diagnosis and prognosis of engineering systems. Beyond RLSS, the granular decomposition of sensing spaces presented in this method is applicable to a wider range of complex socio-technical systems. Questions then arise on how to manage high-dimensional sensing spaces and what type of methods are required to make this approach practical. We suggest the use of other methods in computational intelligence in combination with FAM to arrive at solutions applicable to larger-scale systems.

4.2 Situation-oriented Integration of Human-automation Systems

This section proposes a multi-sensor fusion method that elaborates on a granular approach to the operation and automation of RLSS [135]. The approach employs an agent architecture based on FAM in an effort to allow for *situation observability*, *i.e.* the capability of non-expert human operators to probe for information about the situation of the system. Such attribute may also provide users with operational margin [11] to detect and respond to anomalies in a timely manner. However, the abundance of sensor information may result in a combinatorial explosion unsuited for the manual design of monitoring and automation systems. The core of this method consists of taking advantage of the interaction of human-experts with the RLSS to generate and collect data useful for the development of the FAM that constitutes the perception function of the agents. In particular, the method proposed in this section makes use of particle swarm optimization [148] (PSO) to *compress* sensor data and a set of human-expert situation assessments into a granular representation of their SKB. Such representation enables the transformation of sensor data into situation-rich signals useful for monitoring and automation purposes.

4.2.1 Granular Multi-Sensor Data Fusion Method

An advantage of the FAM-based agent architecture is the possibility of combining a large number of sensors, to gather information beyond the internal state of systems and towards enabling it to have a better assessment of its situation. A disadvantage of this approach is the combinatorial explosion that makes it impractical to manually define membership functions $\mu_{X_i^\alpha}(x_i)$ for situations α detected by each sensor $i = 1, 2, \ldots, n$. Therefore, this subsection proposes the use of human-system interaction and the application of methods in computational intelligence to overcome this challenge. The method shown in Figure 24 collects situation assessments from expert human operators, i.e. system snapshots, to obtain situation-rich data sets that may be useful to generate a representation of the SKB of experts. Datasets containing a number of N snapshots are aggregated (compressed) into a parametric representation. The aggregation consists of a particle swarm optimization process that adapts π-membership functions to the data contained in the data set for each sensor and each situation. The result is a granular structure useful for decision support tools and, when coherent, susceptible for adoption as the perception function of the FAM-based agent architecture. The following subsections describe each one of these steps.

4.2.1.1 Data Collection

Data collection consists of taking advantage of the interaction between expert human operators and the system to obtain situation rich data sets. These data sets include measurements of the *operating condition* of the system (internal state), its *context* (external state), and an *identifier* of the expert. Datasets contain N snapshots of the system at times t_j for $j = 1, 2, \ldots, N$ as shown in Figure 31.

Measurements of the system state, both internal and external, include values x_{ij} recorded by sensors x_i for $i = 1, 2, \ldots, n$. If sensors are not available, values may be

	Measurements					Expert Input		
	Time	x_1	x_2	$\cdots$	x_n	Situation	Confidence	User Code
Dataset	t_1	x_{11}	x_{21}	$\cdots$	x_{n1}	s_1	c_1	h_1
	t_2	x_{12}	x_{22}	$\cdots$	x_{n2}	s_2	c_2	h_2
	$\vdots$	$\vdots$	$\vdots$		$\vdots$	$\vdots$	$\vdots$	$\vdots$
	t_N	x_{1N}	x_{2N}	$\cdots$	x_{nN}	s_G	c_N	h_N

Figure 31: Data set description for the data collection process

systematically obtained and introduced by the expert through a user interface, depending on the nature of the measurement. In addition to measurements, the data set includes *expert input* that defines to which situation s_γ the snapshots belong in each case, for $\gamma = 1, 2, ..., G$, and with what degree of confidence $c_j \in [0, 1]$. If $c_j = 1$, the expert is fully confident that the system snapshot taken at t_j belongs to situation s_γ. The number $G \geq l$ depends on the presence of hierarchical structures in the situation assessments according to the notion of *levels of resolution* in granular computing [59]; *i.e.* a situation assessed as "nominal" may be subdivided in more specific situations, such as "nominal-high" and "nominal-low." This subsection does not address hierarchical granular structures, making $G = l$. Finally, the user code h_j allows the data collection process to identify the expert that contributed to each snapshot of the data set, enabling approaches in crowdsourcing [111, 112]. The intention of the following steps is to compress the data set into a more compact and meaningful representation.

4.2.1.2 Aggregation or Data Compression

The aggregation algorithm transforms (compresses) situation-rich data sets into granular structures described by an array of parameters that define membership functions $\mu_{X_i^\alpha}$ for each situation γ susceptible to detection by sensors i. How situation knowledge is represented, how it is obtained from data sets, and a suggested approach to achieve coherence of the fuzzy sets are described in the following paragraphs.

Knowledge Representation: Given the need to allow for flexible adaptation of a membership function $\mu_{X_i^\alpha}$ to collections of snapshots found in the data sets, the aggregation algorithm makes use of a piece-wise differentiable function defined by four parameters and known as a π-membership function, as defined in Equation 16:

$$\mu_{X_i^\alpha}(x_i; a, b, c, d) = \begin{cases} 0 & x_i \leq a \\ 2\left(\frac{x_i - a}{b-a}\right)^2 & a < x_i \leq \frac{a+b}{2} \\ 1 - 2\left(\frac{x_i - b}{b-a}\right)^2 & \frac{a+b}{2} < x_i \leq b \\ 1 & b < x_i \leq c \\ 1 - 2\left(\frac{x_i - c}{d-c}\right)^2 & c < x_i \leq \frac{c+d}{2} \\ 2\left(\frac{x_i - d}{d-c}\right)^2 & \frac{c+d}{2} < x_i \leq d \\ 0 & x_i \geq d \end{cases} . \tag{16}$$

The π-membership function results in the curve shown in Figure 32, with parameters $P = [a, b, c, d]$ defining the "feet" and "shoulders" of the curve. Each membership function in the aggregation process represents a single situation $\gamma = 1, ..., G$ for a single sensor x_i. The PSO process obtains the four parameters in each case, as described next.

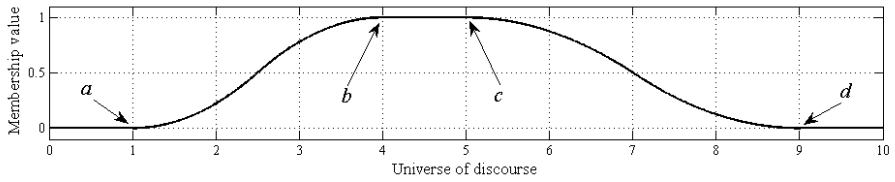

Figure 32: π-Membership function for $P = [a, b, c, d] = [1, 4, 5, 9]$.

Particle Swarm Optimization: PSO [148] is the process that transforms data sets into a granular structure. For each situation γ and sensor i, find $P^* \in X_i$ such that the condition in Equation 17 is found, where $f(x_i) = \sum \left(\mu_{X_i^\alpha}(x_{ij}) - c_j\right)^2$ for $j = 1, 2, \ldots, N$ and in each case subject to the initial constraints shown in Table 7.

$$P^* = \arg\min_{x_i \in X_i} f(x_i) = \{x_i^* \in X_i : f(x_i^*) \leq f(x_i) \forall x_i \in X_i\} \tag{17}$$

Table 7: Initial constraints of the particle swarm optimization.

	Constraints
1:	$a \leq b \leq c \leq d$
2:	$\min x_{ij} - 0.25 \left\lvert \max x_{ij} - \min x_{ij} \right\rvert \leq a \leq \min x_{ij}$
3:	$\min x_{ij} \leq b \leq \max x_{ij}$; $\min x_{ij} \leq c \leq \max x_{ij}$
4:	$\max x_{ij} \leq d \leq \max x_{ij} + 0.25 \left\lvert \max x_{ij} - \min x_{ij} \right\rvert$

The swarm is subject to random variables $\zeta_1 \in [0, 1]$ and $\zeta_2 = 1 - \zeta_1$, to parameters $W = 0.99$, $\varphi = 0.02$, and follows the steps enumerated in Table 8 with p representing an agent (particle) in the population.

Table 8: Particle swarm optimization algorithm

Step	Description
1.	Randomly distribute particle swarm (or swarm of agents) in the search space.
2.	Evaluate the performance of each particle according to $f(x_i)$.
3.	If the current position is better than previous ones, then update with the best.
4.	Determine the best particle so far according to their previous and present positions.
5.	Update velocities with $v_p^{t+1} = W \cdot v_p^t + \varphi \left[\zeta_1 \left(x_{lp}^t - x_p^t\right) + \zeta_2 \left(x_g^t - x_p^t\right)\right] \leq \frac{\left\lvert \max x_{ij} - \min x_{ij} \right\rvert}{100}$.
6.	Update positions of particles according to $x_p^{t+1} = x_p^t + v_p^{t+1}$.
7.	Repeat from (2) until $f(x_i^*) < \frac{\left\lvert \max x_{ij} - \min x_{ij} \right\rvert}{500}$ or iterations = 2000.

The process results in a granular structure described by an array of dimensions $G \times n \times 4$ as shown in Figure 33. Although the PSO may converge to a "best" result, the irregularities introduced by the data collection step make it necessary to employ a coherence operation to obtain granular structures that comply with the Ruspini condition in Equation 12. The advantage of using PSO is the flexibility it provides to vary the computation power invested in the aggregation process.

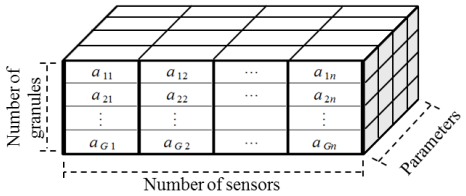

Figure 33: Three dimensional array containing granular structure

4.2.1.3 Coherence Operation

The coherence operation adjusts parameters $P = [a, b, c, d]$ of each fuzzy set $\mu_{X_i^\alpha}$ by determining their similarity or adjacency, and performing operations on these parameters in each case. It performs searches of fuzzy sets that are similar or adjacent, making use of its descriptive parameters. The coherence operation separates the search for similar or adjacent conditions by employing two sub-operations: the *similarity operation* and the *adjacency operation*. Each sub-operation separately performs searches in the granular structure (shown in Figure 33) described by parameters $P = [a, b, c, d]$ for each sensor and situation. The following paragraphs describe the sub-operations.

4.2.1.4 Similarity Operation

The similarity operation searches for fuzzy sets in each sensor for all situations. The search identifies those sets that comply with specific similarity conditions based on the parameters illustrated in Figure 34.

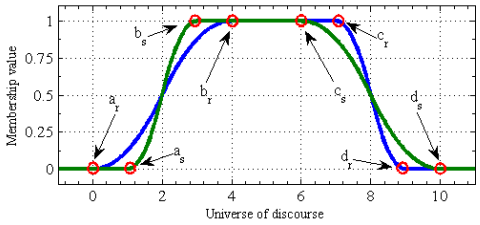

Figure 34: Plot of two similar fuzzy sets.

Two sets of parameters are defined in Figure 34: $P_r = [a_r, b_r, c_r, d_r]$ and $P_s = [a_s, b_s, c_s, d_s]$. During the search, P_r serves as the set of parameters that describes the

current *reference* fuzzy set of a given situation for a particular sensor. Each fuzzy set is used as the reference set during the search of similar fuzzy sets in each sensor. The fuzzy sets described by P_s are those to which P_r is compared. The algorithm explores the entire partition for each sensor comparing the reference parameters P_r to all other parameters P_s being searched. Similar sets are identified when:

$$a_r < \langle P_s \rangle < d_r \tag{18}$$

with $\langle P_s \rangle$ being the average of parameters a_s, b_s, c_s, and d_s. Once similar fuzzy sets $P_{r,s}$ have been identified, their value is updated to $P'_{r,s} = \left[a'_{r,s}, b'_{r,s}, c'_{r,s}, d'_{r,s}\right]$ as in Equation 19.

$$P'_{r,s} = \left[\min\left(a_{r,s}\right), \langle b_{r,s} \rangle, \langle c_{r,s} \rangle, \max\left(d_{r,s}\right)\right] \tag{19}$$

4.2.1.5 Adjacency Operation

The adjacency operation, in analogy to the similarity operation, searches for fuzzy sets in the partition of each sensor. In this case, however, the search will focus on the fuzzy sets adjacent to the reference fuzzy set defined by parameters $P_r = [a_r, b_r, c_r, d_r]$, shown as the central fuzzy set (in blue) in Figure 35.

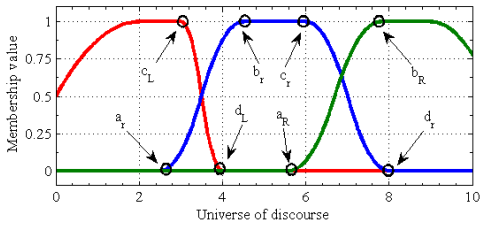

Figure 35: Plot of three adjacent fuzzy sets.

Two other fuzzy sets are shown in Figure 35 to the right (in green) and to the left (in red), with parameters $P_R = [a_R, b_R, c_R, d_R]$ and $P_L = [a_L, b_L, c_L, d_L]$, respectively. The adjacency operation makes use of these parameters to search for fuzzy sets in each sensor that are adjacent to a reference fuzzy set in all situations. As with the similarity operation, here again each fuzzy set in the partition serves as the reference

in one opportunity. However, in this case the condition used to identify adjacent fuzzy sets to the right and to the left are expressed as inequalities in Equations 20 and 21, respectively.

$$b_r < a_R < d_r \tag{20}$$

$$a_r < d_L < c_r \tag{21}$$

Once adjacent fuzzy sets have been identified, the parameters of the central fuzzy set are updated to $P'_{RL} = [a_{RL}, b_{RL}, c_{RL}, d_{RL}]$ as in Equation 22.

$$P'_{RL} = [\langle a_r, c_L \rangle, \langle b_r, d_L \rangle, \langle c_r, a_R \rangle, \langle d_r, b_R \rangle] \tag{22}$$

The terms $\langle a_r, c_L \rangle$, $\langle b_r, d_L \rangle$, $\langle c_r, a_R \rangle$, and $\langle d_r, b_R \rangle$ are the average of a parameter in P_r and the corresponding parameters of all adjacent fuzzy sets found to the right or to the left. Such correspondence is illustrated in Figure 35. The purpose of the adjacency operation is to obtain fuzzy partitions that comply with the Ruspini condition in Equation 12.

4.2.2 Numerical Example on the Aquatic Habitat Model

The model of the aquatic habitat presented in Chapter 3 was used to perform simulations of anomalies that exhibit transitions between various operation conditions. The purpose was to operate under all possible situations so that data could be collected. This example makes use of two sensors: dissolved oxygen(DO) and pH. Possible levels of pH are high, good, or low levels, while DO levels are good or low, resulting in six possible situations. Expert human operators were modeled as a prototype granular structure to collect data for confidence values greater than 0.1. They read a different situation every 5 minutes throughout 21 days, allowing for each situation to be monitored every 30 minutes. The data obtained is processed with steps (A), (B), and (C) of Section 4.2.1.

4.2.2.1 Results and Discussion

Figure 36 shows four 3-D graphs comparing results obtained from the sensor fusion algorithm with the prototype granular structure. Each situation is defined by a different color. Figure 36(A) provides a spatial distribution of the confidence values c_j. The number of data points collected in each situation is not uniform. The algorithm obtains granules independently of the number of data points. Figure 36(B) shows the resulting granules. The output of step (B) is processed with a coherence operation based on similarity and proximity, resulting in Figure 36(C).

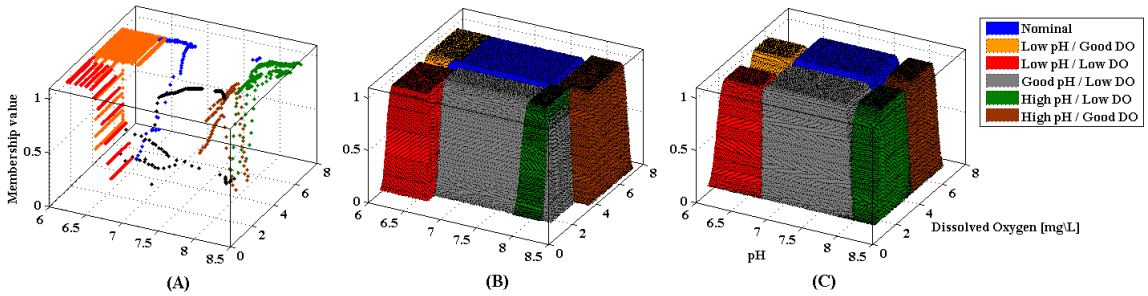

Figure 36: Steps (A), (B), (C), and prototype granular structure.

The lack of uniformity in the distribution of data points collected by expert human operators poses a challenge to the application of tools in computational intelligence for the development of decision aids and automation systems. Special attention should be given to how experts collect data and on the number of data points needed to guarantee coherence of granular structures. With better data sets, the particle swarm optimization should arrive at solutions without excessive overlaps or holes, as those shown in Figure 36(B). However, the result also exhibits regularity in the distribution of the granules, even if some situations register a few number of data inputs. This regularity can be observed when comparing Figure 36(B) to the prototype granular structure used to model the SKB of expert human operators. Another question related to quality of data sets is how parameters of the particle swarm may compensate for the lack of human inputs. One advantage of making use of PSO is the

flexibility it provides to increase computing power to arrive at solutions to the optimization problem. This supports and suggests the need for research that may help to characterize the performance of the particle swarm aggregation algorithm working under different search parameters, particle population sizes, and sizes of data sets. A final observation can be made on the borders of the output granular structures as compared to the prototype. Because the granules obtained are product of the data sets used, they are not able to define situations beyond those values. In other words, those areas not covered by the granules represent *unknown* situations. This implies that under such conditions a non-expert human operator should request assistance from experts, either to record new assessments in the data sets or to evaluate the need for intervention.

4.2.2.2 Remarks from the Numerical Example

This subsection presented a numerical example of the granular multi-sensor data fusion method. It collected assessments from expert human operators to generate a granular structure suitable for decision support tools and automation systems. The methodology presented offers an approach to overcome the combinatorial explosion of merging information from a large number of sensors. It makes use of human-system interaction to generate data sets that are processed with tools in computational intelligence. Expert assessments define the operational condition of the system with a subjective assessment of its situation. An algorithm based on particle swarm optimization obtains a representation of the SKB of human experts.

4.3 Summary

This chapter introduced a granular approach to the automation of the habitat that enhances situation observability [135]. It presented the FAM-based agent architecture as a granular approach to automate systems in engineering. The FAM acts as

the perception function of the agent, decomposing sensing spaces into granular structures. Each granule represents a different operating condition, to which a different control action may be associated. The information generated by the granules may be used to enhance situation observability and forensic analysis of dynamic systems. Further research is needed to understand how such information may help to design ecological interfaces. Beyond these, other questions remain about how methods in computational intelligence will help to make this approach practical for larger-scale systems. Applications of such solutions could be useful for the integration of larger-scale sensor networks to support situation awareness in mission control centers and systems involving humans and automation.

Advantages and Limitations The granular approach to the automation of RLSS has the advantage of introducing flexibility in automation design in a way that allows for coordination with tasks performed by human operators. The main limitations of this approach is found in its dependence on data sets containing situation assessments collected by human experts with the objective of obtaining a representation of their knowledge useful to operate the system and in providing appropriate training to non-expert operators.

CHAPTER V

AGGREGATION ALGORITHM CHARACTERIZATION

The perception function denoted with A in Figure 25 and described in Section 4.1.1.1 serves to represent the SKB of experts who have previously contributed to the Aggregation Algorithm process described in Section 4.2.1.2 by providing situation assessments of a system. The time of human experts can be expensive. In this Chapter, we employ a methodology that makes use of human assessments to obtain the array of parameters that describes the granular structure of the perception function. As explained previously, such representation of the SKB can be used in user interfaces and automation systems.

Given the potential cost of employing a group of experts to obtain a sufficiently large data set to ensure the proper performance of the Aggregation Algorithm, the question arises of what would be the minimum number of data points required. Considering the non-interactiveness of the perception function as described in Section 4.1.1.1 that employs the minimum operator (Equation 13), this chapter discusses a characterization based on simulated situation assessments for a single sensor. These results are later validated in Section 6 with an experiment incorporating situation assessments from human participants and their interaction with the simulation of a dynamic system through a user interface.

This chapter is organized in five parts: Section 5.1 introduces the experimental design for the characterization of the Aggregation Algorithm; Section 5.2 elaborates in detail on how the data set containing simulated situation assessments is generated; Section 5.3 delivers the experimental procedure used to obtain the results; and

Section 5.4 presents the characterization results and observations. The end of the subsection summarizes the chapter and prepares the reader for the validation presented in Chapter 6.

5.1 Experimental Design

The question arose as to the minimum number of data points needed in a data set to ensure the best performance of the Aggregation Algorithm. From observations made on previous results, in which the Aggregation Algorithm failed to obtain a granular structure compliant with the Ruspini attribute of Equation 12, the Algorithm seemed to perform increasingly better with larger number of data points.

This experimental design is supported by the non-interactiveness of the perception function explained in Subsection 4.1.1.1. This means that making use of only one sensor can lead to a measure of the minimum number of data points needed if a uniform coverage of the sensing domain is assumed. Therefore, the experimental design makes use of data sets of different sizes based on a data-set generator that distributes situation assessments uniformly along a continuous domain. By truncating the data sets obtained, the characterization procedure is expected to deliver results similar to those of Figure 37.

This figure describes a trend (light blue line) by which the mean proportion of Ruspini partitions increases with greater data-set sizes. A low value means that for a number of repetitions, the majority of the results do not comply with the Ruspini condition (Equation 12). Conversely, a high value means that the majority of repetitions result in partitions compliant with the Ruspini condition. However, the blue line is only a trend. In Figure 37, the green circles correspond in each case to the mean value of the number of Ruspini results obtained for a given number of repetitions; in other words, they represent the average proportion of Ruspini results for a given number of repetitions and for a specific data-set size. The dotted line

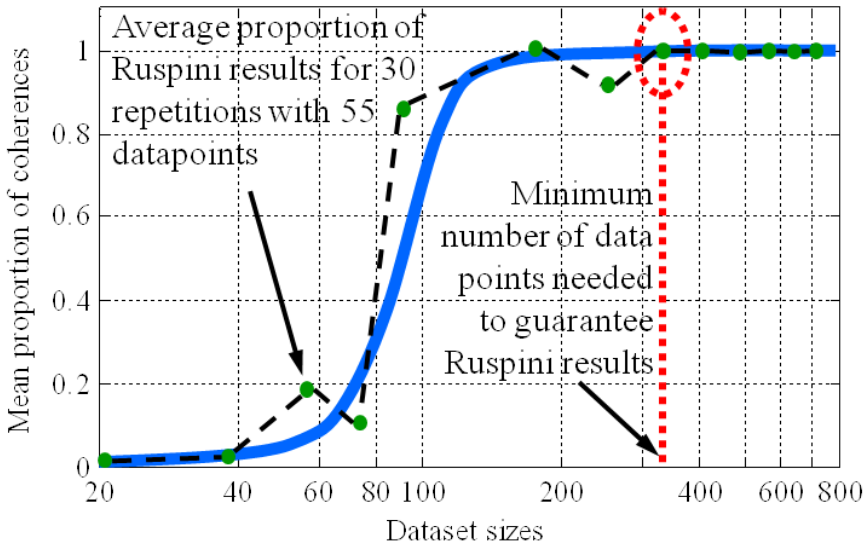

Figure 37: Characterization approach

connects the results for increasing data set sizes. The purpose of this experiment is to find the data set with the fewest number of data points for which the mean proportion of Ruspini results is 1. The independent variables explored are:

- Number of granules: $G = \{2, 3, 4, 5\}$.
- Transition intervals: $TI = \{1, 2, 4\}$.
- Dataset sizes: $\{20, 30, 40, \ldots, 100, 200, \ldots, 800\}$.
- Particle swarm sizes: $N = \{20, 50, 100\}$.

The dependent variables are:

- Number of iterations.
- Proportion (or percentage) or Ruspini results.

The frequency of repetitions for each data-set size is 30. The assumptions in this experiment are the following:

- The universe of discourse is $X \in [-10, 10]$.

- Knowledge of phenomena is complete, i.e. the prototype SKB is Ruspini (Equation 12).
- The distribution of data points collected is random but still uniform along the G granules in the partitions.
- The minimum confidence value reported is 0.1.
- Data points collected in X are generated by a chirp signal (explained in Section 5.2).
- Other PSO parameters remain constant (Section 4.2.1.2).

The following subsections present the data-set generation and a graphical example of the data sets.

5.2 Data-Set Generation

The data set is generated through the MATLAB Simulink simulation presented in Figure 38. The generator contains an oscillator of variable frequency that operates as a chirp waveform generator. The chirp wave oscilates within the domain $X \in [-10, 10]$, with initial frequency $f_0 = 0.0125$ [Hz], target frequency $f_t = 0.00025$ [Hz] and target time $t_t = 4000$ [s]. The situation assessment generator interprets sensor data and provides a data set containing: (1) situation assessments, and (2) values for their corresponding degree of confidence. A random number generator simulates identification codes for a number of humans. The simulated data sets are obtained for prototype partitions with $G = \{2, 3, 4, 5\}$ and $TI = \{1, 2, 4\}$. An example of four data sets for 50 data points generated for $G = \{2, 3, 4, 5\}$ and $TI = 4$ is shown in Figure 39.

For Figure 39, the independent variable is the universe of discourse $X \in [-10, 10]$. Continuous lines show the partitions for $G = \{2, 3, 4, 5\}$. Below the plots with continuous lines, the plot of their corresponding data sets is presented. Similar plots may

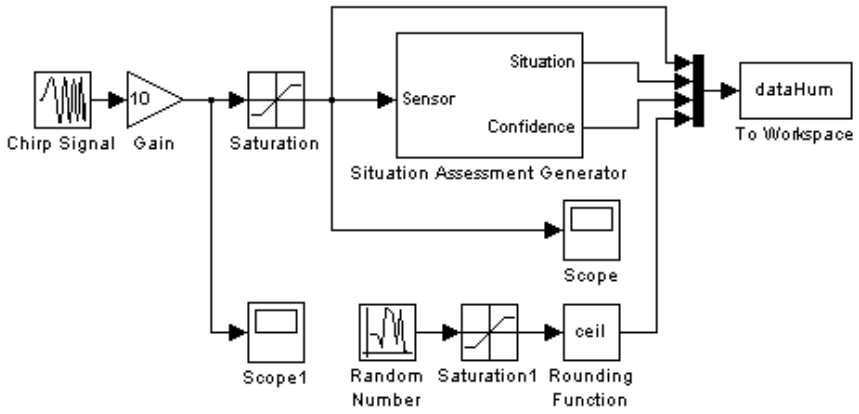

Figure 38: Situation Assessment Generator in Simulink.

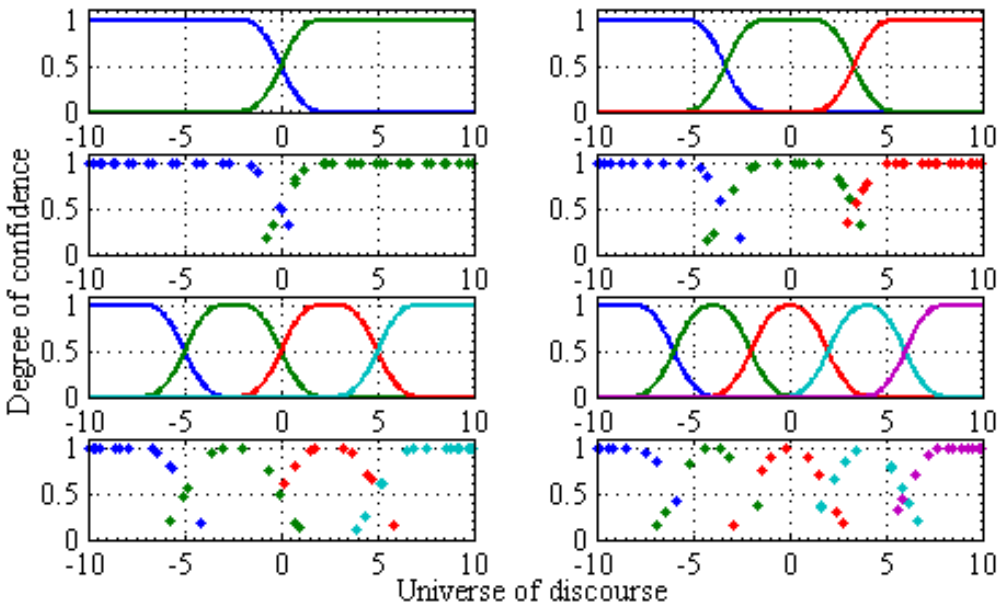

Figure 39: Example of data sets of 50 data points generated for $G = \{2, 3, 4, 5\}$ and $TI = 4$.

be generated for $TI = \{1, 2\}$.

5.3 Experimental Procedure

A script written in MATLAB served to automate the experiment. The script loads data sets for specific number of granules G and transition intervals TI. Considering the swarm sizes, data-set sizes, and number of repetitions, the MATLAB script runs the PSO-based Aggregation Algorithm and coherence operation for each one. The algorithm reports the number of holes, overlaps, Ruspini results, and iterations. The algorithm used in this section is later employed for validation in Chapter 6.

5.4 Characterization Results and Observations

The results of the characterization experiment are presented in Figures 40, 41, and 42 for swarm sizes $N = \{20, 50, 100\}$, respectively. Each figure shows four graphs with plots of the results obtained from running the Aggregation Algorithm with $G = \{2, 3, 4, 5\}$. The graphs reflect the mean proportion of Ruspini results as a function of data-set sizes $\{20, 30, 40, \ldots, 100, 200, \ldots, 800\}$. The mean proportion of Ruspini results for each data-set size is calculated by executing the Aggregation Algorithm 30 times on the specific data-set size. A proportion close to zero indicates that from the number of repetitions (i.e. 30), very few results complied with the Ruspini condition of Equation 12. Alternatively, a mean proportion closer to 1 implies that a majority of results complied with Equation 12.

In each of the 12 graphs there are three traces plotted in blue, red, and green color, which correspond to the three transition intervals tested: $TI = \{1, 2, 4\}$. Observations on these graphs are discussed in Subsection 5.5.

An additional graph is generated comparing the traces for $G = 5$ and $TI = 4$; the graph is shown in Figure 43. Its purpose is to compare the results obtained for a single partition for various swarm sizes and observe changes of performance of the Aggregation Algorithm as the computational power invested increases with

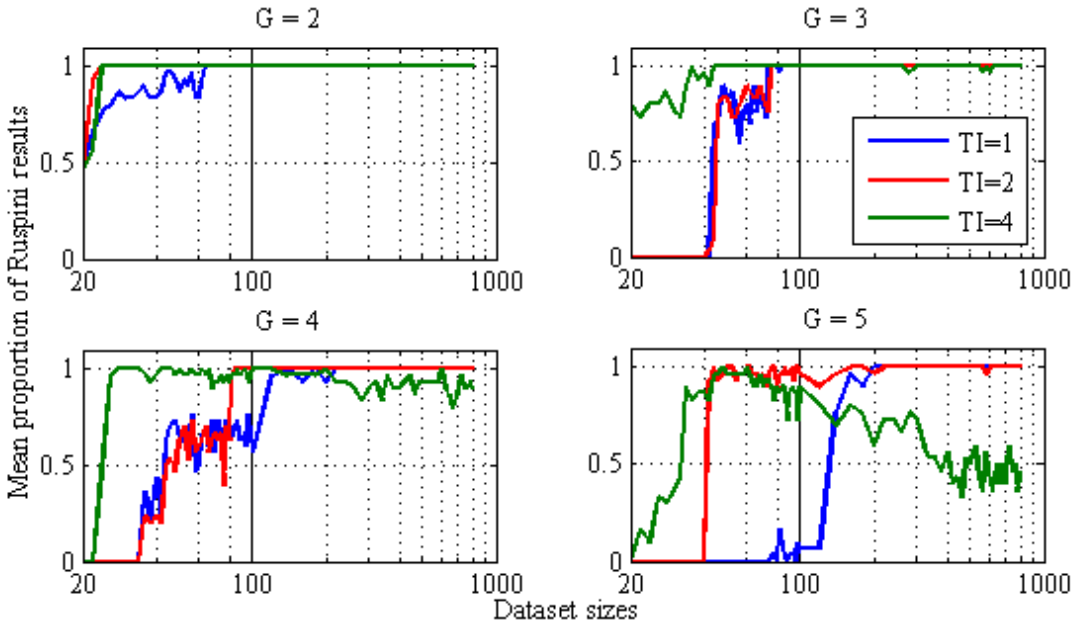

Figure 40: Proportion of Ruspini results for N=20.

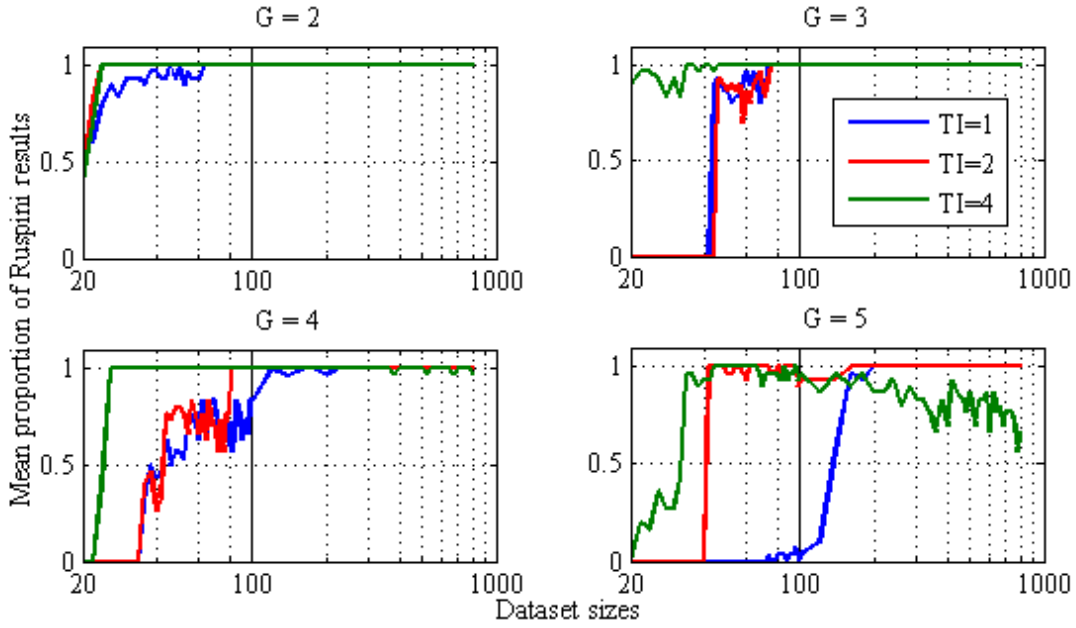

Figure 41: Proportion of Ruspini results for N=50.

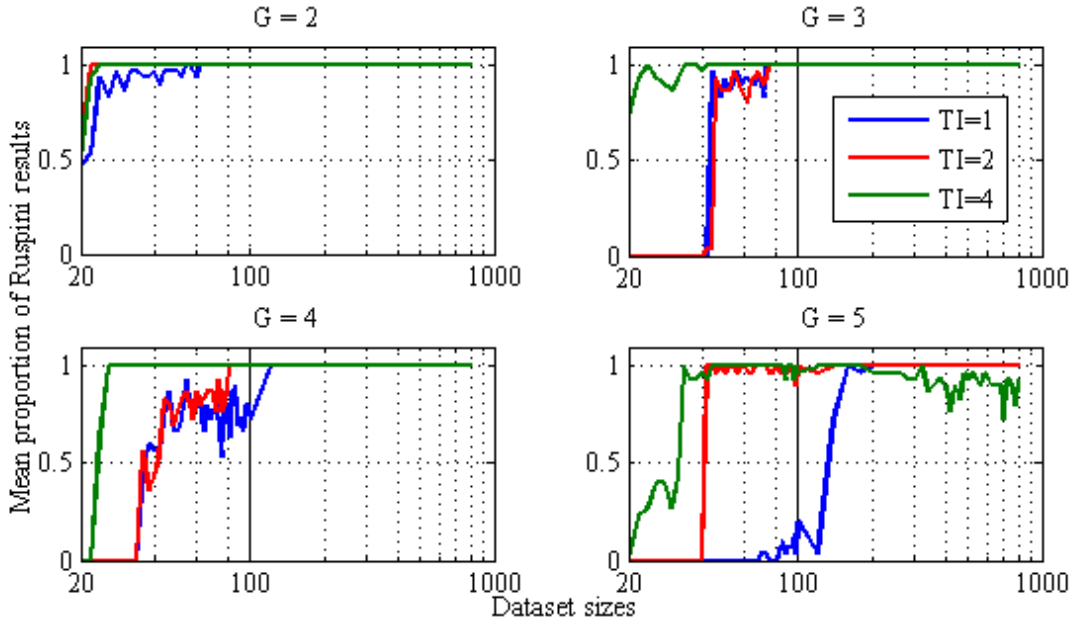

Figure 42: Proportion of Ruspini results for N=100.

$N = \{20, 50, 100\}$.

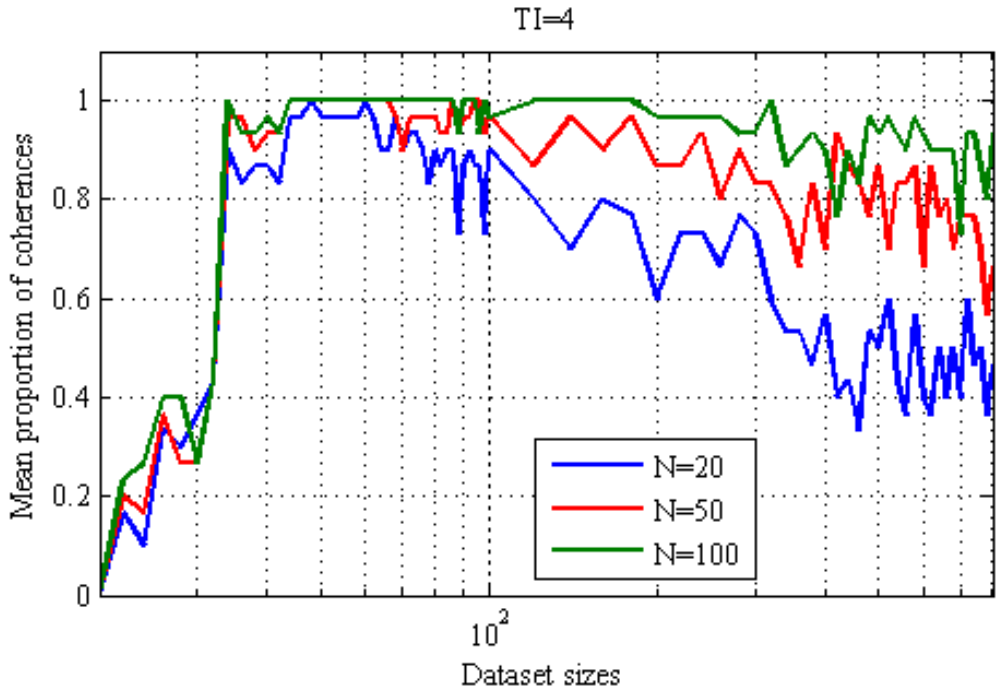

Figure 43: Proportion of Ruspini results for $G = 5$ and $TI = 4$.

5.5 Analysis of Characterization Results

The objective of this experiment was to characterize the Aggregation Algorithm in order to observe and determine the minimum number of data points required in a data set to ensure the Ruspini results under ideal experimental conditions. Figures 40, 41, and 42 contain the proportion of Ruspini results for various conditions depending on increasing data-set sizes, ranging from 20 to 800 data points, as illustrated with Figure 37 in Subsection 5.1. The analysis in this subsection is based on these three figures, which contain information susceptible to comparison as it may be relevant to experiment variables, *i.e.* swarm sizes, number of granules, and transition intervals.

As a first observation, the reader may notice that the Aggregation Algorithm performs better with fewer data points when a fewer number of granules is considered; for each one of the three figures, the graph with a smaller G value achieves a higher proportion of Ruspini results for a smaller data-set size, i.e. $G = 2$. Such performance deteriorates as the number of granules G increases. In this case, the largest value for the number of granules is $G = 5$. One reason for this phenomena is the number of transition intervals, which is equivalent to $G - 1$; the number of transition intervals increases with the number of granules. A larger number of transition intervals increases the chances that one of them may be the cause of anomalies and non-compliance with the Ruspini condition of Equation 12.

Secondly, the reader may appreciate that from Figure 40 to Figure 42 the swarm size in the PSO increases from 20 to 100. By comparing the graphs for a single value of G, in each case the reader may notice how the performance of the Aggregation Algorithm increases consistently for swarm sizes with greater number of particles. Such comparison is also detailed for $G = 5$ in Figure 43. A larger swarm size will increase the ability of the PSO to evaluate more of the search space, and thus to potentially arrive at a better solution than with a swarm with a fewer number of particles. In this observation, it is important to highlight that the PSO performs

searches individually for each granule, fitting the curve of the π-membership function to its corresponding data points. The swarm size has a meaningful impact on the performance of the Aggregation Algorithm even though the parameters obtained from the PSO are subsequently processed through the coherence operation.

As for the number of data points required in data sets to achieve Ruspini results, such number increases with the number of granules. This result is more clearly observed for smaller transition intervals. For example, for $TI = 1$ the data-set size with fewer data points that guarantees Ruspini results is shown in Table 9. For $TI = 2$ and $TI = 4$, their values are presented in Tables 10 and 11, respectively.

Table 9: Minimum number of data points in data sets that guarantee Ruspini Results for $TI = 1$.

	G=2	G=3	G=4	G=5
N=20	66	86	220	200
N=50	64	74	220	200
N=100	62	74	120	200

Table 10: Minimum number of data points in data sets that guarantee Ruspini Results for $TI = 2$.

	G=2	G=3	G=4	G=5
N=20	24	76	84	220
N=50	24	76	82	160
N=100	22	76	82	140

Table 11: Minimum number of data points in data sets that guarantee Ruspini Results for $TI = 4$.

	G=2	G=3	G=4	G=5
N=20	24	620	N/A	N/A
N=50	24	46	N/A	N/A
N=100	24	42	26	N/A

The results contained in Tables 9, 10, and 11 show that a larger number of data points are required for smaller transition intervals. Such observation suggests an advantage in recording data points during situation transitions. Conversely, more computing power (greater swarm size) is required for greater transition intervals and

for greater number of granules. This is evident in Table 11 and Figure 43, where performance deteriorates even for larger number of data points in the data sets. The reason for this phenomena is found in the size of the search spaces: greater transition intervals translate to larger search spaces, which will require a larger number of particles in the PSO step to increase the chance of obtaining Ruspini results. Because the coherence operation is applied to transitions between adjacent fuzzy sets, more data points within transitions may favor Ruspini results. Other parameters of the PSO could be modified to improve the performance of the Aggregation Algorithm; however, for this experiment only the swarm size was considered.

5.6 Summary

In conclusion, the following summarizes the findings discussed in this Chapter:

- The number of situation assessments required increases with the number of fuzzy sets in a partition.
- A greater number of data points is needed for smaller transition intervals.
- The results obtained suggest the advantage of recording situation assessments with confidence values lower than 1; *i.e.* during transitions.
- Because the Coherence operation is applied to transitions between adjacent situations, more data points within transitions may favor Ruspini results.

Limitations There are two main limitations to be considered when approaching this Chapter. First, the data sets used for the characterization are meant to be ideal and thus are generated by a simulation, not by human experts; this limitation may lead to misunderstandings on the capability of the aggregation algorithm. As a consequence, it is suggested that the reader proceeds with caution when addressing data sets that include situation assessments collected by real human experts. Second,

the characterization is conducted for a single sensor; although the non-interactiveness between sensors assumed in the FAM-based agent architecture allows the work of this Chapter to extend to multiple sensors, the results do not include the case when more sensors are considered.

CHAPTER VI

AGGREGATION OF HUMAN-EXPERT INPUTS

Given the results of the characterization of the Aggregation Algorithm in Chapter 5, one of the weaknesses of the experimental approach presented is that the data from the chirp-based situation assessment generator does not represent the inputs that would be provided by real human experts. Hence, a validation experiment that would provide observations based on real human-expert situation assessments was necessary. While the field application of this research has focused on the operation of regenerative life support systems [135, 61, 149, 150, 151, 152], the time needed from human-experts in this field to participate in data collection sessions was a challenge. Therefore, an analogous dynamic system and relevant variables were identified to serve as the basis for data-collection sessions in which more individuals would be eligible to participate. The dynamic system employed consists of the simulation of a cup of hot beverage, i.e. coffee, and the experiment was entitled "The Coffee Cup Experiment." The variables of the dynamic system used are its liquid level, measured in [cm], and its temperature, measured in [°F]. These two variables are respectively used in analogy to the concentration of dissolved oxygen and pH of the water volume of the aquatic habitat employed as a ground-based regenerative life support research platform [152].

The following subsections describe the experiment design, the data collection protocol, the dependence measures employed to assess the performance of participants, the validation results and observations, and a summary of the validation.

6.1 Experimental Design

This section describes the experimental design and setup employed to enable the interaction of human participants with the simulation of a dynamic system running in MATLAB Simulink. The interaction is achieved through a set of user interfaces elaborated in LabVIEW and connected to a simulation of the dynamic system. The software block diagram that illustrates the integration of MATLAB Simulink and LabVIEW to enable this experiment design is shown in Figure 44.

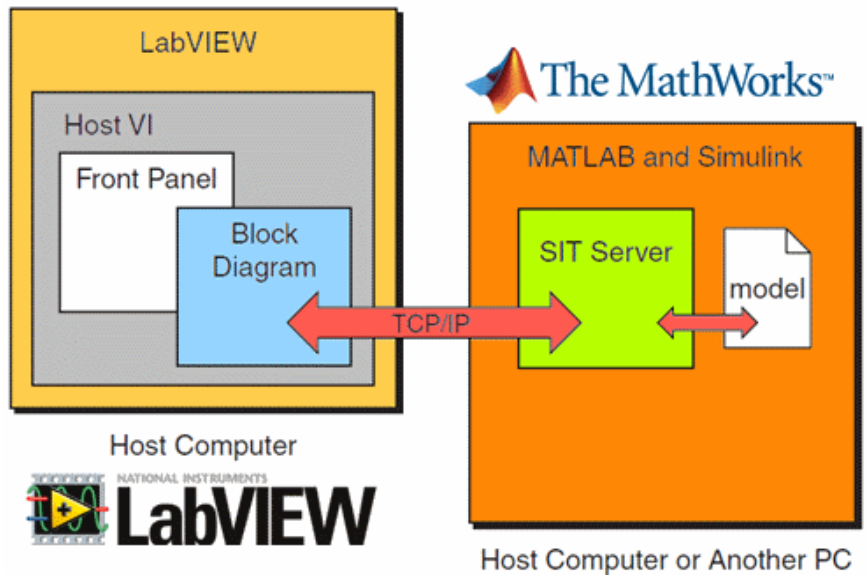

Figure 44: Software diagram combining a MATLAB Simulink model and a LabVIEW user interface.

The software integration of Figure 44 is powered by the Simulation Interface Toolkit of National Instruments. The system is able to register the interaction of the participants with the system by recording a selected number of variables.

The following subsections present (1) the mathematical model and block diagram of the dynamic system of a hot beverage, (2) the block diagram of the experiment in MATLAB Simulink, (3) the user interface designs prepared with LabVIEW, and (4) the simulation data used for this experiment.

6.1.1 Simulation of a Cup of Hot Beverage

The mathematical model of the dynamic system of a cup of hot beverage is presented in Equations 23 and 24.

$$\frac{d}{dt}h(t) = -\frac{4}{\pi d^2}C_{sip} \cdot u(t) \tag{23}$$

$$\frac{d}{dt}T(t) = \frac{1}{c_P h(t)}\left(T_A - T(t)\right)\left[\frac{4C_c}{d}h(t) + C_a + C_c\right] \tag{24}$$

In these Equations, $h(t)$ and $T(t)$ are the state variables. The model takes into consideration the diameter d of the cup, the heat capacity of water C_P, the ambient temperature T_A of the environment surrounding the cup, a coefficient C_c for heat loss through the sides and bottom of the cup, and a coefficient C_a for heat loss through the liquid surface area. The purpose of the model is to describe the behavior of the liquid level and its temperature as the state Equations 23 and 24, respectively. The block diagram of these two equations implemented in MATLAB Simulink is shown in Figure 45.

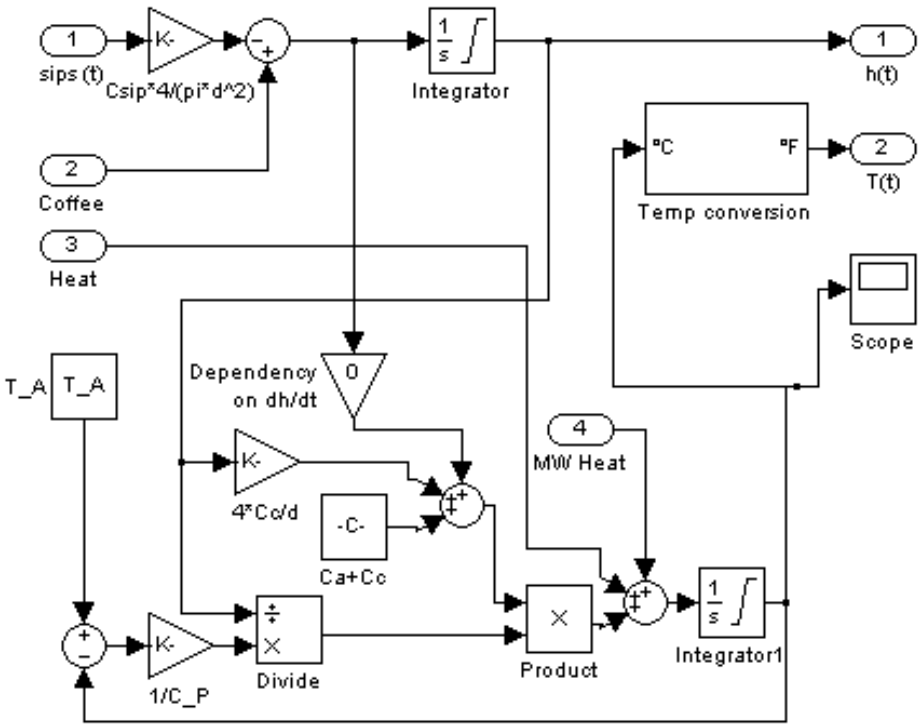

Figure 45: Block diagram of the MATLAB Simulink model of Equations 23 and 24.

As shown in the block diagram, two more inputs were added to the model described in Equation 24. The two terms correspond to the addition of coffee by a barista (Input 2) and the increase of temperature by a microwave oven (Input 4). Their purpose is to enable the exploration of the state space with the simulation data prepared in Subsection 6.1.4. The following assumptions were considered for this model: (1) the thermodynamic properties of coffee are similar to that of water (i.e. $\rho = 1\left[\frac{gr}{cm^3}\right]$ and $C_P = 4.18[\frac{J}{gram \cdot K}]$), (2) the temperature in the volume of liquid is uniform, (3) ambient temperature is constant, and (4) changes in temperature due to changes in liquid volume are discarded. The parameters used for the simulation of the cup of hot beverage are $d = 8[cm]$, $T_A = 20[^\circ C]$, $h_{max} = 5[cm]$, $C_{sip} = 1[cm/s]$, $C_c = 0.001$, $C_a = 0.025$, and $MW_{constant} = 0.55$. The initial values for the variables were $h_0 = 5[cm]$ and $T_0 = 70[^\circ C]$ (or $158[^\circ F]$). The block diagram in Figure 45 constitutes a single block in the experiment block diagram introduced in the following subsection.

6.1.2 Experiment Block Diagram in MATLAB

As mentioned in the previous subsection, the MATLAB Simulink model in Figure 45 is part of a larger simulation that incorporates a barista and a microwave oven, among other subsystems. Their purpose is to allow the exploration of the state space defined by the liquid level height $h(t)$ and the temperature $T(t)$ of the cup of hot beverage. The objective is to force the trajectories of the state variables so that human participants may provide a richer set of assessments during their interaction with the system. The complete block diagram implemented in MATLAB Simulink for this purpose is presented in Figure 46.

The block diagram of Figure 45 is contained in the top right block of Figure 46. Details of the interaction of the blocks *Drink*, *Barista Subsystem*, and *Prototype Granular Structure* are presented in Subsection 6.1.4. The data recorded by the blocks

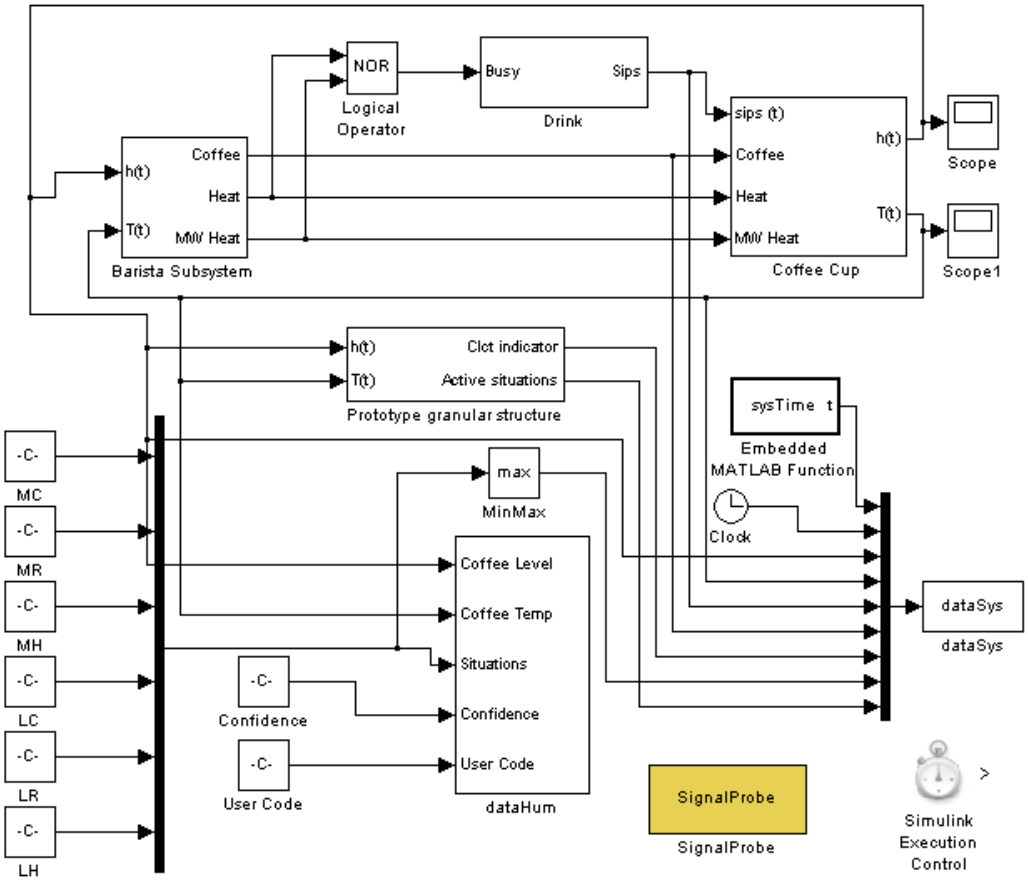

Figure 46: MATLAB Simulink block diagram for the Coffee Cup Experiment.

dataHum and *dataSys* is explained in Subsection 6.2. The six blocks in the lower left of the figure tagged with "MC," "MR," "MH," "LC," "LR," "LH," communicate the activity of six buttons in the user interfaces that allow participants to select between six possible situations. The user interface design is presented in the next subsection and elaborates on three interface versions that allow participants to report their confidence level.

6.1.3 User Interfaces in LabVIEW

Three interface designs were developed for this experiment. Their purpose is to allow for human-system interaction and data collection of situation assessments from human experts. From Subsection 4.2.1.1 and Figure 31, the second column of the expert input refers to the confidence c that the situation s is present in the system at a particular time t. The objective of having three user interface designs is to evaluate the importance and influence of the ability to report confidence values during data collection.

The three user interfaces designed are shown in Figure 47. They are composed of two working areas: (1) the indicator working area, and (2) the participant input working area. The indicator working area is the same for all three interfaces and is shown in Figure 48. The participant input working areas are slightly different between the three interfaces; they are shown in Figure 49.

The indicator working area shown in Figure 48 contains displays of the state variables of the mathematical model of the dynamic system. These are connected to the state variables of Equations 23 and 24 and to their corresponding MATLAB Simulink ports shown in the top right corner of Figure 45. Below each state variable indicator, participants can read a question related to the simulated variable. An image of a cup of coffee is shown between the two state variable indicators to reinforce the thought to participants that these two variables describe the behavior of its liquid level and

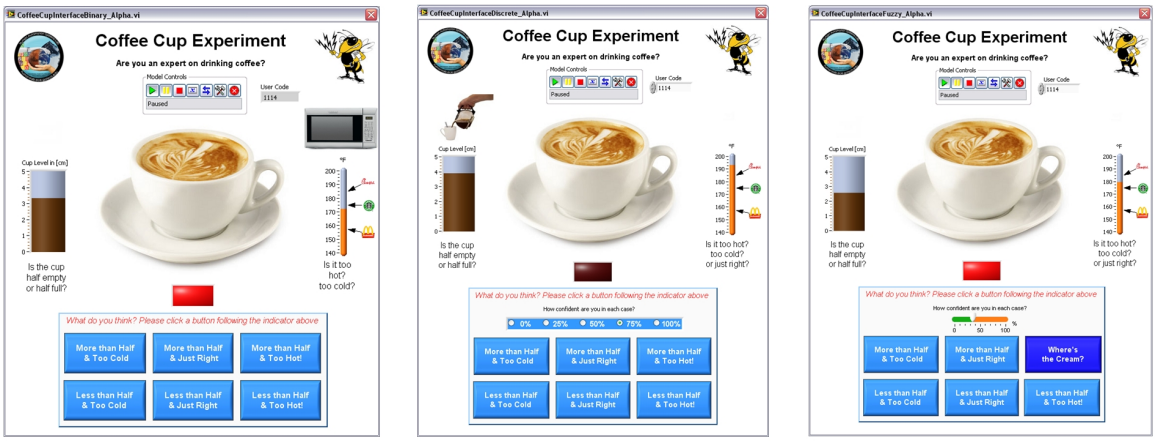

Figure 47: Interfaces of the Coffee Cup Experiment.

Figure 48: Indicator working area of the Coffee Cup Experiment interfaces.

its temperature. The position of the coffee cup between the state variable indicators is designed to create a cognitive load to participants, such attention switches between indicators when developing a situation assessment. The red indicator below the cup correlates to the time and frequency of when recordings are desired or expected. The activity of the red indicator is associated to the prototype granular structure mentioned in Figure 46 (in Subsection 6.1.2), which is explained in more detail in Subsection 6.1.4.3.

The second working area of the user interfaces shown in Figure 47 is the participant input working area. A more detailed (zoomed-in) representation is presented in Figure 49. The three participant working areas are indentified throughout this work as: (a) "buttons alone," (b) "with options," and (c) "confidence bar."

The participant working areas implement different confidence resolution options; i.e. (a) $c = 100\%$, (b) $c \in \{0\%, 25\%, 50\%, 75\%, 100\%\}$, and (c) $c \in [0\%, 100\%]$. The lowest resolution in confidence level for the collection of situation assessments from human experts consists of fixing the value of c to a constant representing the maximum confidence; i.e. $c = 100\%$. This option is implemented in one of the three interfaces considered by not offering the capability to experts to change the confidence value of their situation assessments. Increasing levels of resolution of c for the second and third interfaces offer the capability for experts to select other values between zero and 100. In such a way, those interfaces include a selection device that allows experts to select their confidence level when reporting situation assessments. The second of three interfaces allows experts to report five confidence values; these are $c \in \{0\%, 25\%, 50\%, 75\%, 100\%\}$. The selection device used for the second interface is a radio button selector with the five confidence level values mentioned. The third interface allows experts to report confidence values in a continuous range between zero and 100%. The selection device used in this case is a sliding bar that enables experts to report their confidence level with any value between 0% and 100%, *i.e.*

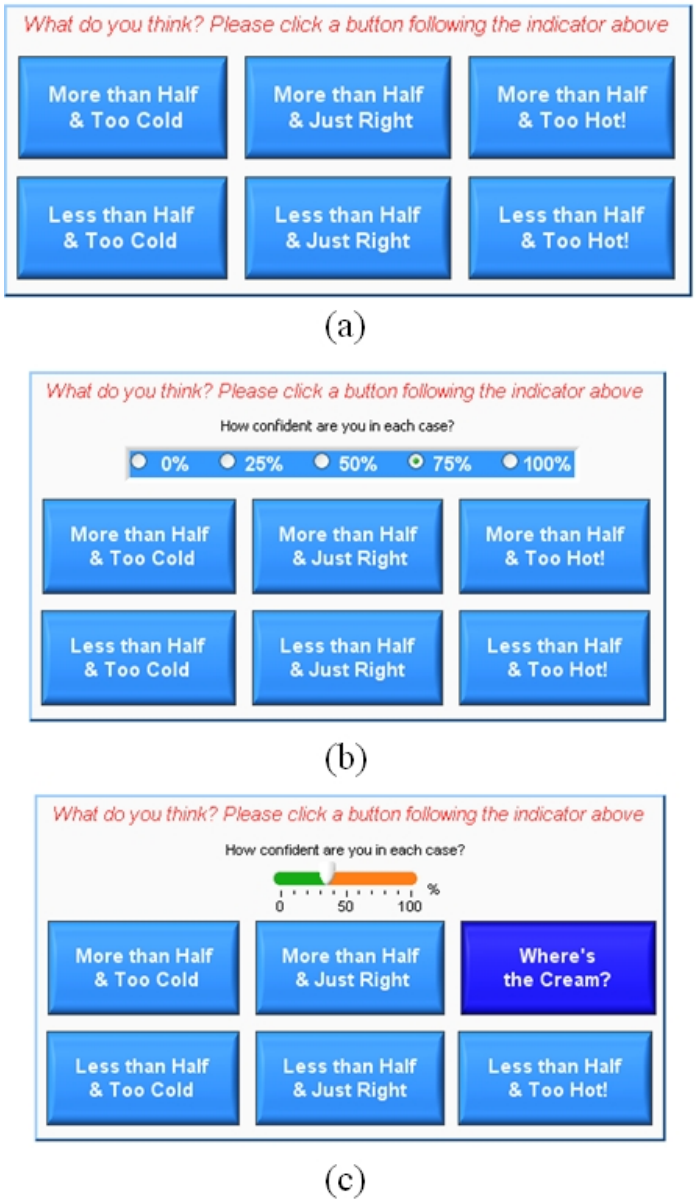

Figure 49: Participant input working areas: (a) buttons alone, (b) with options, and (c) confidence bar.

$c \in [0\%, 100\%]$. These options represent differences in the resolution of confidence levels; the resolution increases as well as the possible confidence values available to participants. All three participant input working areas include six buttons with the following tags:

- More than Half & Too Cold
- More than Half & Just Right
- More than Half & Too Hot
- Less than Half & Too Cold
- Less than Half & Just Right
- Less than Half & Too Hot

These buttons impose a constraint on the possible options that experts may consider and provides a minimum structure to the SKB to be developed from their assessments. These interfaces integrate with the simulation of Subsection 6.1.2 and provide participants with the signals necessary to collect and register their situation assessments. The simulation data and specific signals developed for this experiment are presented in the next subsection.

6.1.4 Simulation Data

The simulation presented in this section and prepared with the system of Figure 46 is employed for all human-system interaction sessions for the three user interfaces of Subsection 6.1.3. Therefore, the state-variable trajectories and all other dependent signals are identical in all simulations. The dynamic behaviors are intended to be sufficiently complex to cover the state space defined by liquid level and temperature variables and also to prevent participants from learning or predicting its behavior with the data collection protocol described in Subsection 6.2.

The simulation time is 600 [s] (10 minutes) in all cases, forced to run in real time by the "Simulink Execution Control" function shown in the lower-right corner of Figure 46. This subsection presents the simulation data in three parts: (a) state-variable trajectories, (b) prototype granular structure and situation-rich signals, and (c) activity of the red indicator.

6.1.4.1 State-Variable Trajectories

The trajectories of the state variables are presented in Figures 50, 51, and 52. They evolve during the 600 seconds of simulation in response to the inputs of the "Drink" and "Barista" subsystems. Figures 50 and 51 indicate the periods of time in which various behaviors are active, such as "drinking," "heating in microwave," and "barista refilling." The barista subsystem refills the cup at 300 [s] into the simulation and it also warms it up in the microwave at 110 [s] and 530 [s].

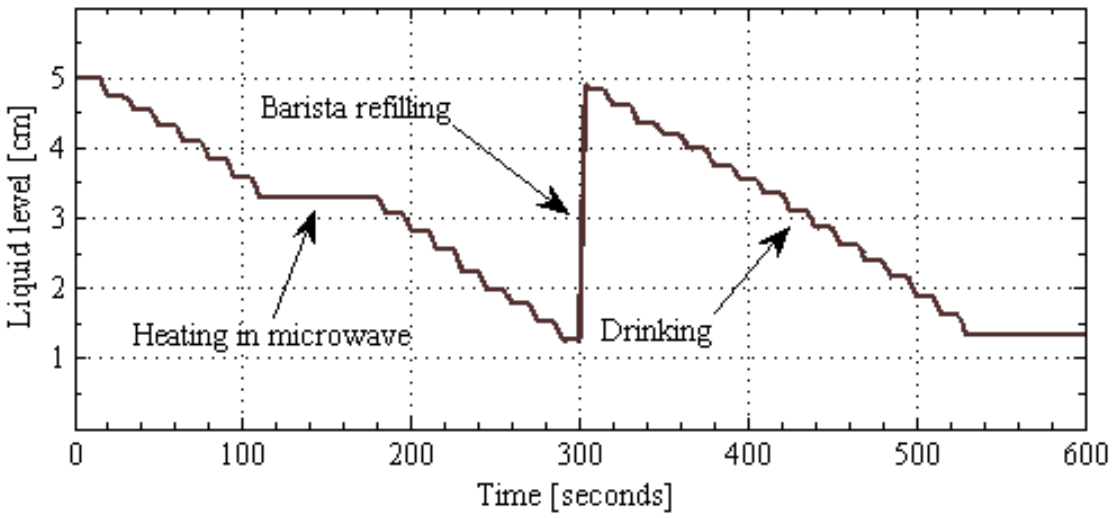

Figure 50: Behavior of the liquid level over time.

The relationship between the state variables in the simulation and their trajectory in the state space is shown in Figure 52. This figure illustrates the coverage of the state space achieved in the simulation by making use of the "Drink" and "Barista" subsystems. As it will be shown in the next subsection, the coverage of the state

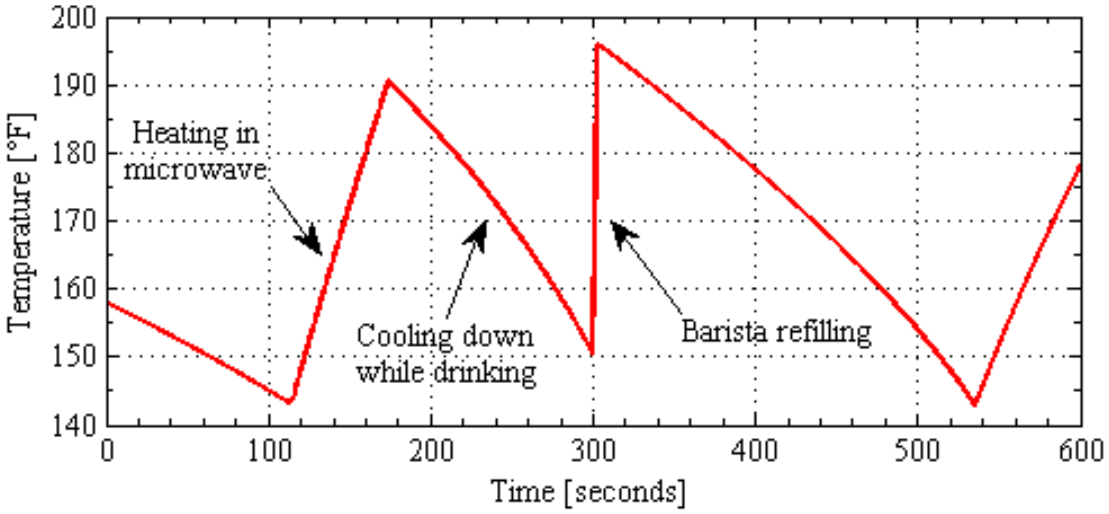

Figure 51: Behavior of the temperature over time.

space achieved in the simulation also allows the exploration and activation of the six situations defined in the prototype granular structure.

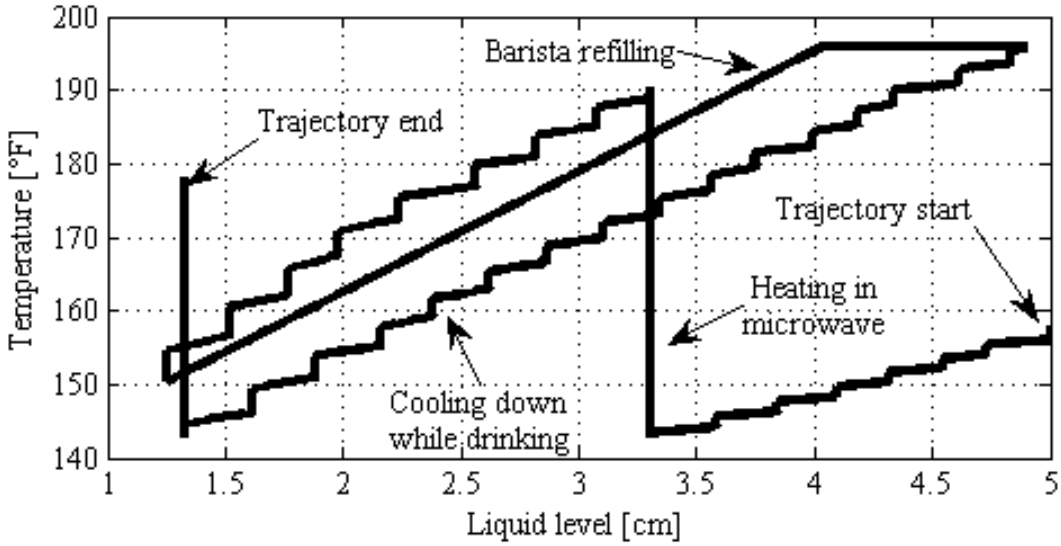

Figure 52: Trajectory of the simulated variables.

6.1.4.2 Prototype Granular Structure

Six situations and their membership functions are predefined as the "truth" for this experiment. The membership function and situation definitions are shown in Figure

53. The partition of the universes of discourse in each case complies with the Ruspini attribute of Equation 12. The resulting prototype granular structure is obtained by applying Equation 13 from Chapter 4.1.1.1 and is presented in Figure 54.

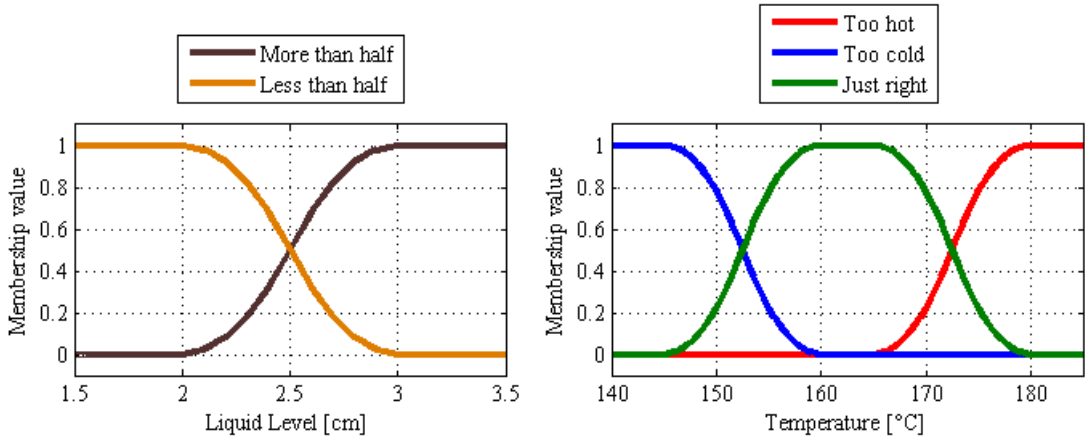

Figure 53: Plots describing liquid level and temperature fuzzy sets for the prototype granular structure.

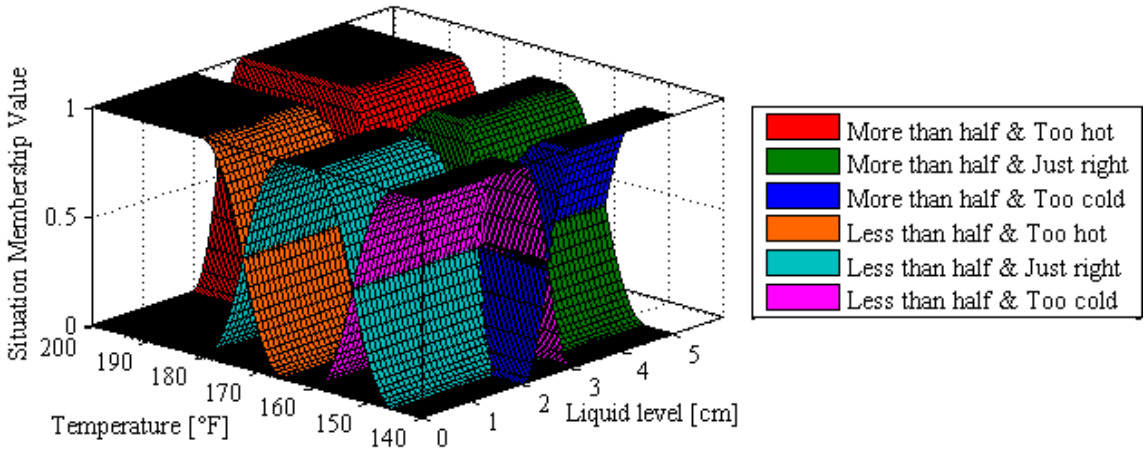

Figure 54: Three-dimensional plot of the prototype granular structure.

The membership values of the trajectory of Figure 52 can be plotted on the surface of the three-dimensional prototype granular structure (Figure 54) as in Figure 55, showing the activity of the system as the membership values of situations transition between 0 and 1. This same activity can be appreciated more clearly in a time-dependent plot for each situation and observing their evolution over time, as shown

in Figure 56.

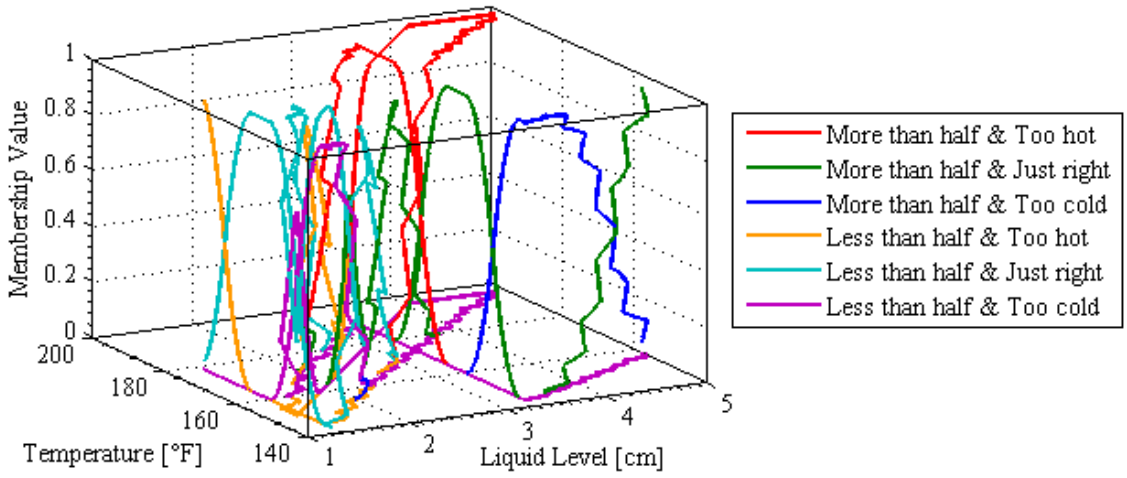

Figure 55: Three-dimensional plot of the trajectory of the simulated variables as they would move on the surfaces of the prototype granular structure.

The simulation data employed in this experiment not only provides coverage of the state space as illustrated in Figure 52, but it also enables the activation of all situations predefined in the prototype granular structure, as shown in Figure 56. This aspect of the simulation data and experiment aims to enable participants to provide situation assessments for all possible situations during the 600 [s] of simulation. The way participants are able to transition between these predefined situations is by associating the activity of the red indicator of the user interfaces (Figure 48) to the maximum value of the situation-rich signals shown in Figure 56. The association between these signals and the red indicator is elaborated in the following subsection.

6.1.4.3 Activity of the Red Indicator

The red indicator in the user interfaces is the mean by which participants are prompted to introduce situation assessments and thus consider transitioning to a new situation or, in other words, to change their situation selection option. The specifics of how the red indicator is used is explained in more detail in Subsection 6.2. As for the simulation data, the relationship between the red indicator and the prototype granular

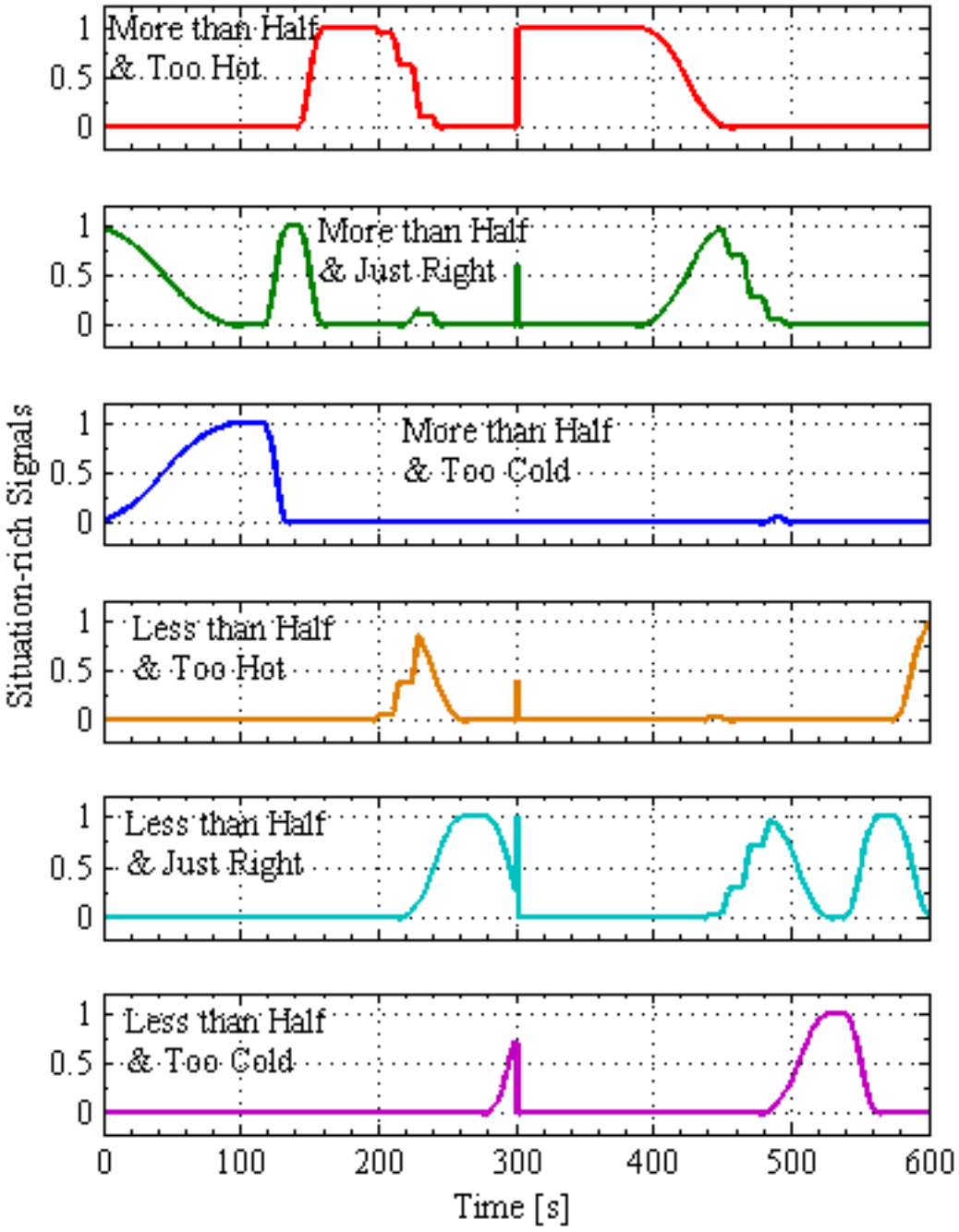

Figure 56: Two-dimensional plot of the membership value of the situation of the dynamic system as it evolves over time.

structure is the following: the red indicator blinks at a minimum base frequency when the maximum membership value of the situation-rich signals in Figure 56 equals 1. As the value of the membership value reaches 0.5, the frequency at which the red indicator blinks increases to its maximum. The behavior of the indicator is the same for all simulations and is plotted in Figure 57.

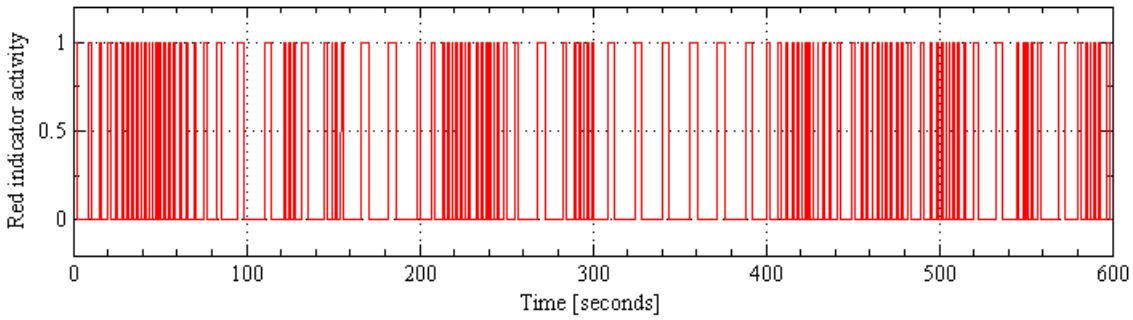

Figure 57: Plot of the red indicator activity during the simulations.

The idea behind this device in the experiment design is to provide the minimum clues to participants about the existence of a prototype granular structure and about the situation definitions contained therein, and still be able to obtain a similar granular structure from the situation assessments recorded during sessions of data collection. The instructions given to participants on how to respond to the red indicator are presented in Subsection 6.2, which corresponds to the data collection protocol.

6.2 Data Collection Protocol

A main aspect of the experiment design is its ability to collect situation assessments from real human participants. Even though very few individuals may be considered experts in the operation of a life support system, many may be considered experts in drinking coffee or other hot beverages, and in assessing the level of liquid in a cup and the value of its temperature. This subsection presents the data collection protocol used in this experiment design in the following four parts: (1) participants, (2) instructions, (3) data collection sessions, and (4) post data collection survey.

6.2.1 Human Participants

The subjects in this study were able-bodied participants and members of our laboratory. They were recruited by word of mouth and confirmed by e-mail. Participants did not have any risk of discomfort during the data collection sessions. Any lab member comfortable using computers could participate in this experience. Eight (8) participants enrolled in this experiment.

6.2.2 Instructions to Participants

The instructions given to participants requested that they provide situation assessments of a cup of coffee based on the variables of liquid level and temperature, indicating that their ranges are $[0, 5]$ [cm] and $[140, 200]$ [°F], respectively. It introduced the six possible situations considered and the layout of their corresponding blue buttons in the user interfaces. Instructions also explained the difference between the three user interfaces, highlighting the possibility of reporting confidence value for situation assessments. A final instruction was given to participants as a "very important note;" it introduced the red indicator and set the goal for participants to report their situation assessments when the indicator lit up, also mentioning that the blinking frequency changes during the simulations. As a final note and key hint, the instructions asked participants to consider changing their situation selection especially as the frequency of the red indicator increased.

6.2.3 Data Collection Sessions

The sessions consisted of exposing human participants to three user interfaces (Figure 47) in order to collect their assessment of the situation of a hot beverage during simulations. As mentioned in previous sections, the duration of each simulation was 10 minutes and took the cup of coffee along six possible situations. The interfaces contain buttons that are associated with each situation. The experiment block diagram in MATLAB Simulink records how participants press each button in their attempt to

assess the situation of the simulated cup of coffee. The variables were recorded in the blocks *dataHum* and *dataSys* shown in Figure 6.1.2. The following variables were recorded from human inputs:

- Situation selection.
- Confidence level.
- User code.

The system variables recorded from the simulation were the following:

- Simulation time (in seconds).
- Liquid level (in centimeters).
- Temperature (in degrees Fahrenheit).
- Behavior of the "Drink" subsystem (in cubic centimeters per second).
- Behavior of the refill function of the Barista subsystem (in cubic centimeters per second).
- Activity of the red indicator (on/off behavior over time).

6.2.4 Post-Data-Collection Survey

At the end of the data collection session, each participant was given a survey to assess their understanding of the simulation, their preferred user interface, and a self-rating of their performance. It presented an image of the three interfaces for reference and asked the following six questions:

1. How would you rate the difficulty of the interface using a slider bar to express your confidence?

2. How would you rate the difficulty of the interface using options to express your confidence?

3. How would you rate the difficulty of the interface without the confidence options?

4. What interface do you prefer when the Red Indicator speeds up?

5. What interface do you prefer when the Red Indicator slows down?

6. How would you rate yourself at following the Red Indicator with each interface?

The response options for Questions 1, 2, and 3 used a six-point Likert scale with the options: a) Very easy, b) Somewhat easy, c) Somewhat hard, d) Very hard, and e) Undecided; for Question 4 and 5, the options were: a) Buttons with Options, b) Buttons Alone, c) Buttons with Confidence Bar, d) None of them, and e) All of them; and finally for Question 6 it presented a table with the following 5-point Likert scale for each interface: a) Very good, b) Somewhat good, c) Somewhat bad, and d) Very bad.

The response of participants to this survey provides a supporting measure to the performance metrics developed for the evaluation of their interaction with the user interfaces, which are presented in the next subsection.

6.3 Dependence Measures

The data collected from the interaction of participants with the three interfaces is analyzed by developing dependence measures that provide performance metrics about:

- individual interaction with the interfaces, and

- outcome metrics from processing the collected data sets through the Aggregation Algorithm.

Consequently, this subsection is organized in two parts. The first part describes the dependence measures used to evaluate the acceptance of the interface designs as tools useful to record situation assessments. The second part analyzes the performance of the aggregation algorithm with data sets generated by real human participants and validates the characterization of the Aggregation Algorithm presented in Chapter 5.

6.3.1 Human-system Interaction Performance

The performance metrics developed to evaluate human-system interaction performance are based on the signals recorded by the *dataHum* and *dataSys* blocks of the MATLAB Simulink block diagram (Figure 46). In particular, they make use of the signals that record the push activity of the blue buttons and the activity of the red indicator in the interfaces (refer to Figures 47, 48, and 49). By observing the activity of how participants respond to the red indicator and make a situation selection by pushing the blue buttons, the performance metrics allow observations about the time response of participants, their ability to track the red indicator while making situation selections, and the rates at which participants change their choice of situation versus the rate at which they change their confidence level.

6.3.1.1 Time-Response Score

The time response of participants is measured and scored as shown in Figure 58.

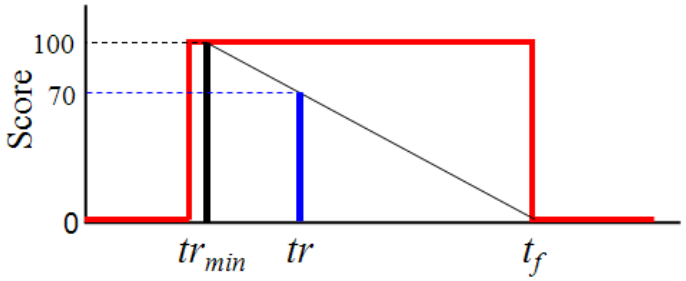

Figure 58: Illustration of the time-response score.

In this figure, the red signal represents the activity of the red indicator as it lights up once. The time-response score is then defined for the time period between

the minimum time response possible tr_{min} [153, 154] and the time t_f at which the indicator turns off. The time-response score is calculated for each single red indicator light-up event according to Equation 25.

$$S_r\% = \frac{|tr - t_f|}{|tr_{min} - t_f|}100 \tag{25}$$

The time-response scores are calculated for the 112 light-up events of the red indicator for each interface with each participant. The results are plotted as the distribution of the average time-response scores among participants for each interface.

6.3.1.2 Indicator-Tracking Score

This performance metric measures the difference between the 112 situation selection inputs s_r expected from participants and the actual number of situation selections s_{in} made. As the difference between s_{in} and s_r grows (for making more or less situation selections than those signaled by the red indicator), the indicator-tracking score $S_{tk}\%$ achieved is lower. The score is expressed as a percentage and is described by Equation 26.

$$S_{tk}\% = \left[1 - \frac{|s_r - \sum s_{in}|}{s_r}\right] 100 \tag{26}$$

As with the time-response score, the mean indicator-tracking scores are calculated with the 112 light-up events of the red indicator for each interface with each participant. The results are plotted as the distribution of the average indicator-tracking scores among participants for each interface.

6.3.1.3 Confidence vs. Situation Selection Change Proportion

The goal of this interaction performance metric is to allow for observations about the use of the interface elements of the input working area, i.e. elements for action selection (blue buttons) and elements to record confidence levels (options or confidence bar). This performance metric is expressed in Equation 27 and measures the

proportion between the rate at which participants change their situation selection and the rate at which they change their confidence level.

$$S_{c/s} = \frac{\sum \Delta c}{\sum \Delta s} \tag{27}$$

The results are plotted as the distribution of the average selection change proportion among participants for the interface with options and with confidence bar. The interface with buttons alone does not have confidence level selection elements and, by Equation 27, its proportion of selection change equals zero.

6.3.2 Aggregation Algorithm Performance

The metrics developed to measure the performance of the Aggregation Algorithm serve two objectives:

- to analyze the performance of the Aggregation Algorithm using data sets from the interaction of humans with the simulated dynamic system and
- to validate the characterization of the Aggregation Algorithm.

The performance metrics used to analyze the performance of the algorithm are the mean percentage of Ruspini partitions among participants for each interface, the mean number of fuzzy sets per sensor, and the mean score of similarity between the granular structure obtained from the algorithm and the prototype granular structure introduced in Subsection 6.1.4.2. The mean value of these metrics per participant is the average of the results from executing the Aggregation Algorithm on their respective data sets with a frequency of 100 times and swarm sizes $N = \{20, 50, 100\}$. The results are plotted as the distribution of the average value of each metric among participants for each interface and for each swarm size.

6.3.2.1 *Mean Percentage of Ruspini Partitions*

The Aggregation Algorithm is executed 100 times with the data sets of each participant with each interface for the three swarm sizes. Each time the result complies with the Ruspini condition of Equation 12, the metric adds one percentage point to that particular execution under those conditions. The results are plotted as the distribution of the average percentage of Ruspini partitions among participants for each interface and for each swarm size.

6.3.2.2 *Mean Number of Sets per Sensor*

From the same execution of the Aggregation Algorithm ran to obtain the mean percentage of Ruspini partitions (above), the mean number of fuzzy sets per sensor is recorded. As with other metrics, the results are plotted as the distribution of the average number of fuzzy sets among participants, for each sensor, for each interface, and for each swarm size.

6.3.2.3 *Similarity Score to Prototype*

The goal of this performance metric is to compare the maximum of the fuzzy sets obtained per sensor with that of the prototype granular structure (presented in Subsection 6.1.4.2) and evaluate how similar they are. An illustration of this performance metric per sensor is presented in Figure 59.

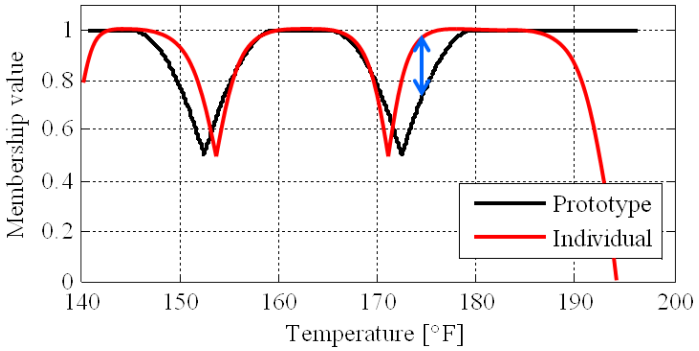

Figure 59: Illustration of the measure of similarity between partitions maxima.

The similarity score $S_p\%$ takes 1000 points uniformly distributed along x_i (as defined in Chapter 4.1.1.1) between parameters $\min(a_{x_i})$ and $\max(d_{x_i})$ and applies Equation 28 for $i = 1, \ldots, n$; the fuzzy sets $\alpha = 1, 2, \ldots, k_i$ and those of the corresponding partition $\alpha_p = 1, 2, \ldots, k_p$ of the prototype granular structure. The metric adds a tenth of a percentage point to the score every time that $\left|\max\left(\mu_{X_i^{\alpha_p}}\right) - \max\left(\mu_{X_i^{\alpha}}\right)\right| \leq 0.05$.

$$S_p\% = \frac{\sum \left|\max\left(\mu_{X_i^{\alpha_p}}(x_i)\right) - \max\left(\mu_{X_i^{\alpha}}(x_i)\right)\right|}{10} \tag{28}$$

As with previous metrics, the results are plotted as the distribution of the average similarity score among participants for the sensors considered, for each interface, and for each swarm size.

6.3.2.4 Percentage of Ruspini Results for Other Data-Set Sizes

This last performance metric operates on the data sets collected from the interaction of participants with the system and reduces their size by uniformly discarding data points. The reduced data-set sizes considered are obtained at 25%, 33%, 50%, 67%, and 75% of their original sizes. The action taken to obtain the reduced size data sets is presented in Table 12.

Table 12: Reduction of data-set sizes

Dataset size	Data point	Action
25%	Every fourth	Keep
33%	Every third	Keep
50%	Every other	Discard
67%	Every third	Discard
75%	Every fourth	Discard

The goal of this metric is to evaluate the performance of the Aggregation Algorithm for reduced data-set sizes obtained from human participants and validate the characterization and observations made in Chapter 5. This performance metric executes the Aggregation Algorithm with a frequency of 100 times for each reduced

data-set size, for each participant, for the three interfaces, and with the three swarm sizes considered. The results are plotted as the average percentage of Ruspini results versus the average sizes of data sets, in both cases calculated among participants. The interface exhibiting the best performance was plotted in more detail, showing the distribution of Ruspini results among participants for various sizes of data set completeness.

6.4 Validation Results and Observations

This chapter organizes results in three parts:

- Results from participant-interface interaction.
- Results from post-interaction survey.
- Results from the Aggregation Algorithm.

The first part presents the results from the performance metrics explained in Subsection 6.3.1 applied to the data sets collected from the interaction of participants with the simulated dynamic system. The second part complements the first by providing the results of the post-interaction survey described in Subsection 6.2.4 as a supporting measure and to evaluate the acceptance of the interfaces. The third part contains the results from processing the data sets collected from participants through the Aggregation Algorithm, as outlined in Subsection 6.3.2.

6.4.1 Results from Participant-Interface Interaction

The results from participant-interface interaction present the distributions of the mean time-response score among participants for each interface, the distribution of the average indicator-tracking scores, and the proportion of selection change between confidence and situation options for interfaces with confidence level devices.

Time-Response Score The distributions of the mean time-response scores among participants for each interface are plotted in Figure 60 and their values are presented in Table 13.

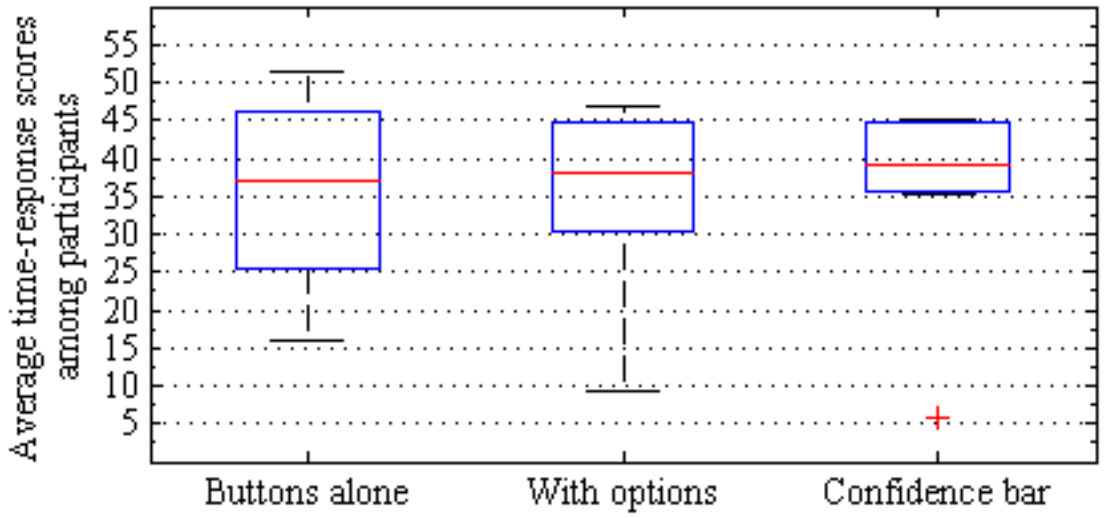

Figure 60: Time-response scores per interface in percentage units.

Table 13: Values for the distribution of time-response scores.

Avg. Time	Buttons alone	With options	Confidence bar
Upper adjacent	51.37	46.70	45.08
75th Percentile	46.09	44.84	44.66
Median	37.07	38.23	39.06
25th Percentile	25.55	30.37	35.71
Lower adjacent	15.82	9.25	35.21
Outliers	0	0	1

For the time-response score results presented in Figure 60 and on Table 13, two main observations can be made. First, the difference between median scores is small, being 37.07 units for the interface with buttons alone, 38.23 for the interface with options, and 39.06 for the interface with confidence bar. Second, the average scores among participants seem to be more consistent when using the interface with confidence bar. This observation is supported by noting the box size in each case: for the interfaces with buttons alone, with options, and with confidence bar the box sizes

are 20.54, 14.47, and 8.95, respectively. From looking at the upper adjacent values of the time-response scores among participants, they seem to have delayed more their response on interfaces with confidence level devices; i.e. for interfaces with options and confidence bar, the maximum time-response score obtained in each case is 46.70 and 45.08, as compared to 51.37 for buttons alone.

Indicator-Tracking Score The distributions of the mean indicator-tracking scores among participants for each interface are plotted in Figure 61 and their values are presented in Table 14.

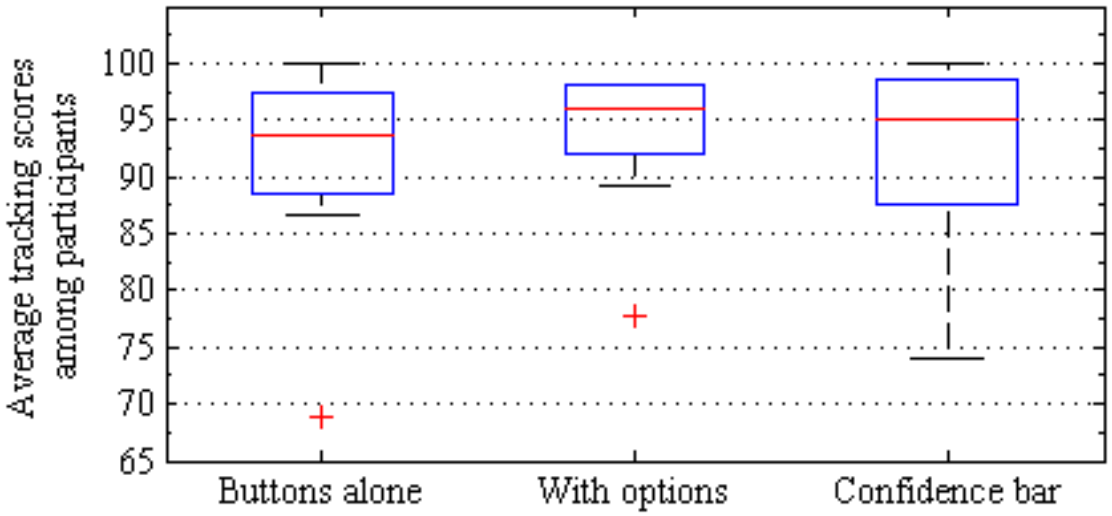

Figure 61: Indicator-tracking scores per interface in percentage units.

Table 14: Values for the distribution of indicator-tracking scores in percentage units.

	Buttons alone	With options	Confidence bar
Upper adjacent	100.00	98.21	100.00
75th Percentile	97.32	98.21	98.66
Median	93.75	95.98	95.09
25th Percentile	88.39	91.96	87.50
Lower adjacent	86.61	89.29	74.11
Outliers	1	1	0

Two observations are worth noting from Figure 61 and Table 14. First, the interface with confidence options shows a better response having a median value of 95.98

and a box size of 6.25; such box size indicates a better consistency of participants in tracking the red indicator when reporting situation assessments. Secondly, results appear to be less consistent when participants report situation assessments through the interface with confidence bar; i.e. its box size is the greatest with a value of 11.16 units. Hence, the interaction of participants show better average tracking scores on interface with confidence options. The decreased performance of participants using the interface with confidence bar may be due to the increased attention demanded to consider the possible range of values that their confidence level may take while making a decision and reporting each assessment. In other words, having to pay more attention to their confidence level may have made tracking-scores less consistent among participants.

Confidence vs. Situation Selection Change Proportion The distributions of the mean proportion of selection change between confidence and situation options among participants for interfaces with confidence level devices are plotted in Figure 62 and their values are presented in Table 15.

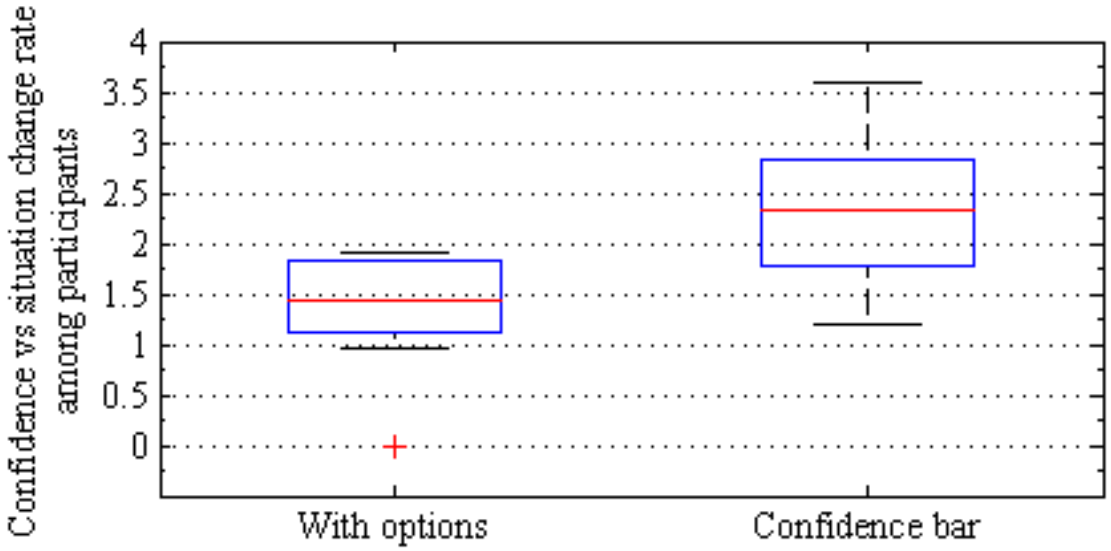

Figure 62: Proportion of change: factor by which confidence level was changed more often than situation selection.

Table 15: Values of the proportion of selection changes.

	With options	Confidence bar
Upper adjacent	1.90	3.59
75th Percentile	1.83	2.83
Median	1.43	2.32
25th Percentile	1.12	1.77
Lower adjacent	0.96	1.20
Outliers	1	0

The observations on the proportion of confidence versus situation selection change are focused on the interface with confidence bar as compared to that with confidence options. One observation to highlight from Figure 62 and Table 15 is that participants tended to take advantage of the capability to change their reported confidence level in both cases. The more possible options they had seemingly translated to a higher rate of proportion of change, evident from the higher median score achieved by participants for the interface with confidence bar. If offered the capacity to change confidence values, participants tended to update their confidence level more often than their situation choice. This observation supports the discussion in Subsection 6.4.1 on the indicator-tracking scores showing that the interface with confidence bar in fact demanded more attention from participants in order to update or change the confidence value reported through the confidence bar.

6.4.2 Results From Post-Interaction Survey

The response of participants to the questions of the post-interaction survey are presented in Figures 63, 64, and 65. The responses about the difficulty of the user interfaces are plotted in Figure 63. The responses for their preferred interface are shown in Figure 64. Finally, their self-rated performances with the user interfaces are shown in Figure 65.

Interface Difficulty Half of the participants found it less difficult to make use of an interface with buttons alone than those with the capacity to report confidence

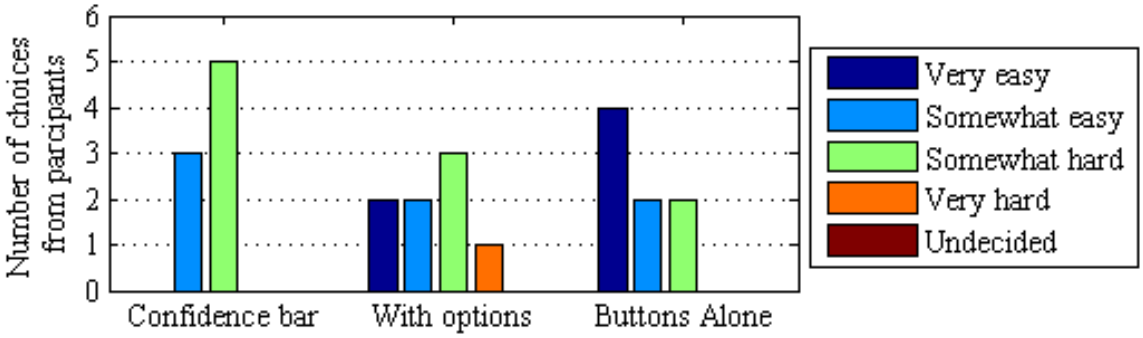

Figure 63: Responses from participants about the difficulty of the interfaces.

values. From those with such capacity, diverse answers were given for the interface with confidence options, with 37.5% responses considering it somewhat hard. And third, most participants (62.5%) found it somewhat difficult to work with the interface employing a confidence bar.

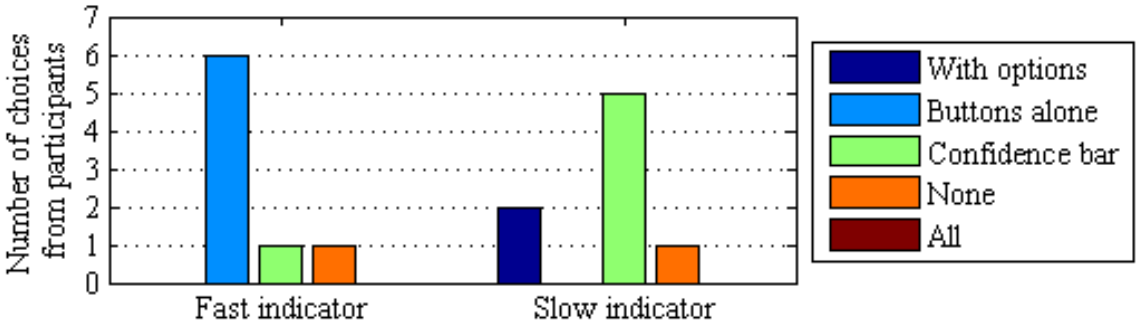

Figure 64: Responses from participants about their interface preferences.

Interface Preference There are four observations to make. First, for periods of time in which the red indicator would blink faster, most participants (75%) agreed on their preference for the interface with buttons alone. Second, for a slow indicator, most participants (62.5%) preferred the interface with a confidence bar. Third, only two participants (25%) preferred the interface with options to report situation assessments for slow indicators. And fourth, only one participant did not express a preference for an interface in reference to indicator speeds. These results show that,

despite its difficulty, participants would accept using a confidence bar to report situation assessments; it also suggests that participants prefer not to report confidence values when the red indicator speeds up or during situation transitions.

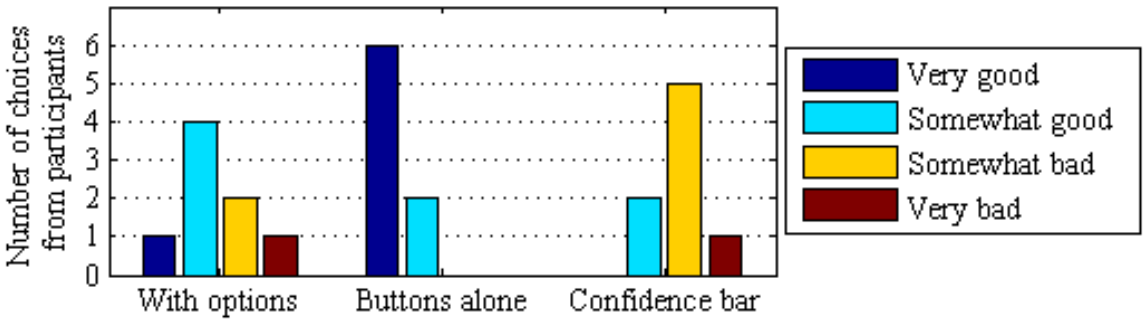

Figure 65: Self-rate of participants about their interaction performance.

Participant Self-Rating Most participants (75%) considered themselves very good when employing the interface with buttons alone. Second, although a confidence bar is preferred during slow indicators, most participants (62.5%) considered themselves somewhat bad when interacting with it. Third, and according to the self-evaluation, participants considered the interface with confidence options their second best alternative. Finally, from the eight participants, nobody self-rated him or herself as very good when using the interface with a confidence bar. The results from the self-rating question is consistent with observation made on the performance through the indicator-tracking score. Although, few positive conclusions may be drawn from the survey for the interface with confidence options, it does appear to have a better acceptance than the interface with a confidence bar.

6.4.3 Results from the Aggregation Algorithm

This subsection organizes the results from the Aggregation Algorithm in four additional subsections. The first subsection reports the mean percentages of Ruspini

partitions obtained among participants; it presents the results with both of the sensors combined, as well as separately per sensor. The second shows the distribution of the mean number of fuzzy sets per sensor among participants. The third provides the distribution of similarity scores in reference to the prototype granular structure. Finally, the fourth presents the performance of the Aggregation Algorithm for various data-set sizes based on the data sets collected from participants.

6.4.3.1 Mean Percentages of Ruspini Partitions

The distribution of mean percentages of Ruspini partitions for the resulting granular structure is presented in Figure 66. Additionally, these results can be analyzed separately per sensor, as shown in Figures 67 and 68 for the liquid level and temperature, respectively.

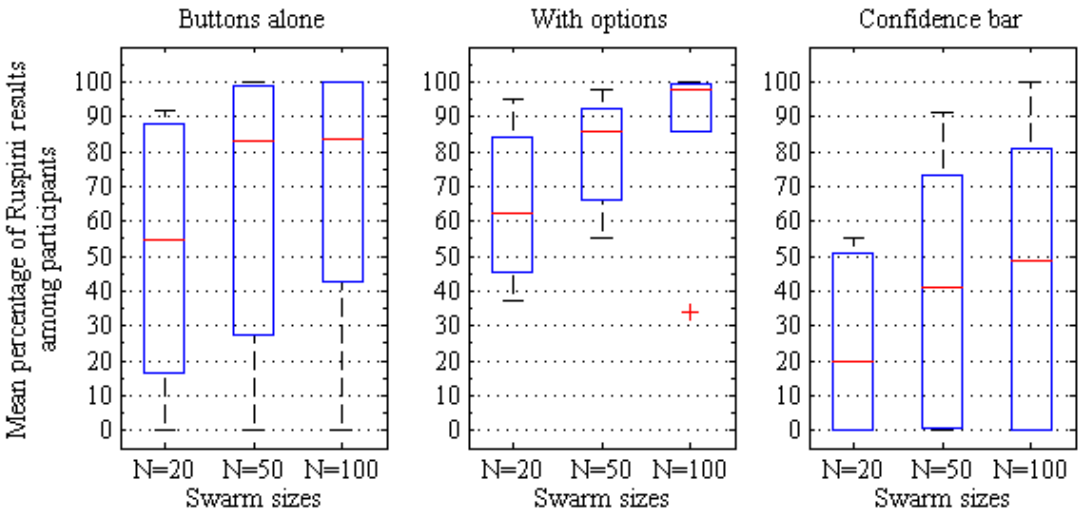

Figure 66: Distribution of the mean percentage of Ruspini partitions per swarm size combined for liquid level and temperature.

The mean proportion of Ruspini results is presented as combined (*i.e.* globally) in Figure 66 and per sensor in Figures 67 and 68. In a similar way, these results are discussed first as combined and then for the individual sensors.

Given the results obtained for both sensors combined, the reader may observe that the outcome is more consistent with data sets collected from participants employing

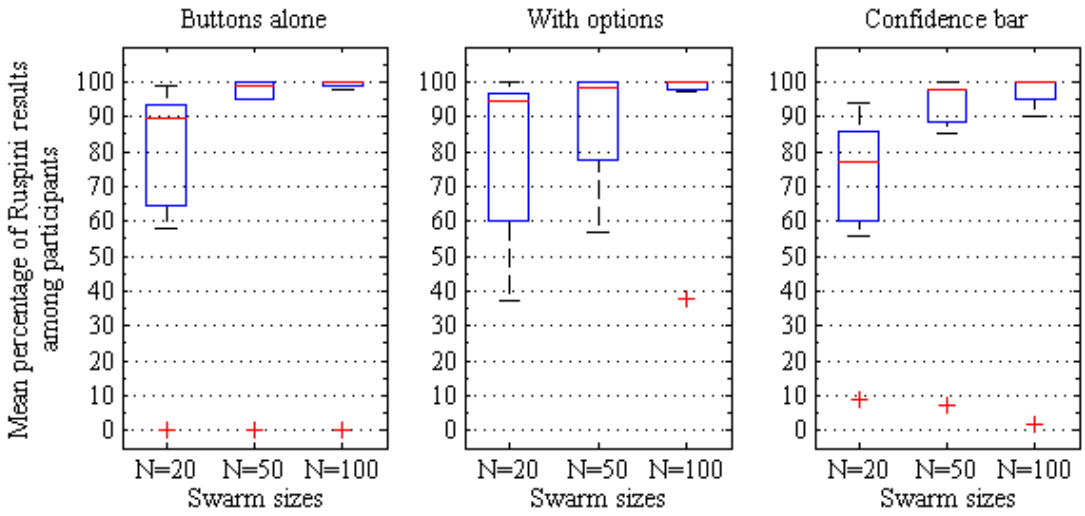

Figure 67: Distribution of the mean percentage of Ruspini partitions per swarm size for the liquid level.

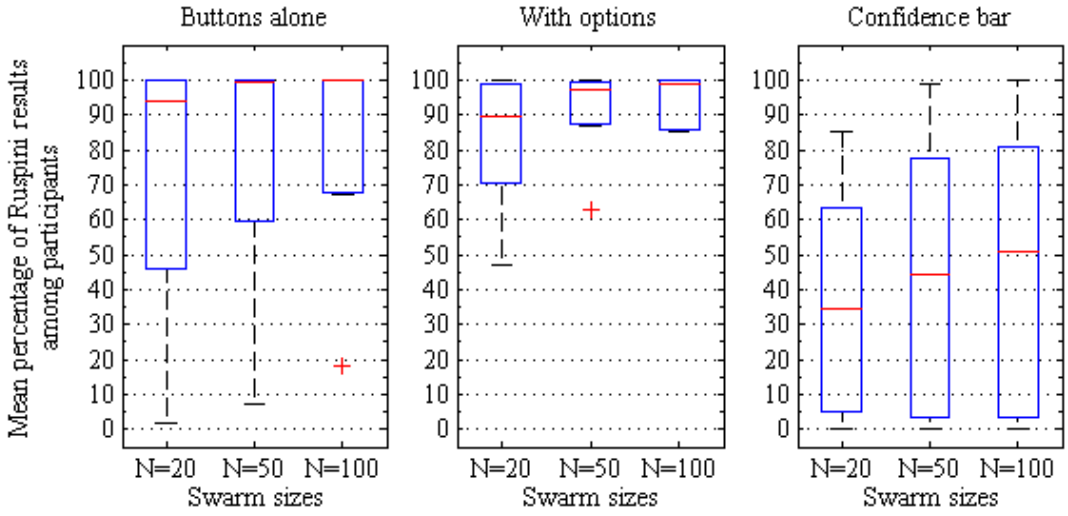

Figure 68: Distribution of the mean percentage of Ruspini partitions per swarm size for the temperature.

the interface with confidence options. As expected from the results obtained from the characterization in Chapter 5, the distribution of proportions of Ruspini results among participants improves as the swarm size increases from $N = 20$ to $N = 100$. With regard to the median, the best value achieved among the data sets produced by participants is obtained for the interface with confidence options and swarm size $N = 100$ with a median proportion of Ruspini results of 97.5%. Conversely, the poorest performance is obtained from most participants employing interface with confidence bar, comparatively achieving a median proportion of Ruspini results of 48.5% with $N = 100$. The least median value (20%) is obtained for the interface with confidence bar and employing $N = 20$. One question arising from these results is the influence of each sensor to the distribution of Ruspini results of the sensors combined. Therefore Figures 67 and 68 become of interest.

For the liquid level sensor (Figure 67), the Aggregation Algorithm evidently converges for increasing swarm sizes. Results are strongly consistent among data sets from participants for $N = 100$ with a maximum box size of 5% and especially for the interface with buttons alone with a box size of 1%. Also with $N = 100$, all interfaces share a median value of 100%, making such condition not useful to discriminate among results. However, for $N = 20$, the median values show some differences. The best median obtained for $N = 20$ is from the interface with options, with a median value of 94.5%, as compared to 89.5% and 77% for the interfaces with buttons alone and with confidence bar, respectively. Another observation is in the presence of outliers. Whereas for the interfaces with buttons alone and with confidence bar there are outliers for all values of N, the interface with options only presents an outlier for $N = 100$. Even though from the liquid level sensor the results seem to be close for the interfaces with buttons alone and with options, it is worth observing the same results for the temperature sensor in Figure 68.

For the temperature sensor (Figure 68), the convergence of the distribution of

Ruspini results is less evident for the three interfaces. In fact, such convergence may only be appreciated for the interfaces with buttons alone and especially for the interface with options. Such convergence may not be evident only from the box sizes, but mostly from the median. The best median value of 100% is obtained for the interface with buttons alone and $N = 100$. The second best median is 99% for the interface with options and $N = 100$. Even though the interface with buttons alone seems to achieve better median values, the box sizes of the interface with options show greater consistency in general with a maximum box size of 28.5% and a minimum box size of 12%. In contrast, the interface with buttons alone achieves a maximum box size of 54% and a minimum box size of 32%.

The ability to discriminate the proportion of Ruspini results obtained per sensor allows us to better evaluate the performance data sets obtained with various interfaces after processed through the Aggregation Algorithm. It also shows advantages in employing an interface with confidence options over other alternatives. These observations, combined with those from the interaction metrics suggest an advantage in having participants pay attention to their confidence level while reporting situation assessments than not doing so. More so, it also supports an argument for cognitive overload when employing a device that may demand excess attention from participants, *e.g.* an interface employing a confidence bar.

Although making observations on the distribution of Ruspini results may seem sufficient, it is important to exploit the capacity to analyze the number of fuzzy sets obtained as they are relevant to the corresponding number of fuzzy sets used in the prototype granular structure (presented in Subsection 6.1.4.2).

6.4.3.2 Mean Number of Fuzzy Sets per Sensor

Additional evidence is necessary to evaluate the performance of the Aggregation Algorithm processing data sets collected from humans. One such evidence factor is the

distribution of the mean number of fuzzy sets per sensor among participants. For this experiment, such distributions are plotted for the liquid level in Figure 69 and for temperature in Figure 70.

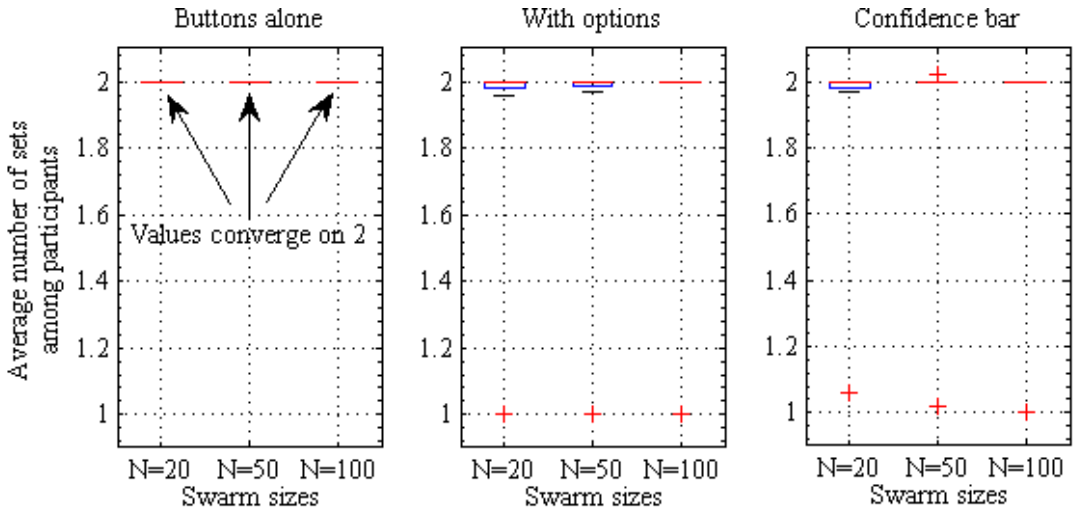

Figure 69: Distribution of the average number of sets per sensor for the liquid level.

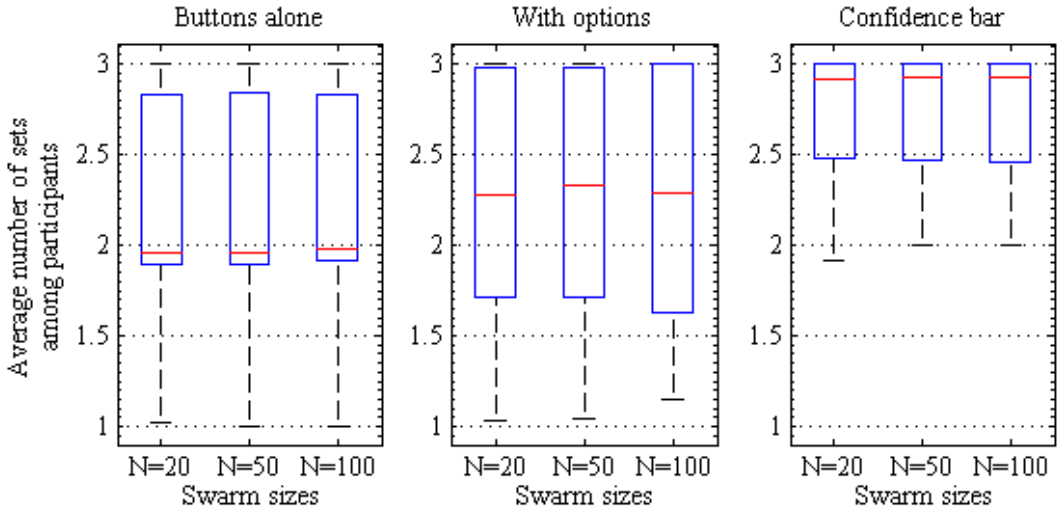

Figure 70: Distribution of the average number of sets per sensor for the temperature.

For the liquid level, the algorithm does not present any problem arriving at $k_1 = 2$ (using the notation from Subsection 4.1.1.1). However, a few outcomes from some participants did not achieve $k1 = 2$ when $N <= 50$ for interfaces including any type of confidence assessments. This is expressed by the presence of the boxes and

lower adjacent values. At least one participant was not consistent at distinguishing between situations relevant to the liquid level sensor; such inconsistency is evident by the inability of the Aggregation Algorithm to distinguish clearly between situations and thus arriving at a single fuzzy set, i.e. $k_1 = 1$.

As for the temperature sensor, the distribution of results among participants is more diverse with $k_2 \in [1, 3]$. This means that in a number of repetitions of the Aggregation Algorithm, some data sets obtained partitions that would not distinguish among situations, *i.e.* with $k_2 = 1$. Some other data sets would arrive at results that partially distinguish the situations, with $k_2 = 2$. Some others, however, would be able to distinguish and discriminate between the three situations defined for the temperature, achieving $k_2 = 3$. From the results displayed in Figure 70 it seems that, despite all the disadvantages of employing the interface with confidence bar, its results tend to be more consistent in achieving the goal value of $k_2 = 3$ (also refer to Figure 53, right hand side). The difficulty in assessing situations based on the temperature variable can be caused by the inability of participants to have a tactile sensation of the simulated temperature values. Another possible cause for inconsistencies in temperature assessments among participants can be the difficulty of establishing clear boundaries between situations. The liquid level variable does not present such challenge because it may be less difficult to establish the point in which it is more than half or less than half. Such observation begins to suggest the need for additional devices to facilitate the perception of values from indicators by human participants. One such device could be similar to the speed bugs used in aircraft cockpits to assist the pilot and co-pilot to establish and share information about speed velocities.

However, while some data sets may achieve both good Ruspini results and a good number of fuzzy sets for each sensor, it is worth exploring how similar is the resulting granular structure to the prototype. This exploration is performed by looking at the

similarity scores to the prototype.

6.4.3.3 Similarity Score to Prototype

The similarity score allows for comparing the contour resulting from taking the maximum membership value along the universe of discourse of the fuzzy sets obtained for each sensor and their distribution among participants. The distribution of the combined similarity score is obtained from the lowest of the sensor scores in each iteration. The results for the liquid level and temperature are presented in Figures 71 and 72, respectively. The similarity score for both sensors combined is presented in Figure 73.

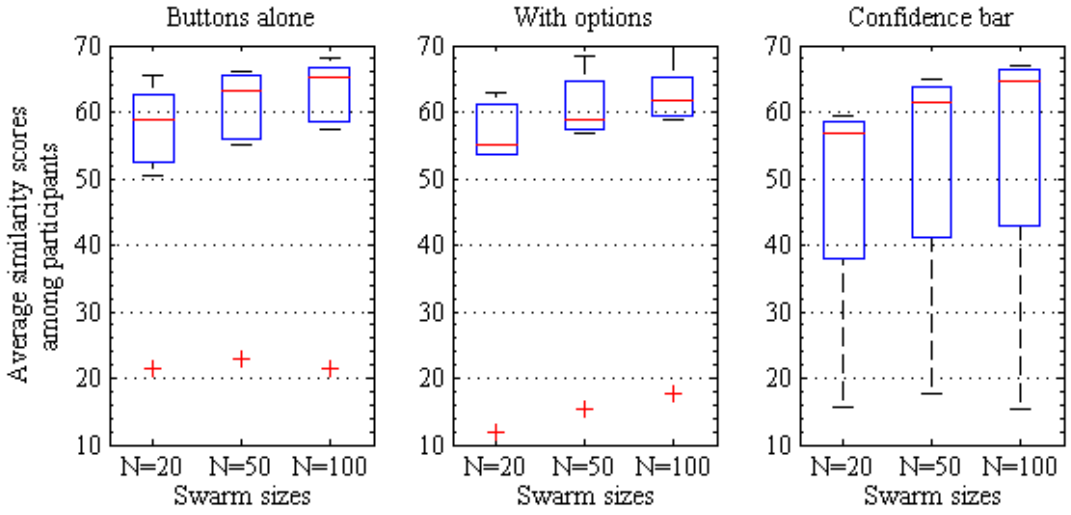

Figure 71: Distribution of scores to prototype for liquid level at 5% error margin.

For the liquid level sensor (Figure 71), the most consistent results are obtained for data sets collected with the interface with options for a maximum box size of 7.47% with $N = 20$. Nevertheless, the best median values are found in data sets obtained through interfaces employing buttons alone for a maximum median score of 65.25% with $N = 100$. Conversely, the less consistent results are obtained from employing interfaces with confidence bar for a maximum box size of 23.35% with $N = 100$. However, it is worth noting that, even if results from the interface with options are

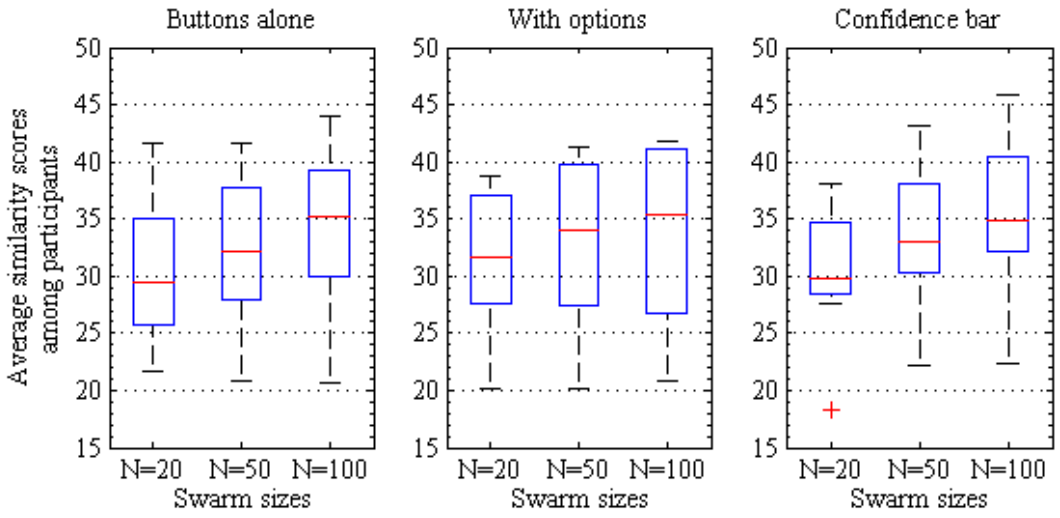

Figure 72: Distribution of scores to prototype for temperature at 5% error margin.

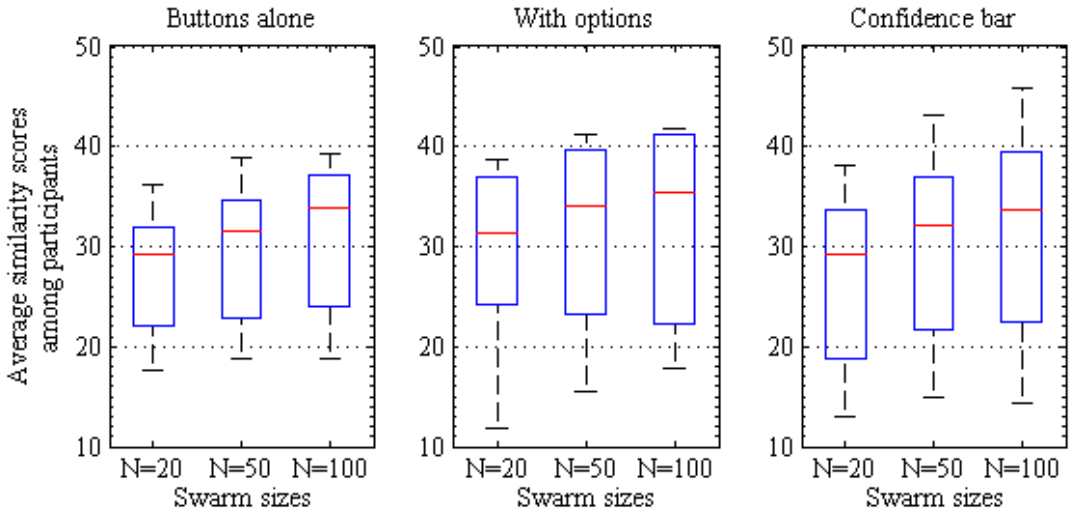

Figure 73: Distribution of scores to prototype for the minimum of both variables at 5% error margin.

more consistent, the median of those from the interface with confidence bar are second in achieving the highest similarity scores after the interface with buttons alone.

In the case of the temperature sensor (Figure 72) and for both sensors combined (Figure 73), the results exhibit a poorer performance than for the liquid level sensor alone with a maximum median value 35.42% for both the temperature sensor alone and for both sensors combined, for the interface with options and $N = 100$. They are in both cases distributed more evenly than for the liquid level sensor, which makes it difficult to make a comparison among various interfaces or swarm sizes. The results reflect that those fuzzy sets obtained for temperature are not similar to those from the prototype considering the 5% margin used in the calculation (refer to Subsection 6.3.2.3). If it was for the similarity scores of the temperature sensor alone, it would not be possible to distinguish which interface produced the best results. This decreased performance may be due to the difference among participants in their definition of what is hot, what is cold, and what is a nominal temperature for a hot beverage. This is one of the challenges of fuzzy logic in employing linguistic variables [155, 143]: the mapping from physical variables into the membership function of the linguistic variables may turn out to be considerably subjective. The results show a poorer perfomance for both sensors combined as well, because of the minimum operator obtained in their calculation (refer to Subsection 6.3.2.3). Once more, such results suggest the possible advantage of adding "speed bugs" to the data collection protocol as devices that could assist participants in achieving more consistency or a higher degree of agreement among them; cognitive aids supporting working memory may help to improve the distribution of scores among individuals.

An interesting question at this point is the following: What should determine the best interface for data collection: consistency (box size) or performance (the median)? From the results and observations made to all other dependence measures in this experiment, the answer favors consistency. This is because median values alone

do not provide a complete measure of the quality of the data sets among participants and the granular structures obtained. Hence, in this analysis, the box size is a useful tool to evaluate the outcome of processing the data sets through the Aggregation Algorithm, as they portray some degree of the quality of the data sets collected from participants. This observation becomes pertinent for the discussion that employs the data sets collected in this experiment for crowdsourced approaches to the aggregation of SKB's, which is to be presented in future work.

6.4.3.4 Percentage of Ruspini Results for Various Data-Set Sizes

An important exploration for the validation of the characterization presented in Chapter 5 is the distribution of Ruspini results for data sets of various sizes containing situation assessments provided by human participants. Such exploration is presented in Figure 74. Given that this experiment made use of three interfaces, the plots compare the performance of the Aggregation Algorithm for the three cases and also includes results for the swarm sizes considered: $N = \{20, 50, 100\}$.

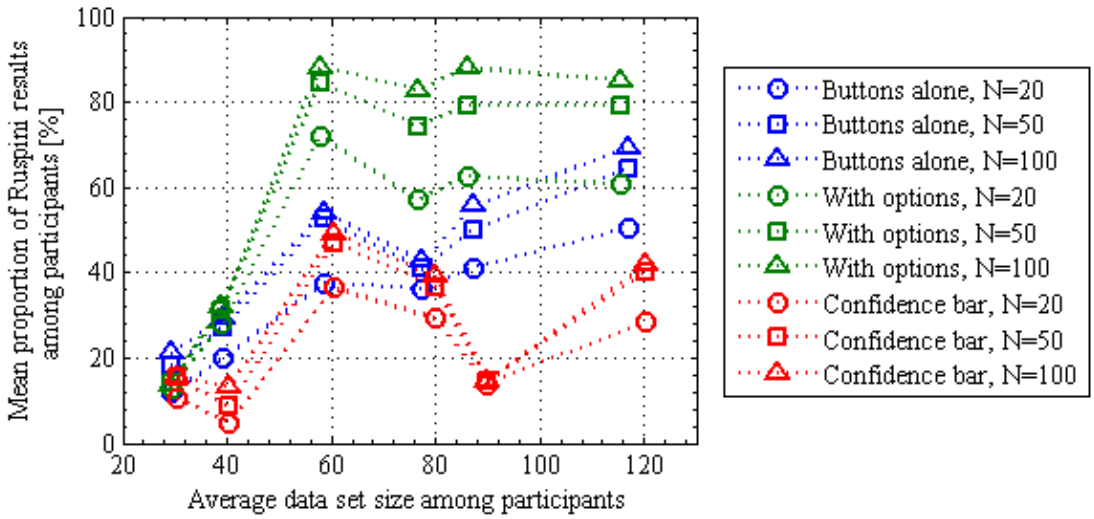

Figure 74: Mean proportion of Ruspini results among participants for various data set sizes with three interfaces.

In addition to the comparison of results for the three interfaces, it was interesting

to see the distribution among participants of Ruspini results for various data-set sizes for the interface with options and $N = \{20, 50, 100\}$. A plot for each swarm size with such distributions is presented in Figure 75. The results are expressed as a function of the percentage of data set completeness, as described with Table 12.

The results obtained in Subsection 6.4.3.1 were repeated for fewer data points than those contained in the original data sets. This was achieved by truncating the size of the data sets (refer to Table 12). Each participant achieved an individual performance in tracking the red indicator. Therefore, each participant was able to collect a number of data points employing the three interfaces considered. The independent variable in Figure 74 is the average data-set size among participants for each interface. The dependent measure is the mean proportion of Ruspini results among participants for each data-set size considered (refer to Table 12).

The main purpose of the results displayed in Figure 74 is to validate the performance obtained for the characterization experiment in Chapter 5. It does so by testing the performance of the mean proportion of Ruspini results for data sets sizes containing fewer data sets and observing the transition from lower to higher mean proportions of Ruspini results. Each color in Figure 74 corresponds to a different interface. The three symbols that describe the results (circle, square, and triangle) correspond to swarm sizes of 20, 50, and 100 particles, respectively. The results obtained show a much better performance for the interface with options. There is a sharp transition in the mean proportion of Ruspini results between the average data-set sizes of 39 and 58 data points. Something similar appears to occur for the other two interfaces (blue and red), but they exhibit a poorer performance.

Interestingly, when compared to the results of Subsection 6.4.3.1, the results obtained in this case support the conclusion that the interface with options exhibits better performance in general than the other two. In addition, these results also support the observation that the second best performance is obtained from the data

sets collected with the interface with buttons alone, finally leaving the interface with confidence bar as the least performing of the three. These observations are especially true when considering the values for the maximum data-set sizes in the plot for each case. These results also show the repeatability of the distribution of results. Evidence from this experiment suggests a convenient balance in the cognitive load of participants from the interface with options, providing a higher demand of attention than the interface with buttons alone, but without reaching an attention overload as the interface with confidence bar.

Finally for this analysis section, the detailed distribution of results among participants for the interface with options and various swarm sizes was presented in Figure 75. The figure highlights the statistical convergence of results toward 100% for increasing data-set sizes and for three swarm sizes. From $N = 20$ to $N = 100$, results show a transition of performance taking place with data sets at 33% of completeness. After the transition, i.e. for data-set sizes with 50% or greater completeness, the median value converges to the performance value that corresponds to the specific swarm size. As such, the best performance is obtained for $N = 100$ with data set complenetess of 75% for a median value of 97%. Of course, this does not mean that a greater data-set size will not perform as well necessarily, but such variability should instead be attributed to the number of participants considered or other defects in the data collection process relative to the coverage of the sensing space by the simulation of the dynamic system.

6.5 Summary

In conclusion, the following observations try to summarize some of the important aspects from this experiment. First, that the aggregation results may be analyzed in a combined fashion or per sensor. The Aggregation Algorithm allows for in-depth evaluation of results and provides opportunities to evaluate data collection strategies.

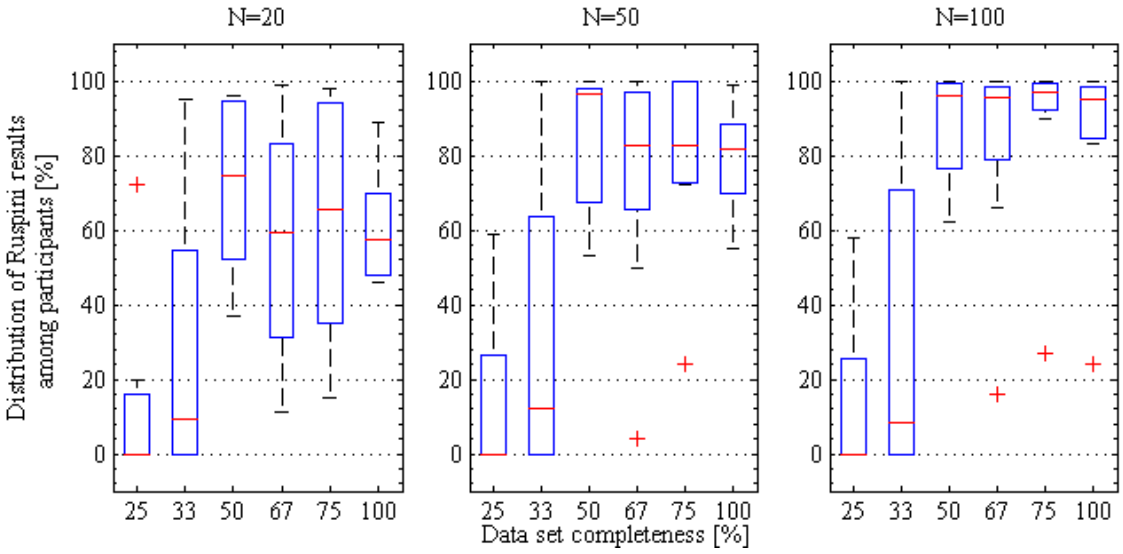

Figure 75: Distribution of Ruspini results among participants for the interface with options, for various swarm sizes.

Second, the best performance of the Aggregation Algorithm was obtained for the interface with confidence options and greater swarm sizes, i.e. N=100. Even though it was expected that a larger swarm size would improve performance, there was no expectation as to which of the interfaces would be better. This was true both for liquid level and temperature variables. Third, artifact support during data collection to distinguish among situations may help improve proportion of Ruspini results and other performance metrics. These artifacts include markers (like "speed bugs"), color scales, and references by convention. Fourth, this experiment validates the results of the characterization experiment. Finally, the question of the minimum number of data points necessary to ensure the best performance of the Aggregation Algorithm will be looked at the Chapter 8.

Advantage and Limitations The main advantage of the experiment presented in this Chapter is the use of data sets containing situation assessments collected by real human participants. It shows the performance of the various dependence measures considered as distributions among participants. Such distribution shows the challenge

of obtaining good measures of performance from the interaction of the participants with the data collection interfaces. However, the distributions also show the capacity of the Aggregation Algorithm to obtain considerably better results when more computing power is employed. The main limitations of the work conducted in this Chapter are two: The first limitation has to do with the assumption that the dynamics of the system are able to cover most of the sensing space available. This may not be the case in real systems, more specially if a large number of sensors is considered. Another limitation of the work conducted in this Chapter and on this manuscript has to do with the omission of possible various levels of granularity resolution. This means that different situations in one dimension may have different ways to define situations in other dimensions. This work may be addressed by elaborating on concepts of granular computing and looking at hierarchical relationships in the definition of situations.

CHAPTER VII

CROWDSOURCED SITUATION KNOWLEDGE BASES

This chapter elaborates on a sensor data fusion approach that collects discrete situation assessments from human experts and sensor measurements to generate a so-called "coherent" representation of their SKB. In particular, this chapter combines situation assessments from multiple human experts with the purpose of obtaining a crowdsourced SKB. This is accomplished using a statistically-based optimization method to compress data from experts and develop a granular representation of the SKB. The techniques employed are applied either before data compression or after; the latter compares two alternatives with granular computing. Results show the advantage of obtaining SKB for individual experts and combining them into a single crowdsourced SKB by means of granular computing. The ability to successfully obtain crowdsourced SKB's enables operators to detect anomalies, avoid human error, and increase the overall reliability of human-automation systems. In particular, the methodology employed explores two distinctive ways to combine data sets collected from crowds of human experts to generate a crowdsourced SKB. Results exhibit a clear advantage with techniques in granular computing [145, 59, 144] to overcome inconsistencies and disagreements in crowdsourced data sets. In such a way, this work aims to address the imperfections present in data sets containing situation assessments collected by humans, which are in most cases will not exhibit the coherence of a Ruspini partition. Instead, data sets collected by humans will contain inconsistencies from individuals in their definition of situations considered at different times. Furthermore, it is very reasonable to expect that there will be disagreements in the

assessments collected by a crowd of human experts. Such problems are the motivation to explore various data-set combination techniques in the effort to obtain crowdsourced situation knowledge bases.

7.1 Background on Crowdsourcing and Human Sensing

Crowdsourcing and human sensing are two main areas of application in the field of *human computation* (HC) [156], which according to literature is "a paradigm for utilizing human processing power to solve problems that computers cannot yet solve" [157, 158]. The idea of HC finds an early use in work related to philosophy and psychology during 1838 [159] and is adopted in the field of computer science in 1950 [160]. The goal of HC is to harmonize the work of human and computer processors, promoting the integration of humans and machines that share a common problem solving objective [156]. Participants may have a role in HC systems as *requesters* or as *workers*.

Because of its breadth of applications, HC is an inherently multidisciplinary topic. Disciplines that contribute to its development include sociology, behavioral economics, cognitive psychology, software engineering, human-computer interaction (HCI), network analysis, security & privacy, workflow management, and knowledge discovery & data mining. The following subsections elaborate on the crowdsourcing and human sensing applications of HC for their relevance to this research. Other applications include the so-called *games with a purpose* (GWAP's), in which problems in need of a solution are embedded in gaming experiences that are found to be enjoyable by users; and mobilization, which goal is to distribute information to crowds with the aim of having an influence on them and triggering actions [156].

7.1.1 Crowdsourcing

The idea of crowdsourcing was first used by Jeff Howe in 2006 as the action of "outsourcing a task that is traditionally performed by an employee to a large group of

people in the form of an open call" [161]. Crowdsourcing increasingly takes advantage of the widespread availability of Internet access [162] and the variety of computing platforms and architectures [156]. As a field of application of HC, crowdsourcing can be classified according to the following [158]:

- *Motivation of participants*: May be caused by a reward, altruism, enjoyment, reputation, or implicit work.
- *Quality control of data sets*: It may be based on the nature of agreements reached by participants, economic models, defensive task designs, redundancy, statistical filtering, or a reputation system.
- *Aggregation of data sets*: This includes the bare collection of inputs, searches, methods in computational intelligence, or iterative improvement.
- *Human skills of participants*: For example, human perception and natural language.
- *Process order*: Depends on the sequence followed between the computer system, the worker, and the requester to achieve the goal of the crowdsourced system.
- *Task-request cardinality*: Is defined according to how workers are assigned to one or more tasks, *e.g.* one-to-one, many-to-many, many-to-one, few-to-one.

Examples of crowdsourced systems are the Amazon Mechanical Turk, iStockPhoto, 99designs, Innocentive, and Microtask.

7.1.2 Human Sensing

Human sensing consists of assigning data collection tasks to groups of participants. They are supported by information and communication technologies (ICT's) and the increasing availability of sensors to collect real-time data relevant to a decision support system or an emergency management system. Sensors commonly used are,

for example, the global positioning system (GPS), camera, barometer, light sensor, and compass, which are nowadays commonly included in mobile platforms. The availability of such devices enables the collection of physical data with human sensed observations. Areas of application are mostly found today in environmental protection for air and water quality control, monitoring of invasive species, and noise pollution [156]. Other applications make use of social media platforms, such as Twitter, to provide geo-tagged information using controlled terminology to address particular events, e.g. "power outage," "pest control," or "flooding alert." In this way, this research finds support in human sensing and computation to explore the ability of crowds to provide human sensed observations relevant to situation awareness.

7.2 Methodology

In this research, we seek to contrast results from combining data sets collected from individuals while obtaining a crowdsourced SKB from them. The goal is to distinguish a technique by which data sets from individuals may be combined in a crowdsourced data set and processed through the Aggregation Algorithm, presented in Subsection 4.2.1, to obtain a SKB that is comparable to a prototype granular structure. This section presents the data-set-combination techniques employed and the dependence measures used to evaluate and compare results. Subsection 7.2.1 describes the data-set-combination techniques and Subsection 7.2.2 explains the dependence measures used.

7.2.1 Data-Set-Combination Techniques

The data-set-combination techniques considered can be characterized by the sequence in which they are applied in relation to the Aggregation Algorithm; i.e., the data-set-combination techniques are applied before the execution Aggregation Algorithm or afterwards. In each case, the data sets contain different information. In the former, data sets contain either the raw input data collected from participants or a

representation of their collective input in the form of median values. In the latter, the data sets are a collection of the SKB's of all participants; their SKB's are obtained from applying the Aggregation Algorithm to their raw data sets individually. The following subsections elaborate on each one of these data-set-combination techniques.

7.2.1.1 Data Sets Before Aggregation: Working with Raw Data Input

There are two data-set-combination techniques considered before aggregation: (1) merging data sets and (2) taking the median values from participant inputs.

Merged Data Sets This variable consists of making use of the recorded simulation time to merge together the data collected from individual participants. It results in a data set containing a total number of situation assessments equivalent to the sum of the individual number of situation assessments reported by participants. Data sets are merged for each one of the three user interfaces employed in the experimental design discussed in Section 6.1. The resulting data sets are then processed through the Aggregation Algorithm and performance metrics are obtained for the resulting granular structures.

Median of Participants This variable consists of comparing individual data inputs collected from participants for each data collection event driven by the red indicator. For each blink event of the red indicator, situation assessments of participants are compared and a median is obtained from them. Each situation assessment is characterized by a situation selection, a confidence level, and a selection time. For each of these values, the median is obtained and considered as the collective choice. The total number of situation assessments is equivalent to the number of red indicator events for which there is at least one situation assessment reported from a participant.

7.2.1.2 After Aggregation: Employing Granular Computing

As mentioned above, data sets processed after aggregation are a collection of the SKB's obtained for individual participants. Those collections of SKB's are then processed through a granular computing operation similar to the coherence operation presented in Section 4.2.1.3. The result is a SKB of the same dimensions but containing new parameters describing a new granular structure. Such granular structure is composed of fuzzy sets that represent an agreement of situation assessments among participants for each sensor considered. Their performance metric is obtained for comparison with other data-set-combination techniques.

The SKB's of individuals are obtained by executing the Aggregation Algorithm on their individual raw data sets with a frequency of 100 repetitions and for $N = 100$ only. The parameters describing the granular structures of situation assessments of individual participants are the average of the parameters obtained from the 100 repetitions of the Aggregation Algorithm on their respective data sets. The following paragraph explain the difference between two variations of the granular computing operation used in this experiment.

Nominal Coherence Operation This variation employs an operation identical to the coherence operation in Subsection 4.2.1.3.

Less Tolerant Coherence Operation This variation modifies the similarity and adjacency operation of Subsection 4.2.1.3. For this variation, the similarity and adjacency operations no longer make use of the average of the parameters describing fuzzy sets to search for similar fuzzy sets as expressed in Equation 18. Instead, it searches for all fuzzy sets that comply with $b_s < c_r$ and $c_s > b_r$, with $P_r = [a_r, b_r, c_r, d_r]$ being a reference set during the search and $P_s = [a_s, b_s, c_s, d_s]$ all other fuzzy sets searched in the granular structure for a given sensor (refer to Subsection 4.2.1.3). All other

characteristics used in the coherence operation remain unaltered.

7.2.2 Dependence Measures

The performance metrics used to analyze the performance of the algorithm are the percentage of Ruspini partitions among participants for each interface, the number of fuzzy sets per sensor, and the score of similarity between the granular structure obtained from the algorithm and the prototype granular structure.

7.2.2.1 Before Aggregation Only

Percentage of Ruspini Partitions This performance metric is executed for the technique combining data sets before the Aggregation Alorithm, for each interface. Each time the result complies with the Ruspini condition of Equation 12, the metric adds one percentage point to that particular execution under those conditions. The results are tabulated as the percentage of Ruspini partitions for the crowdsourced data set for each interface.

7.2.2.2 Before and After Aggregation

Similarity Score to Prototype The goal of this performance metric is to compare the maximum membership values of the resulting fuzzy sets for each sensor with those of the prototype granular structure and evaluate how similar they are. An illustration of this performance metric is presented in Figure 76.

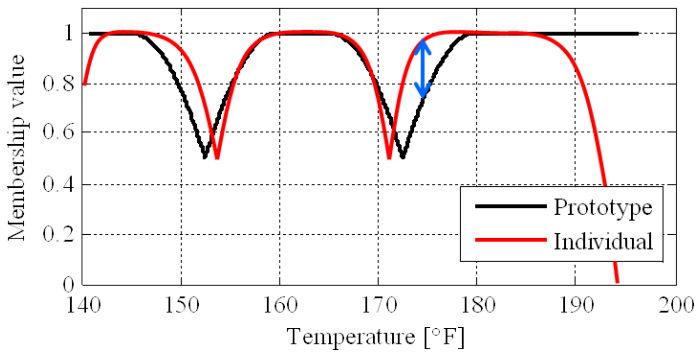

Figure 76: Illustration of the measure of similarity between partitions maxima.

The similarity score $S_p\%$ takes 1000 points uniformly distributed along x_i (as defined in Section 4.1.1.1) between parameters $\min(a_{x_i})$ and $\max(d_{x_i})$ and applies Equation 29 for $i = 1, \ldots, n$; the fuzzy sets $\alpha = 1, 2, \ldots, k_i$ and those of the corresponding partition $\alpha_p = 1, 2, \ldots, k_p$ of the prototype granular structure. The metric adds a tenth of a percentual point to the score every time that $\left|\max\left(\mu_{X_i^{\alpha_p}}\right) - \max\left(\mu_{X_i^{\alpha}}\right)\right| \leq 0.05$.

$$S_p\% = \frac{\sum \left|\max\left(\mu_{X_i^{\alpha_p}}(x_i)\right) - \max\left(\mu_{X_i^{\alpha}}(x_i)\right)\right|}{10} \tag{29}$$

As with previous metrics, the results are tabulated for each sensor separately and both sensors combined, for each interface, and for each swarm size if the case applies.

Number of Fuzzy Sets per Sensor For each result, the number of fuzzy sets per sensor is recorded. As with other metrics, the results are tabulated for each sensor, for each interface, and for each swarm size if the case applies.

7.3 Experiment Data

This section illustrates the data-sets used in this experiment. For data sets combined before the Aggregaton Algorithm, datasets are presented in their raw form as they compare to the situation-rich signals generated from the prototype granular structure. Data sets combined after the Aggregation Algorithm show the collection of fuzzy sets contained in the granular structures obtained for each individual.

7.3.1 Data Employed Before Aggregation

As mentioned above, the data sets obtained before the Aggregation Algorithm are two: the first contains the data sets from individuals merged into one, while the second is obtained from the median of individual situation assessments of participants in each event of the red indicator.

7.3.1.1 Merged Data Sets

Figures 77, 78, and 79 contain the data sets merged from individual participants for each interface. The six plots contained in each of the three figures describe the input of participants for each situation considered. Their inputs are displayed as pulses of various colors illustrating the raw activity of the crowd of participants.

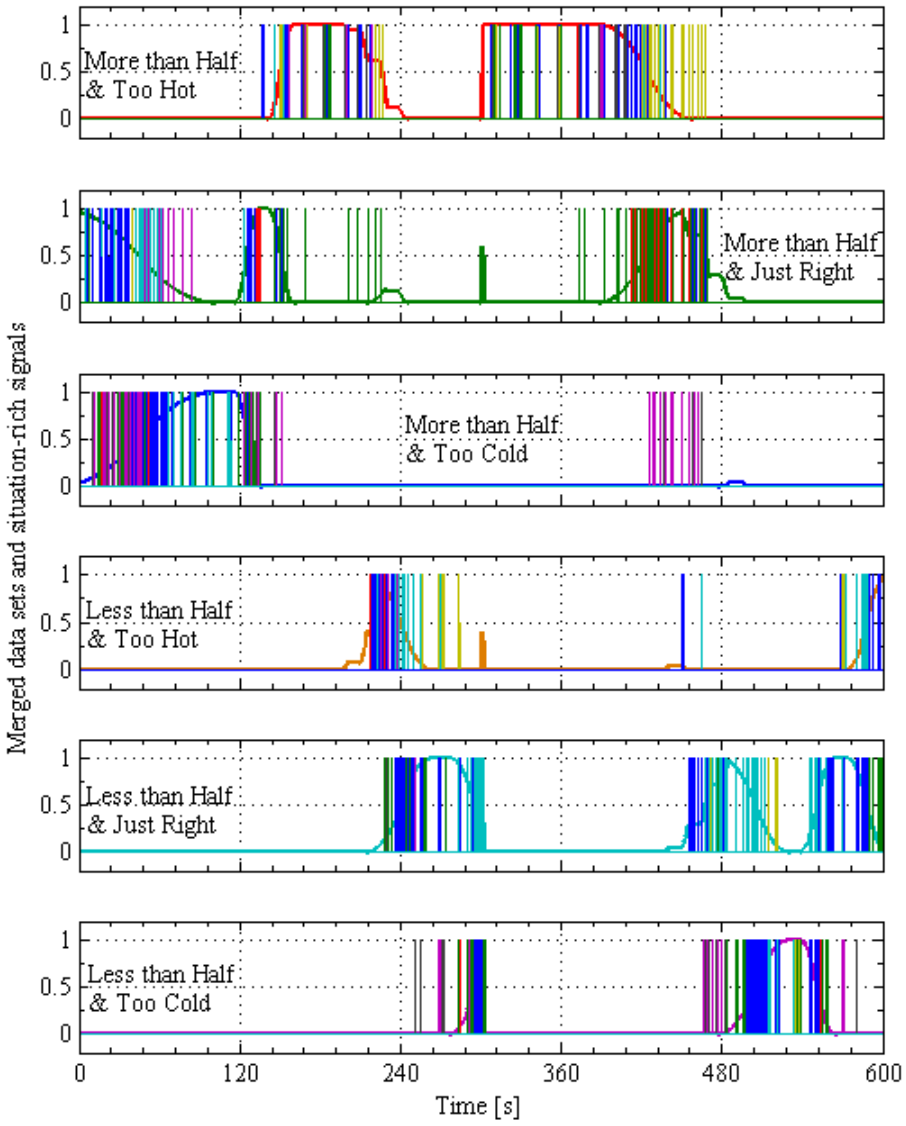

Figure 77: Merged datasets collected through the interface with buttons alone.

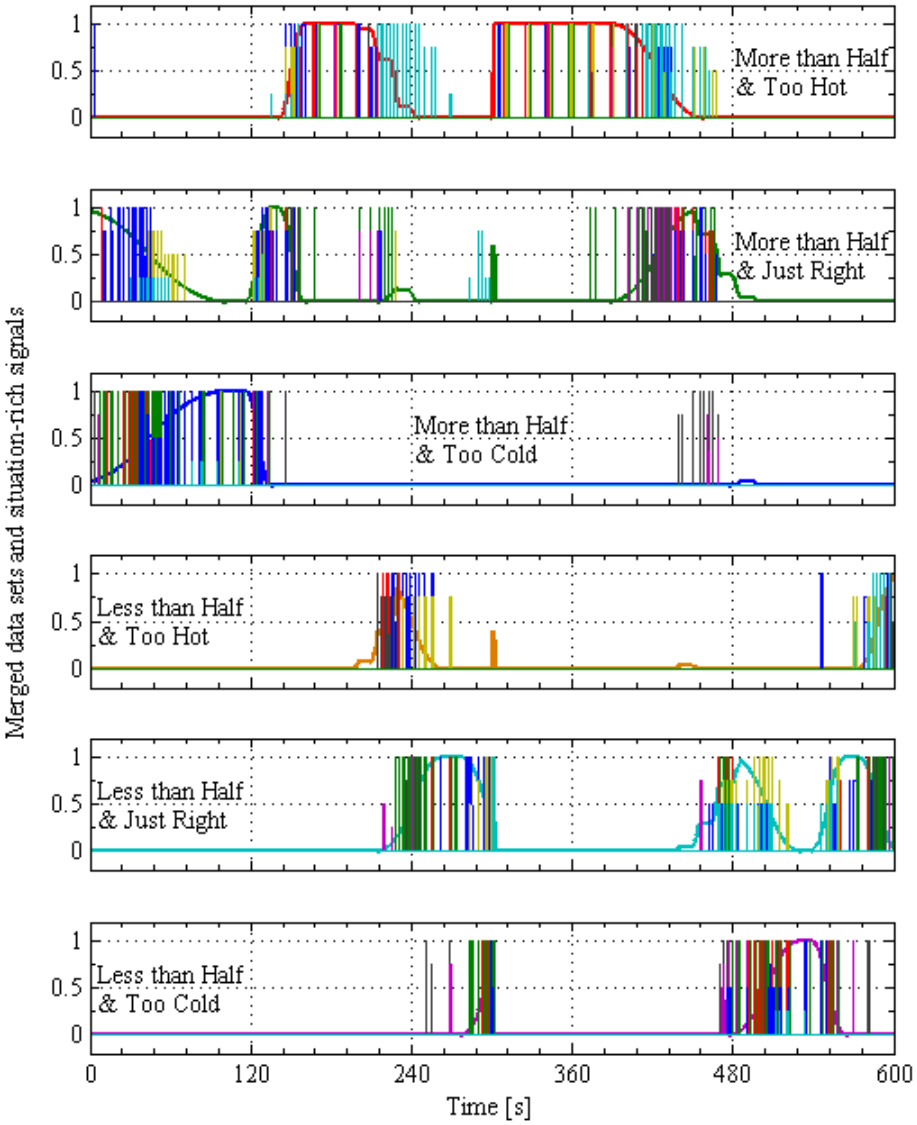

Figure 78: Merged datasets collected through the interface with options.

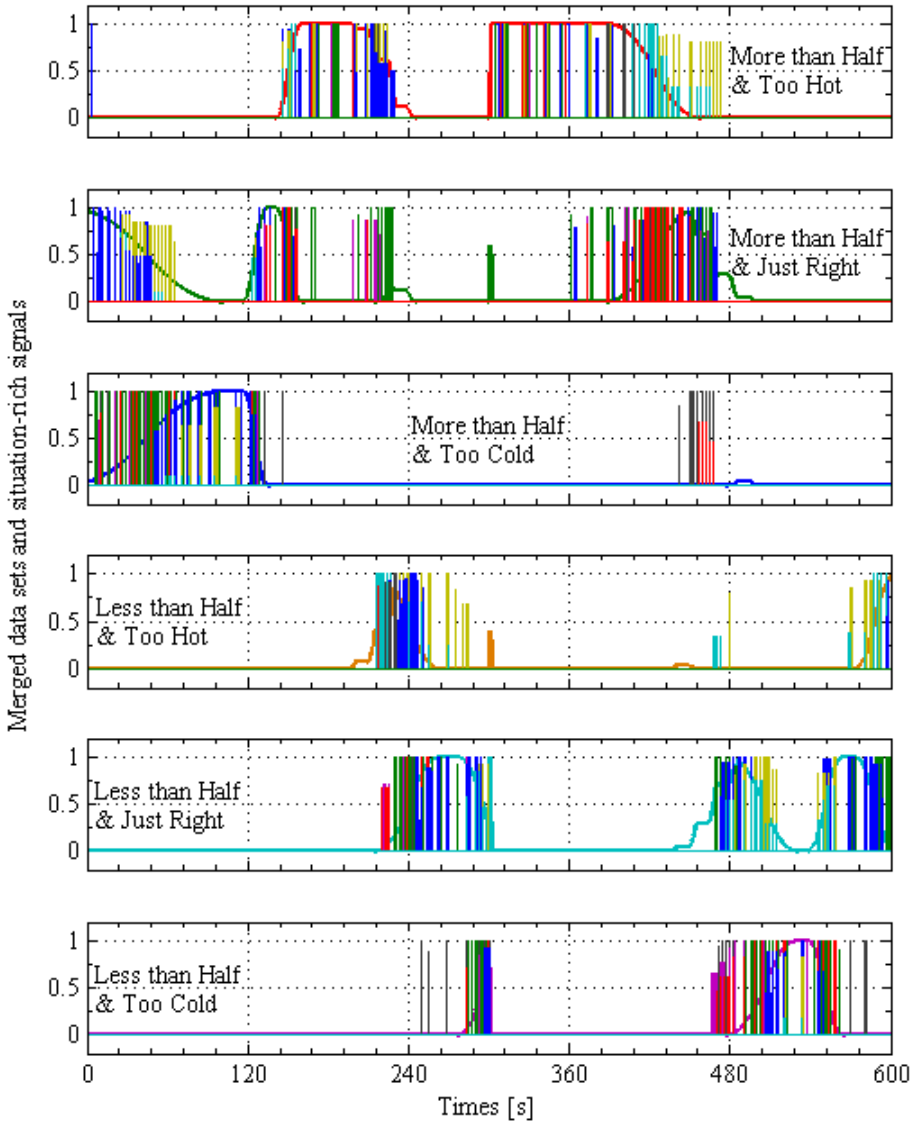

Figure 79: Merged datasets collected through the interface with confidence bar.

7.3.1.2 Median of Participants

Figures 80, 81, and 82 contain the data sets calculated with the median from individual choices per red indicator event for each interface. The six plots contained in each of the three figures describe the median situation assessment from participants for each situation considered. Their inputs are displayed as pulses in a single color, illustrating the combined activity of participants.

7.3.2 Data Employed After Aggregation

The data sets combined after the Aggregation Algorithm are a collection of granules obtained from the raw data sets of each participant as described in Subsection 7.2.1.2. The data sets used after Aggregation are the same for both data-set-combination techniques considered. This section illustrates the data sets employed by plotting them for each of the interfaces used for data collection. Two plots are presented in each figure for each interface. The fuzzy sets obtained from all participants for the liquid level sensor are presented on the left-hand side; the fuzzy sets for temperature are shown on the right-hand side. Figures 83, 84, and 85 show a representation of the granular structure obtained with the interface with buttons alone for all participants combined.

7.4 Results and Analysis

This section presents the results obtained from applying the methodology of Section 7.2 to the experiment data of Section 7.3. It is organized to match the presentation of the experiment data, dividing the section in two parts: before aggregation and after aggregation. The results provide the values obtained for the dependence measures described in Section 7.2.

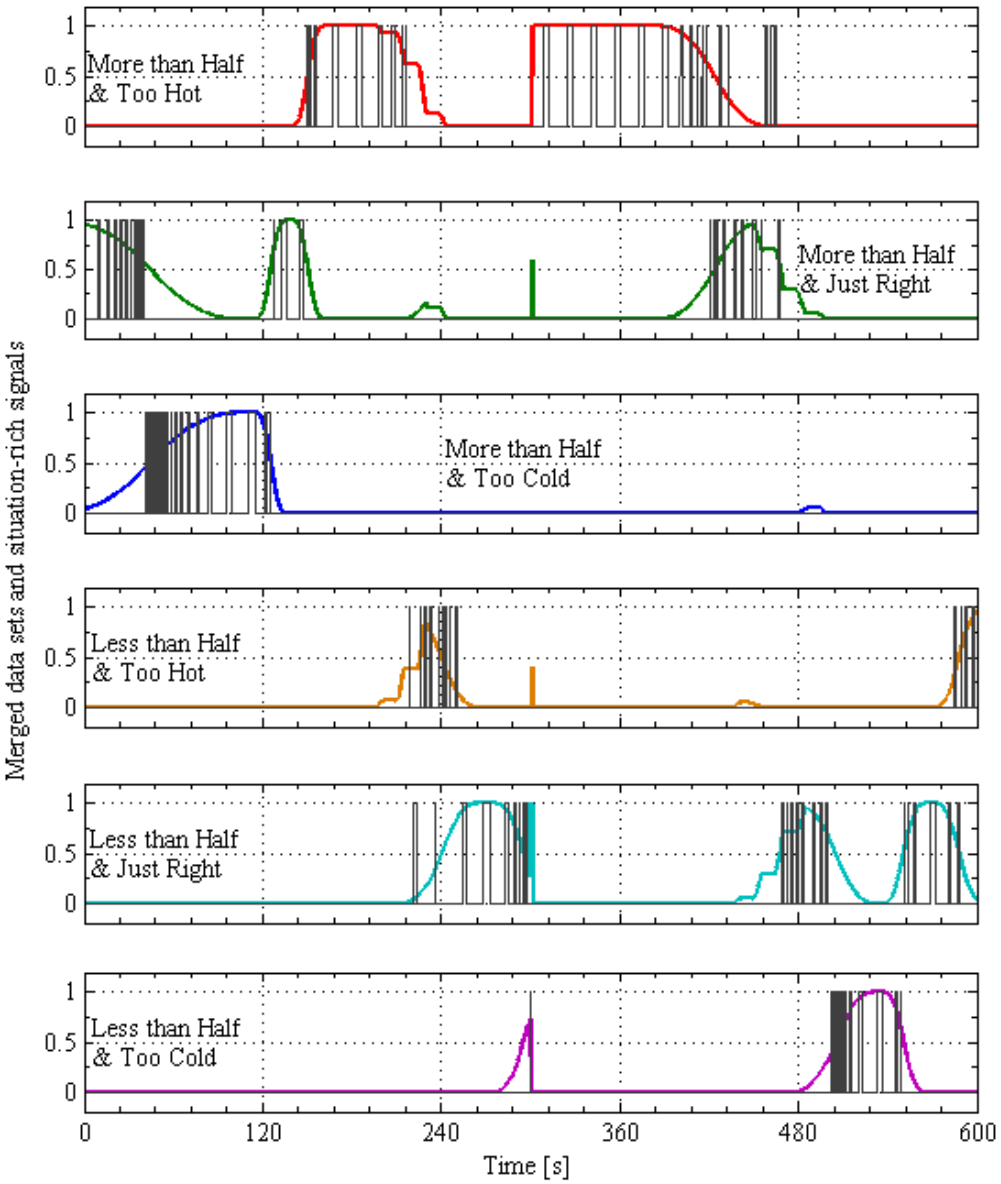

Figure 80: Median of input collected from participants through the interface with buttons alone.

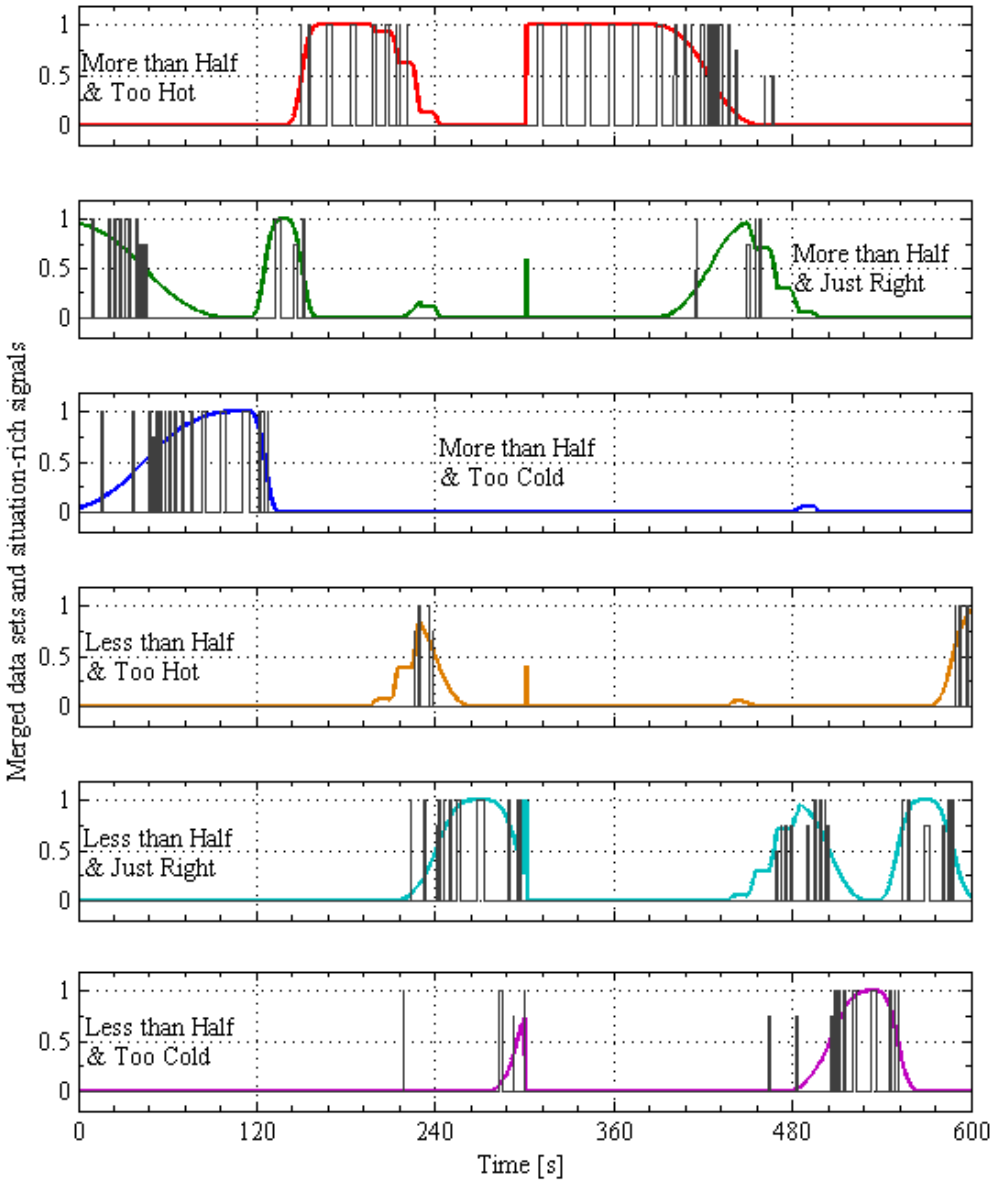

Figure 81: Median of input collected from participants through the interface with options.

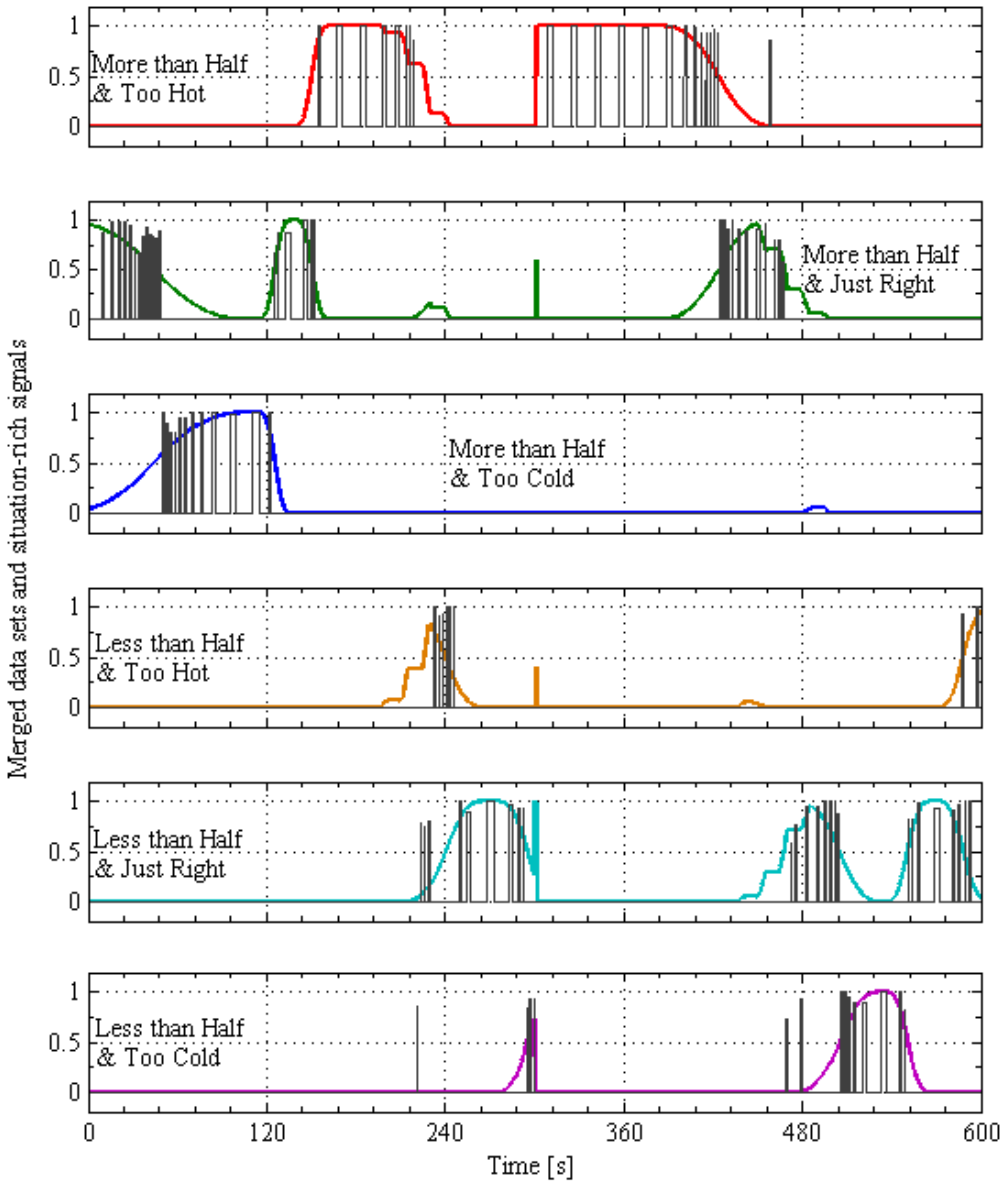

Figure 82: Median of input collected from participants through the interface with confidence bar.

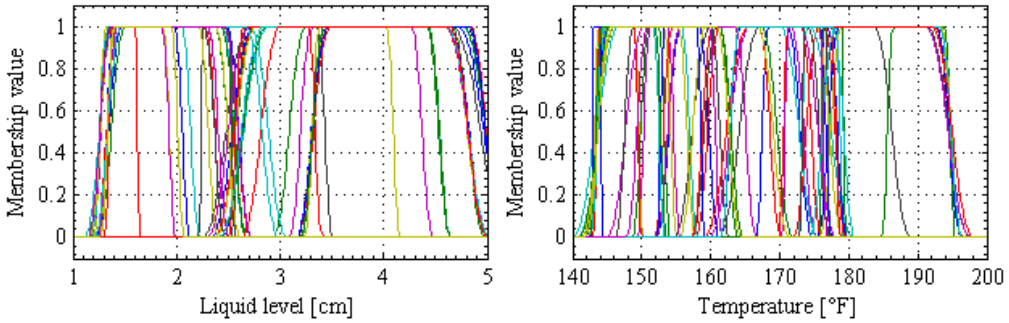

Figure 83: Individual granules obtained from participants employing an interface with buttons alone.

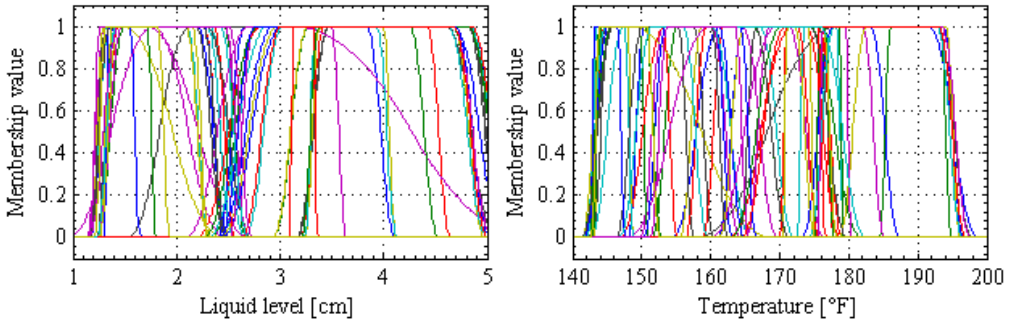

Figure 84: Individual granules obtained from participants employing an interface with options.

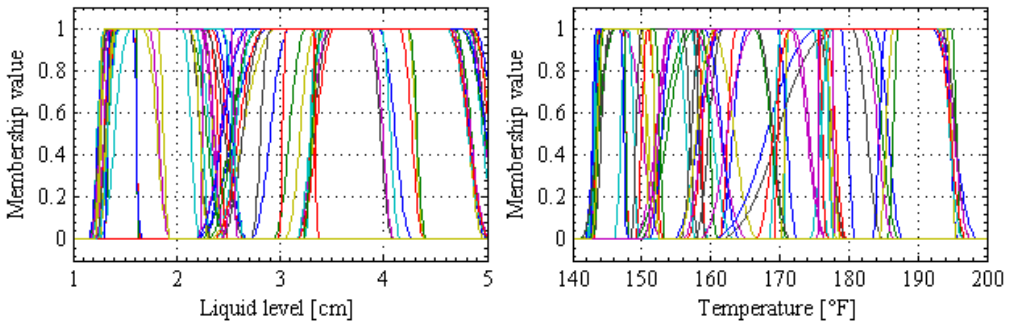

Figure 85: Individual granules obtained from participants employing an interface with confidence bar.

7.4.1 Results from Data Sets Combined Before Aggregation

Tables 16 through 21 present the results obtained with data sets combined before aggregation. Tables 16, 17, and 18 correspond to results from merged datasets, while Tables 19, 20, and 21 belong to the results of the data sets with the median of the input of participants. Each table contains the values obtained for the dependence measures presented in Subsection 7.2.2 out of 100 repetitions of the Aggregation Algorithm on the corresponding data set. The tables organize the following performance metrics in each column: the percentage of Ruspini results per sensor and the total value for sensors combined, similarity score to prototype per sensor and the total score for sensors combined, and the number of fuzzy sets per sensor and for sensors combined. The rows of the tables correspond to the swarm size used to run the 100 repetitions of the Aggregation Algorithm, *i.e.* $N = \{20, 50, 100\}$.

7.4.1.1 Results with Merged Data Sets

The results from merged data sets collected with the interfaces with buttons alone, with options, or with confidence bar are presented in Tables 16, 17, and 18, respectively.

Table 16: Results with merged data sets for interface with buttons alone.

	R_1	R_2	R_T	S_1	S_2	S_T	k_1	k_2
N=20	98	100	98	55.53	20.93	20.88	1.93	1.00
N=50	100	100	100	60.25	22.68	22.68	1.97	1.00
N=100	100	100	100	63.20	24.29	24.29	2.00	1.00

Table 17: Results with merged data sets for interface with options.

	R_1	R_2	R_T	S_1	S_2	S_T	k_1	k_2
N=20	100	100	100	20.84	20.95	19.32	1.00	1.00
N=50	100	100	100	24.22	21.54	21.16	1.00	1.00
N=100	100	100	100	27.34	22.08	22.04	1.00	1.00

For the interface with buttons alone, Table 16 highlights the high frequency of Ruspini results for all sensors and for its total value, *i.e.* R_1, R_2, and R_T. Such high

Table 18: Results with merged data sets for interface with confidence bar.

	R_1	R_2	R_T	S_1	S_2	S_T	k_1	k_2
N=20	96	100	96	61.21	21.84	21.80	1.98	1.00
N=50	100	100	100	67.13	22.16	22.16	2.00	1.00
N=100	100	100	100	69.02	22.44	22.44	2.00	1.00

frequency of Ruspini results indicate that coherence was achieved by the Aggregation Algorithm by applying the coherence operation of Subsection 4.2.1.3. This would translate to a desirable result if the partition was composed of at least two fuzzy sets, i.e. $\{k_1, k_2\} > 1$. Such is the case for the liquid level sensor, *i.e.* for R_1 and k_1, for which minimum values obtained with $N = 20$ are 98 [%] and 1.93, respectively. However, a different result is obtained for the temperature sensor; in this case the frequency of Ruspini results R_2 is maximum (100%) for all values of N, but the number of sets obtained in every case is $k_2 = 1.00$. This is evidence of inconsistencies in the situation assessments provided by participants. This means that participants had different mappings for what hot or cold means, and thus, their collective inconsistency in assessing situations resulted in a partition with a single fuzzy set, i.e. $k_2 = 1.00$. A better performance metric than the percentage of Ruspini results to evaluate the quality of crowdsourced data sets is the similarity scores to prototype S_1, S_2, and S_T. For the interface with buttons alone, S_1 and S_2 show a sharp contrast between the scores for the liquid level and temperature sensors. In fact, the minimum score obtained for the liquid level ($N = 20$) is more than twice the maximum score obtained for the temperature sensor ($N = 100$). A similar contrast is obtained for S_1 and S_2 with the interface with confidence bar (Table 18); the difference in this case is that the minimum score for the liquid level is almost three times the maximum score for the temperature sensor. As with the interface with buttons alone, the number of fuzzy sets obtained for the interface with confidence bar reflects the values of the similarity scores, with a minimum value of 1.98 for the liquid level sensor and 1.00 for the temperature. Surprisingly, the results obtained from data sets collected with the

interface with options are considerable poorer than the other two (Table 17). In this case, the similarity scores are no greater than 30% for any of them, and the number of fuzzy sets obtained in all cases is evidence that the Aggregation Algorithm is not able to distinguish situations reported by the crowd, *i.e.* $\{k_1, k_2\} = 1$.

The results obtained with merged data sets indicate that inconsistencies present in the data reported by the crowd can result in an apparent lack of agreement between participants. It suggests the need to pre-process the raw data collected to a representation that may help to overcome such inconsistencies. One such pre-processing technique is to take the median of the situation assessments of the crowd for each instance of data collection (in this case for each lit-event of the red indicator). This was the motivation that led to the results reported in Subsection 7.4.1.2.

7.4.1.2 Results with Median of Participants

The results of pre-processing the merged data sets by employing the median technique explained in Section 7.2.1.1 are presented in Tables 19, 20, and 21 for the interfaces with buttons alone, with options, and with confidence bar, respectively.

Table 19: Results with median of crowd for interface with buttons alone.

	R_1	R_2	R_T	S_1	S_2	S_T	k_1	k_2
N=20	95	100	95	60.17	24.91	24.91	2.00	1.63
N=50	100	100	100	65.92	28.33	28.33	2.00	1.78
N=100	100	100	100	67.09	30.83	30.83	2.00	1.84

Table 20: Results with median of crowd for interface with options.

	R_1	R_2	R_T	S_1	S_2	S_T	k_1	k_2
N=20	95	100	95	61.94	21.53	21.53	2.00	1.00
N=50	100	100	100	67.07	20.84	20.84	2.00	1.00
N=100	100	100	100	69.75	20.71	20.71	2.00	1.00

With this technique, results are more uniform among the interfaces employed to collect situation assessments. The values of S_1 are greater than S_2 in all cases, for any of the three tables and with any swarm size. The high similarity scores obtained for

Table 21: Results with median of crowd for interface with confidence bar.

	R_1	R_2	R_T	S_1	S_2	S_T	k_1	k_2
N=20	99	100	99	59.30	20.88	20.88	2.00	1.00
N=50	100	100	100	63.60	20.27	20.27	2.00	1.00
N=100	100	100	100	69.75	20.71	20.71	2.00	1.00

the liquid level sensor, S_1, are consistent with the number of fuzzy sets obtained, *i.e.* $k_1 = 2.00$. In contrast, the values obtained for the temperature sensor, S_2, are not higher than 31% in the best case, with most of the scores falling under 25%. These scores reflect the number of fuzzy sets obtained for each interface for the temperature sensor. The highest value is $k_2 = 1.84$ for the interface with buttons alone when it should be closer to 3.00 for all of them. This continues to indicate that deficiencies in the results obtained may be caused by inconsistencies in the assessments reported by the crowd during data collection. The question is if there is any other technique that may help to overcome such inconsistencies. This was the motivation to obtain individual granular structures before combining such information into crowdsourced SKB's. The following section analyzes the results obtained from employing principles in granular computing to combine individual SKB's into a single crowdsourced SKB.

7.4.2 Results from Combining SKB's

This approach pre-processes the data sets obtained from individual participants with the Aggregation Algorithm presented in Subsection 4.2.1 and generates a SKB for each individual, described as granular structures (refer to Figure 33). It is after this step is performed that the information obtained from participants is combined (merged) into a single crowdsourced SKB by stacking together their corresponding three-dimensional arrays. An illustration of the fuzzy sets contained in the merged SKB for this experiment was given in Figures 83, 84, and 85. Just as introduced in Subsection 7.2.1.2, the results are organized in terms of two variations of the coherence operation that is applied to the merged SKB. The first variation is the original, which

was presented in Subsection 4.2.1.3 and has been successfully employed in previous work [149, 150]. The second was presented in Subsection 7.2.1.2 and makes use of a more restrictive (or less tolerant) variation of the original coherence operation. Subsections 7.4.2.1 and 7.4.2.2 present and analyze the results for a swarm size of $N = 100$.

7.4.2.1 Results with the Original Coherence Operation

The result from combining individual SKB's making use of the original coherence operation is presented in Table 22 and Figure 86. Because this alternative to combining information from a crowd of participants does not depend on the entire Aggregation Algorithm but on the coherence operation, the results shown on Table 22 correspond to the performance metrics for similarity scores, *i.e.* S_1, S_2, and S_T, and the number of fuzzy sets obtained per sensor, *i.e.* k_1 and k_2. Because the swarm size is fixed at $N = 100$, the results for all interfaces are organized in a single table. In this case, the similarity scores are low for both sensors; none of them exceeds 30%. The scores reflect the fact that none of the interfaces exhibit an agreement among partipants about their situation assessments for either sensor; i.e. $\{k_1, k_2\} = 1.00$. This result is illustrated in the curves shown in Figure 86. Each curve in the two plots corresponds to one of the three interfaces. As evident, this approach falls short from producing the desired results. Obtaining a better result was the motivation for exploring more restrictive variants of the coherence operation, results of which are presented in Subsection 7.4.2.2.

Table 22: Results from employing the original coherence operation to the merged SKB.

	S_1	S_2	S_T	k_1	k_2
Buttons alone	29.70	26.10	26.10	1.00	1.00
With options	28.60	26.80	26.80	1.00	1.00
Confidence bar	28.60	26.40	26.40	1.00	1.00

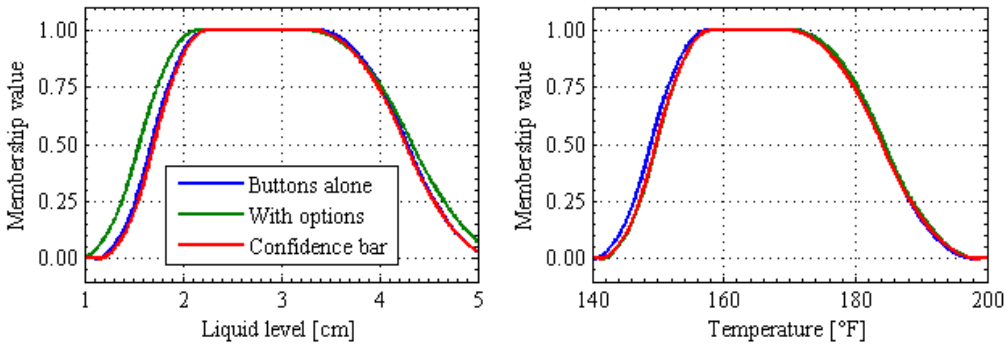

Figure 86: Fuzzy sets obtained for each sensor and interface with the original coherence operation.

7.4.2.2 Results with a More Restrictive Coherence Operation

The result from combining individual SKB's making use of the more restrictive (or less tolerant) variant of the coherence operation is presented in Table 23 and Figures 87, 88, and 89. Similar to the results with the original coherence operation, Table 23 only provides values for the similarity scores S_1, S_2, and S_T and the number of fuzzy sets obtained per sensor k_1 and k_2.

Table 23: Results with less tolerant coherence operation.

	S_1	S_2	S_T	k_1	k_2
Buttons alone	67.00	54.50	54.50	2.00	4.00
With options	66.70	35.50	35.50	2.00	3.00
Confidence bar	41.30	38.80	38.80	3.00	3.00

In this case, the similarity scores obtained for the interface with buttons alone are at least twice the scores from the original coherence operation. Such increase in the similarity score is favored by the increase in the number of fuzzy sets for each sensor: $k_1 = 2$ and $k_2 = 4$. The value of k_2 exceeds the number of fuzzy sets expected by one fuzzy set. However, the fourth fuzzy set (shown in a purple dotted line on the temperature plot of Figure 87) is only one set of 48 contained in the crowdsourced SKB, thus indicating that it is a single anomaly in the collection of fuzzy sets for the temperature sensor. Anomalies like this may be disregarded depending on the

method for data collection used. In this case, given that it is known that the goal value is $k_2 = 3$, the anomalous fuzzy set can be ignored.

For the other two interfaces, the scores are high for the liquid level sensor, but not so for the temperature sensor. This may be due to the presence of anomalous fuzzy sets in the crowdsourced SKB's, as in the temperature sensor in Figure 88, or because of a failure to obtain a coherent partition from the merged SKB as in the plot for the same sensor in Figure 89 (green curve). Nevertheless, these observations are evidence that a more restrictive coherence operation is able to manage the merged SKB and becomes an alternative to obtain crowdsourced SKB's.

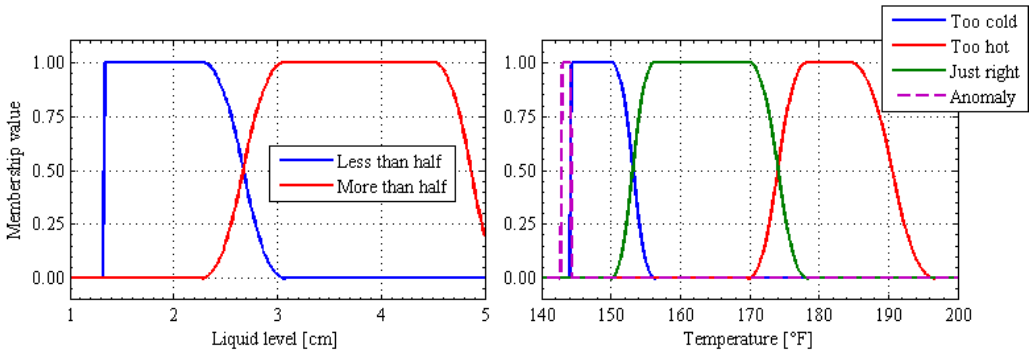

Figure 87: Fuzzy sets obtained from the crowd through the interface with buttons alone.

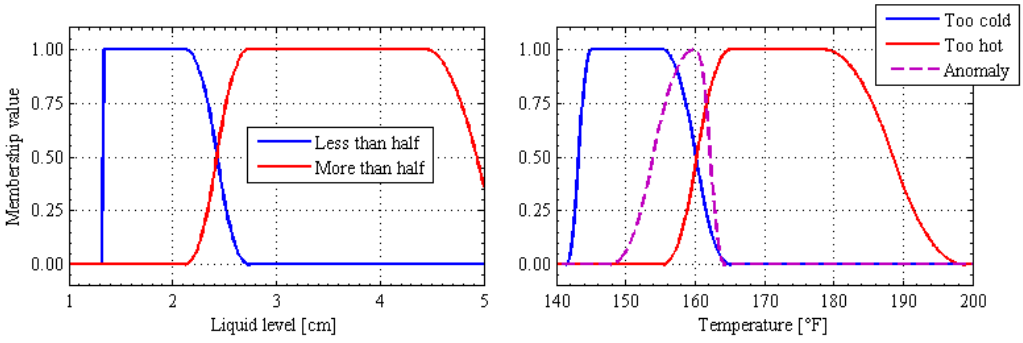

Figure 88: Fuzzy sets obtained from the crowd through the interface with options.

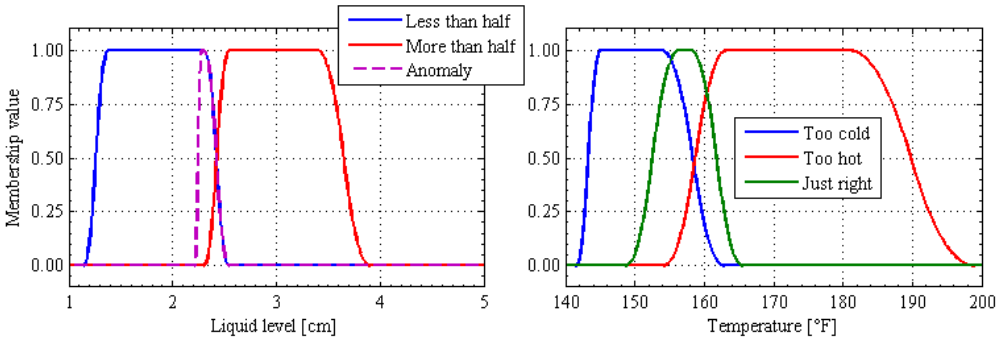

Figure 89: Fuzzy sets obtained from the crowd through the interface with confidence bar.

7.5 Summary

This chapter elaborated on the FAM-based architecture and its perception function. In particular it focused on the sensor data fusion approach that makes use of granular structures to represent SKB's. The approach used collected discrete situation assessments from human experts and sensor measurements and explored ways to combine their situation assessments to obtain a single crowdsourced SKB. This was accomplished by employing a statistically-based optimization method to compress data from experts. The techniques employed were applied before or after the compression of data. Results show the advantage of employing granular computing to filter inconsistencies and disagreements contained in the data sets. Future research will explore other alternatives in granular computing to manage crowdsourced data sets in support of situation-oriented and user-centered design approaches.

Limitations The work in this chapter elaborates on the advantage of employing granular computing to manage inconsistencies and disagreements present in situation assessment data sets collected by human participants. However, results obtained only consider data sets from eight human subjects. In addition, although it describes one variant of the coherent operation that leads to desirable results, other techniques based on granular computing may lead to comparable or even better results.

CHAPTER VIII

DISCUSSION AND GENERAL CONCLUSIONS

8.1 On the Integration of Humans and Automation

Issues in the integration of humans and automation pose challenges that will continue to evolve with innovations in sensing, processing, and actuation. Situation awareness research in particular will play an important role in preventing accidents and promoting the safety and reliability of systems in which humans and automation are meant to interact. This research presented an effort that aims to contribute to situation-oriented and user-centered design approaches. It does so by incorporating human expert assessments in the development of the perception function of agents developed using the FAM-based architecture. As demonstrated in Chapter 4, the use of the FAM-based agent architecture can be useful both to automate systems and to provide means for operators to interact with automated systems.

8.2 On the Bioregenerative Life Support Platform

The aquatic habitat served as a ground-based self-contained bioregenerative life support system, enabling independent research relevant to space-based life support. Its animal and botanical components posed novel challenges and questions for the integration and operation of closed-loop life support systems. Aditionally, its low cost and size also makes it an interesting tool for the classroom, providing hands-on opportunities for experiences that otherwise are not available from conventional research platforms. Such platforms in control engineering are rather electro-mechanical; *e.g.* the ball and beam, inverted pendulum, and flexible arm. The aquatic habitat was inspired by work conducted by Volker Blüm and flown in three Space Shuttle missions.

8.3 On the Granular Approach to Sensor Fusion

This dissertation made use of the FAM-based agent architecture as an approach that enables the interaction of humans and automation. Although the work presented here focused on life support systems, the granular approach and observations on the perception function of the FAM-based agent architecture may also be relevant in fields of application beyond life support systems. One such observations is that the non-interactiveness of the FAM makes the results obtained in this work scalable to more than two sensors. This is why the characterization presented in Chapter 5 makes use of one sensor only, while Chapter 6 employs two sensors instead. Other observations relevant to the results obtained are treated in the next two subsections.

8.4 On the Generation of Situation Knowledge Bases

Most of the data-based analysis in this research focused on the perception function of the FAM-based agent architecture. In particular, it approached the challenge of overcoming the combinatorial explosion when multiple situations and sensors are considered. This was achieved by evaluating the interaction of humans with a system and proposing the collection of situation assessments. One of the research questions was the minimum number of situation assessments needed to ensure that a coherent granular structure was achievable, assuming a uniform coverage of the sensing space for all sensors. This question was answered by performing the characterization presented in Chapter 5. But such characterization was performed with data sets generated by a simulation, so the next task consisted in validating it by employing data sets collected by real human participants. Chapter 6 presented an experiment in which eight human subjects provided situation assessments about the simulation of a dynamic system. The experiment was designed to achieve the best coverage possible of the sensing space, as to approximate the experimental condition of the characterization. However, the data collection process resulted in observations about

inconsistencies in the situation assessments provided by individual participants; inconsistencies were evidenced by poor performance in the dependence measures used. Such observation suggested the advantage of employing devices on future interface designs, such as speed bugs, to increase the consistency of situation assessments from individual human participants.

8.5 On Crowdsourced Situation Knowledge Bases

Finally, having used the simulation of a dynamic system to collect situation assessments sharing the same time reference, the question about obtaining crowdsourced SKB's arose. This contribution explored various ways to combine data sets with situation assessments known to have inconsistencies. Additionally, situation assessments also expressed disagreements among participants. The experiment presented in Chapter 7 explored techniques for the combination of data sets from a crowd of participants. The data-set-combination techniques were classified mainly by its application sequence in relation to the Aggregation Algorithm presented in Chapter 4. The results obtained illustrate the challenge in achieving agreement about situation definitions among a crowd of human experts. Such challenge can be overcome by employing techniques in granular computing. Results obtained with a more restrictive coherence operation were shown to overcome problems inherent to low quality data sets caused by inconsistencies and disagreements. However, the ability to obtain crowdsourced SKB supports team-oriented methods to design and develop complex systems, such as the Integrated Product and Process Development (IPPD) Methodology mentioned in Chapter 2.

8.6 Future Directions

Future research will continue to elaborate on the generation of SKB's in support of situation awareness in user-centered design methodologies. In particular, it will consider focusing on the role of attention in the development of high-quality situation-assessment data sets. One of the tools considered for this purpose is electroencephalography (EEG), which is able to provide measures of unattention from electrical activity in the cerebral cortex. Recent developments in dry-electrode EEG systems make it easier to employ such tools in work relevant to cognitive engineering.

Another area for future research is how to address unknown situation in SKB's. Such information will be increasingly useful in the development of life support systems with higher levels of closure; the interaction of chemical species may lead to unexpected situations during long-term spaceflight missions. The ability to manage such situations in a safe way remains as an open area of research.

Finally, the approach and methods used in this work are suited to fields of application beyond life support systems. Other possible areas include robotics, energy systems, emergency management systems, battlefield command and control, intelligence, and financial systems, among others.

REFERENCES

[1] P. M. Fitts, "Human engineering for an effective air navigation and traffic control system," tech. rep., National Research Council, Washington, DC, 1951.

[2] T. B. Sheridan, *Humans and Automation: System Design and Research Issues*. New York, NY, USA: John Wiley & Sons, Inc., 2002.

[3] S. J. Czaja and S. N. Nair, *Handbook of Human Factors and Ergonomics*, ch. 2, pp. 32–49. John Wiley & Sons, Inc., 2006.

[4] M. Diftler, J. Mehling, M. Abdallah, N. Radford, L. Bridgwater, A. Sanders, R. Askew, D. Linn, J. Yamokoski, F. Permenter, B. Hargrave, R. Piatt, R. Savely, and R. Ambrose, "Robonaut 2 - the first humanoid robot in space," in *Robotics and Automation (ICRA), 2011 IEEE International Conference on*, pp. 2178 –2183, May 2011.

[5] A. Cesetti, C. Scotti, G. Di Buó, G. Angione, L. Lattanzi, C. Cristalli, and S. Longhi, "Development of a flexible test platform for household appliance testing based on mobile agents," in *Proceedings of the 2010 IEEE International Conference on Automation Science and Engineering*, 2010.

[6] J. P. Trevelyan, S.-C. Kang, and W. R. Hamel, *Springer Handbook of Robotics*, ch. 48, pp. 1101–1126. Springer-Verlag Berlin Heildelberg, 2008.

[7] D. Schrage, "Office of the secretary of defense system of systems engineering workshop," tech. rep., Georgia Institute of Technology, 2006.

[8] T. B. Sheridan, *Handbook of Human Factors and Ergonomics*, ch. 38, pp. 1025–1052. John Wiley & Sons, Inc., 2006.

[9] P. T. Grogan, C. Lee, , and O. L. de Weck, "Comparative usability study of two space logistics analysis tools," in *Proceedings of the AIAA Space 2011 Conference and Exposition*, (Long Beach, California), 20-22 September 2011.

[10] P. O. Wieland, *Designing for human presence in space an introduction of environmental control and life support systems*. National Aeronautics and Space Administration, Office of Management, Scientific and Technical Information Program, National Technical Information Service, 1994.

[11] T. McCoy, S. Flint, J. Straub, D. Gazda, and J. Schultz, "The story behind the numbers: Lessons learned from the integration of monitoring resources in addressing an iss water quality anomaly," in *41st International Conference on Environmental Systems*, 2011.

[12] H. Lambers, F. S. Chapin, and T. L. Pons, *Plant Physiological Ecology*. Springer-Verlag New York Inc., 2 ed., 2008.

[13] V. Blüm, M. Andriske, C. Ludwig, U. Paassen, and D. Voeste, "The cebas mini-module: A self-sustaining closed aquatic ecosystem for spaceflight experimentation," *Advances in Space Research*, vol. 31, no. 1, pp. 201–210, 2003.

[14] N. Lane, E. Miluzzo, H. Lu, D. Peebles, T. Choudhury, and A. Campbell, "A survey of mobile phone sensing," *Communications Magazine, IEEE*, vol. 48, pp. 140 –150, September 2010.

[15] H. Alemdar and C. Ersoy, "Wireless sensor networks for healthcare: A survey," *Computer Networks*, vol. 54, no. 15, pp. 2688 – 2710, 2010.

[16] O. A. Sadik, S. K. Mwilu, and A. Aluoch, "Smart electrochemical biosensors: From advanced materials to ultrasensitive devices," *Electrochimica Acta*, vol. 55, no. 14, pp. 4287 – 4295, 2010.

[17] M. Vinyals, J. A. Rodriguez-Aguilar, and J. Cerquides, "A survey on sensor networks from a multiagent perspective," *The Computer Journal*, vol. 54, no. 3, pp. 455–470, 2011.

[18] R. McGrath, "Image sensor technology," in *Single-Photon Imaging*, vol. 160 of *Springer Series in Optical Sciences*, pp. 27–47, Springer Berlin, 2011.

[19] S. Venkataraman and R. Haftka, "Structural optimization complexity: what has moore's law done for us?," *Structural and Multidisciplinary Optimization*, vol. 28, pp. 375–387, 2004.

[20] A. Aizcorbe, "Moore's law, competition, and intel's productivity in the mid-1990s," *The American Economic Review*, vol. 95, pp. 305–308, May 2005.

[21] A. Llarena, "Here comes the robotic brain !," in *Trends in Intelligent Robotics* (P. Vadakkepat, J. Kim, N. Jesse, A. A. Mamun, T. K. Kiong, J. Baltes, J. Anderson, I. Verner, and D. Ahlgren, eds.), vol. 103 of *Communications in Computer and Information Science*, pp. 114–121, Springer Berlin Heidelberg, 2010.

[22] R. Dreslinski, M. Wieckowski, D. Blaauw, D. Sylvester, and T. Mudge, "Near-threshold computing: Reclaiming moore's law through energy efficient integrated circuits," *Proceedings of the IEEE*, vol. 98, pp. 253 –266, feb. 2010.

[23] H.-H. Chen and C. Wang, "Advances in wireless communications and networks," *Mobile Networks and Applications*, vol. 16, pp. 529–530, 2011.

[24] F. Khalid and J. Speidel, "Advances in mimo techniques for mobile communications – a survey," *Int. J. Communications, Network and System Sciences*, vol. 3, pp. 213–252, 2010.

[25] B. Wang and K. Liu, "Advances in cognitive radio networks: A survey," *Selected Topics in Signal Processing, IEEE Journal of*, vol. 5, pp. 5 –23, February 2011.

[26] D. Gavalas, P. Bellavista, J. Cao, and V. Issarny, "Mobile applications: Status and trends," *Journal of Systems and Software*, vol. 84, no. 11, pp. 1823 – 1826, 2011. Mobile Applications: Status and Trends.

[27] R. Lau, R. Klamma, S.-C. Chen, and B. Wah, "Advances in ubiquitous media technologies and applications," *World Wide Web*, vol. 14, pp. 217–222, 2011.

[28] A. Brown and R. Salter, "Can smart grid technology fix the disconnect between wholesale and retail pricing?," *The Electricity Journal*, vol. 24, no. 1, pp. 7 – 13, 2011.

[29] V. Giordano and G. Fulli, "A business case for smart grid technologies: A systemic perspective," *Energy Policy*, vol. 40, no. 0, pp. 252 – 259, 2012. Strategic Choices for Renewable Energy Investment.

[30] K. Giannoutakis and F. Li, "Developing sustainable e-business models for intelligent transportation systems (its)," in *Building the e-World Ecosystem* (T. Skersys, R. Butleris, L. Nemuraite, and R. Suomi, eds.), vol. 353 of *IFIP Advances in Information and Communication Technology*, pp. 200–211, Springer Boston, 2011.

[31] N. Shah, S. Kumar, F. Bastani, and I.-L. Yen, "Optimization models for assessing the peak capacity utilization of intelligent transportation systems," *European Journal of Operational Research*, vol. 216, no. 1, pp. 239 – 251, 2012.

[32] F.-y. Wang, A.-m. Yan, X.-z. Li, and L.-f. Yang, "Cloud computing based business intelligence platform and its application in the field of intelligent power consumption," in *Electronics, Communications and Control (ICECC), 2011 International Conference on*, pp. 3612 –3616, sept. 2011.

[33] S. M. Davey, M. Brennan, B. J. Meenan, and R. McAdam, "Innovation in the medical device sector: an open business model approach for high-tech small firms," *Technology Analysis & Strategic Management*, vol. 23, no. 8, pp. 807–824, 2011.

[34] G. Turchetti, S. Micera, F. Cavallo, L. Odetti, and P. Dario, "Technology and innovative services," *Pulse, IEEE*, vol. 2, pp. 27 –35, march-april 2011.

[35] A. Howard, C. Park, and S. Remy, "Using haptic and auditory interaction tools to engage students with visual impairments in robot programming activities," *Learning Technologies, IEEE Transactions on*, vol. PP, no. 99, p. 1, 2011.

[36] R. Parks and D. Duggan, "Principles of cyberwarfare," *Security Privacy, IEEE*, vol. 9, pp. 30 –35, sept.-oct. 2011.

[37] D. Elliott, "Deterring strategic cyberattack," *Security Privacy, IEEE*, vol. 9, pp. 36 –40, sept.-oct. 2011.

[38] A. Aissa, R. Abercrombie, F. Sheldon, and A. Mili, "Defining and computing a value based cyber-security measure," 2011. 10.1007/s10257-011-0177-1.

[39] S. D. Cunningham, J. Silver, and J. McDonnell, "Rates of change : online distribution as disruptive technology in the film industry," *Media International Australia incorporating Culture and Policy*, vol. N/A, pp. 119–132, August 2010.

[40] C. Feijo Ando, J. Gomez-Barroso, and S. Ramos, "An analysis of mobile gaming development," in *Intelligence in Next Generation Networks (ICIN), 2010 14th International Conference on*, pp. 1 –7, oct. 2010.

[41] L. Stone, C. Keller, T. Kratzke, and J. Strumpfer, "Search analysis for the underwater wreckage of air france flight 447," in *Information Fusion (FUSION), 2011 Proceedings of the 14th International Conference on*, pp. 1 –8, july 2011.

[42] D. C. Nagel, "Human error in aviation operations," in *Human Factors in Aviation* (E. L. Wiener and D. C. Nagel, eds.), pp. 263–303, Academic Press, 1 ed., 1988.

[43] M. Sanders and E. J. McCormick, *Human factors in engineering and deign*. McGraw-Hill, 1992.

[44] C. Hartel, K. Smith, and C. Prince, "Defining aircrew coordination: Searching mishaps for meaning," in *Proceedings of the 6th International Symposium on Aviation Psychology*, (Columbus, OH), 1991.

[45] M. R. Endsley, "A taxonomy of situation awareness errors," in *Proceedings of the 21st Conference of the European Association for Aviation Psychology (EAAP).*, (Trinity College, Dublin, Ireland), 1994.

[46] P. Eckart, *Spaceflight Life Support and Biospherics*. USA: Springer, 2 ed., 2010.

[47] J. E. Straub, D. K. Plumlee, J. R. Schultz, and J. T. McCoy, "Chemical analysis results for potable water from iss expeditions 21 through 25," in *41st International Conference on Environmental Systems*, AIAA, July 2011.

[48] J. A. Rutz, J. R. Schultz, C. M. Kuo, H. E. Cole, S. Manuel, M. Curtis, P. R. Jones, O. D. Sparkman, and J. T. McCoy, "Discovery and identification of dimethylsilanediol as a contaminant in iss potable water," in *41st International Conference on Environmental Systems*, 2011.

[49] S. Skogestad and I. Postlethwaite, *Multivariable Feedback Control: Analysis and Design*. Wiley-Interscience, 2 ed., November 2005.

[50] K. J. Astrom and B. Wittenmark, *Adaptive Control*. Dover Publications, 2 ed., December 2008.

[51] N. Hovakimyan and C. Cao, *L1 Adaptive Control Theory: Guaranteed Robustness with Fast Adaptation*. Society for Industrial & Applied Mathematics, September 2010.

[52] L. Vu and D. Liberzon, "Supervisory control of uncertain linear time-varying systems," *Automatic Control, IEEE Transactions on*, vol. 56, no. 1, pp. 27 –42, 2011.

[53] H. Lin and P. Antsaklis, "Stability and stabilizability of switched linear systems: A survey of recent results," *Automatic Control, IEEE Transactions on*, vol. 54, no. 2, pp. 308 –322, 2009.

[54] D. Liberzon, *Switching in Systems and Control*. Birkhäuser, 2003.

[55] J. P. Hespanha, D. Liberzon, and A. S. Morse, "Overcoming the limitations of adaptive control by means of logic-based switching," *Systems & Control Letters*, vol. 49, no. 1, pp. 49 – 65, 2003. Adaptive Control.

[56] M. R. Endsley, "Design and evaluation for situation awareness enhancement," in *Human Factors Society, Annual Meeting, 32nd*, (Anaheim, CA), pp. 97–101, October 1988.

[57] M. Endsley and D. G. Jones, *Designing for situation awareness: an approach to user-centered design.* Taylor & Francis Group, 2nd. ed., 2012.

[58] L. A. Zadeh, "Toward a theory of fuzzy information granulation and its centrality in human reasoning and fuzzy logic," *Fuzzy Sets and Systems*, vol. 90, no. 2, pp. 111 – 127, 1997. Fuzzy Sets: Where Do We Stand? Where Do We Go?

[59] Y. Yao, "Perspectives of granular computing," in *Proceedings of 2005 IEEE International Conference on Granular Computing*, vol. 1, pp. 85–90, 2005.

[60] G. Drayer and M. Strefezza, "A fam-based agent for a ball and beam," in *IEEE-SOFA 2007. 2nd IEEE International Workshop on Soft Computing Applications*, (Gyula, Hungary, and Oradea, Romania), pp. 89–94, August 21-23 2007.

[61] G. Drayer and A. Howard, "A fam-based switched control approach for the automation of bioregenerative life support systems," in *41st International Conference on Environmental Systems*, (Portland, Oregon), AIAA, July 2011.

[62] M. S. Sanders and E. J. McCormick, *Human Factors In Engineering and Design*. McGraw-Hill Science/Engineering/Math, 7 ed., January 1993.

[63] H. W. Hendrick and B. M. Kleiner, *Macro ergonomics: An Introduction to Work System Design*, vol. 2 of *HFES Issues in Human Factors and Ergonomics Book Series*. Human Factors and Ergonomics Society, December 2000.

[64] Aristotle, *Metaphysics*. Ann Arbor: University of Michigan Press, 1966. Book XVIII, Part 6.

[65] R. Descartes, *Discourse On The Method Of Rightly Conducting The Reason And Seeking Truth In The Sciences*. General Books LLC, July 2010.

[66] D. Meister, *Conceptual Aspects of Human Factors*. The Johns Hopkins University Press, July 1989.

[67] J. Rasmussen, "Cognitive engineering, a new profession?," in *Tasks, errors, and mental models*, pp. 325–334, Bristol, PA, USA: Taylor & Francis, Inc., 1988.

[68] J. Rasmussen, A. M. Pejtersen, and L. P. Goodstein, *Cognitive Systems Engineering*. Wiley-Interscience, August 1994.

[69] D. D. Woods, "Commentary: Cognitive engineering in complex and dynamic worlds," in *Complex Engineering in Complex Dynamic Worlds* (E. Hollnagel, G. Mancini, and D. D. Woods, eds.), pp. 115–129, New York: Academic Press, 1988.

[70] C. D. Wickens, J. D. Lee, Y. Liu, and S. Gordon-Becker, *Introduction to Human Factors Engineering*. Upper Saddle River, NJ.: Prentice Hall, 2 ed., 2004.

[71] D. Schrage, D. DeLaurentis, and K. Taggart, "Ippd concept development process for future combat system," in *9th AIAA/ISSMO Symposium and Exhibit on Multidisciplinary Analysis and Optimization*, (Atlanta, GA), September 2002.

[72] W. A. Pasmore, *Designing Effective Organizations: The Sociotechnical Systems Perspective*. Wiley Series on Organizational Assessment and Change, Wiley, 1988.

[73] K. J. Vicente, "Ecological interface design: Progress and challenges," *Human Factors*, vol. 44, pp. 62–78, 2002.

[74] E. L. Hutchins, J. D. Hollan, and D. A. Norman, "Direct manipulation interfaces," *Human-Computer Interaction*, vol. 1, no. 4, pp. 311–338, 1985.

[75] J. Rasmussen, *Information Processing and Human-Machine Interaction: An Approach to Cognitive Engineering*. Elsevier Science Ltd., 1986.

[76] J. Rasmussen, "Skills, rules, and knowledge; signals, signs, and symbols, and other distinctions in human performance models," *IEEE Transactions on Systems, Man and Cybernetics*, vol. SMC-13, pp. 257–266, May/June 1983.

[77] K. D. Eason, *Information Technology and Organizational Change*. London, UK: Taylor & Francis, 1991.

[78] J. Rasmussen, "Human factors in a dynamic information society: where are we heading?," *Ergonomics*, vol. 43, no. 7, pp. 869–879, 2000.

[79] R. Brooks, "A robust layered control system for a mobile robot," *Robotics and Automation, IEEE Journal of*, vol. 2, pp. 14 – 23, mar 1986.

[80] R. Brooks, "Intelligence without reason," in *Proceedings of 12th International Joint Conferece on Artificial Intelligence*, (Sydney, Australia), pp. 569–595, August 1991.

[81] R. A. Brooks, "Intelligence without representation," *Artificial Intelligence*, vol. 47, no. 13, pp. 139 – 159, 1991.

[82] G. Drayer and M. Strefezza, "Integral control with error modulation in a fam-based agent for a furuta inverted pendulum," in *2008 IEEE World Congress on Computational Intelligence*, (Hong Kong), pp. 1590–1597, June 01-06 2008.

[83] J. B. Rosenborough and T. B. Sheridan, "Aiding human operators with state estimates.," tech. rep., Defense Technical Information Center OAI-PMH Repository [http://stinet.dtic.mil/oai/oai] (United States), 2002.

[84] L. Bainbridge, "Ironies of automation," *Automatica*, vol. 19, no. 6, pp. 775 – 779, 1983.

[85] H. M. Parsons, "Automation and the individual: Comprehensive and comparative views," *Human Factors: The Journal of the Human Factors and Ergonomics Society*, vol. 27, no. 1, pp. 99–111, 1985.

[86] R. Parasuraman, T. Sheridan, and C. Wickens, "A model for types and levels of human interaction with automation," *Systems, Man and Cybernetics, Part A: Systems and Humans, IEEE Transactions on*, vol. 30, pp. 286 –297, may 2000.

[87] C. E. Billings, *Aviation Automation: The Search for A Human-centered Approach*. CRC Press, 1997.

[88] W. Rouse and J. Hammer, "Assessing the impact of modeling limits on intelligent systems," *Systems, Man and Cybernetics, IEEE Transactions on*, vol. 21, pp. 1549 –1559, nov/dec 1991.

[89] C. D. Wickens, A. S. Mavor, R. Parasuraman, and J. P. McGee, *The Future of Air Traffic Control:Human Operators and Automation, Panel on Human Factors in Air Traffic Control Automation*. The National Academies Press, 1998. National Research Council.

[90] D. Broadbent, *Perception and Communication*. Permagon Press, 1958.

[91] U. Neisser, *Cognitive Psychology*. Prentice-Hall, 1967.

[92] M. I. Possner, *Chronometric Explorations of the Mind*. Lawrence Erlbaum Associates, 1978.

[93] C. D. Wickens and C. M. Carswell, *Handbook of Human Factors and Ergonomics*, ch. 5, pp. 111–149. John Wiley & Sons, Inc., 2006.

[94] P. Hancock, J. Flash, J. Caird, and K. Vicente, *Local applications of the ecological approach to human-machine systems*. Lawrence Erlbaum Associates, 1995.

[95] J. Flach, P. Hancock, J. Caird, and K. Vicente, *Global perspectives on the ecology of human-machine systems*. Lawrence Erlbaum Associates, 1995.

[96] A. M. Howard, S. Remy, and H. W. Park, "Learning of arm exercise behaviors: Assistive therapy based on therapist-patient observation," in *RSS: Workshop on Interactive Robot Learning*, 2008.

[97] A. M. Howard, S. Remy, C. Hyuk Park, H. Won Park, and D. Brooks, "Intelligent robotics for assistive healthcare and therapy," in *The Path to Autonomous Robots* (G. Sukhatme, ed.), pp. 1–17, Springer US, 2009.

[98] D. Brooks and A. M. Howard, "Upper limb rehabilitation and evaluation of children using a humanoid robot," in *Proceedings of the 2nd Workshop on Child, Computer and Interaction*, WOCCI '09, (New York, NY, USA), pp. 21:1–21:5, ACM, 2009.

[99] S. Das, S. Chita, N. Peterson, B. Shirazi, and M. Bhadkamkar, "Home automation and security for mobile devices," in *Pervasive Computing and Communications Workshops (PERCOM Workshops), 2011 IEEE International Conference on*, pp. 141 –146, march 2011.

[100] S. Ahmad, "Smart metering and home automation solutions for the next decade," in *Emerging Trends in Networks and Computer Communications (ETNCC), 2011 International Conference on*, pp. 200 –204, april 2011.

[101] P. Wallich, "Mindstorms: not just a kid's toy," *Spectrum, IEEE*, vol. 38, pp. 52 –57, sep 2001.

[102] B. Gerkey and K. Conley, "Robot developer kits (ros topics)," *Robotics Automation Magazine, IEEE*, vol. 18, p. 16, sept. 2011.

[103] T. Yonezawa, H. Yamazoe, A. Utsumi, and S. Abe, "Gaze-communicative behavior of stuffed-toy robot with joint attention and eye contact based on ambient gaze-tracking," in *Proceedings of the 9th international conference on Multimodal interfaces*, ICMI '07, (New York, NY, USA), pp. 140–145, ACM, 2007.

[104] K. Pitsch and B. Koch, "How infants perceive the toy robot pleo. an exploratory case study on infant-robot-interaction," in *Proceedings Second International Symposium on New Frontiers in Human-Robot Interaction* (K. Dautenhahn and J. Saunders, eds.), (De Montfort University, Leicester, UK), 2010.

[105] S. Maeso, M. Reza, J. A. Mayol, J. A. Blasco, M. Guerra, E. Andradas, and M. N. Plana, "Efficacy of the da vinci surgical system in abdominal surgery compared with that of laparoscopy: A systematic review and meta-analysis," *Annals of Surgery*, vol. 252, pp. 254–262, August 2010.

[106] M. Kroh, K. El-Hayek, S. Rosenblatt, B. Chand, P. Escobar, J. Kaouk, and S. Chalikonda, "First human surgery with a novel single-port robotic system: cholecystectomy using the da vinci single-site platform," *Surgical Endoscopy*, vol. 25, pp. 3566–3573, 2011. 10.1007/s00464-011-1759-1.

[107] K. Naohiro, K. Masatoshi, U. Jitsuo, U. Osamu, O. Tatsuo, K. Norihiko, and I. Norihiko, "Training in robotic surgery using the da vinci surgical system for left pneumonectomy and lymph node dissection in an animal model," *Annals of Thoracic and Cardiovascular Surgery*, vol. 17, no. 5, pp. 446–453, 2011.

[108] M. Cummings, A. Clare, and C. Hart, "The role of human-automation consensus in multiple unmanned vehicle scheduling," *Human Factors: The Journal of the Human Factors and Ergonomics Society*, vol. 52, no. 1, pp. 17–27, 2010.

[109] M. L. Cummings and A. S. Brzezinski, "Global vs. local decision support for multiple independent uav schedule management," *International Journal of Applied Decision Sciences*, vol. 3, pp. 188–205, 2010.

[110] M. L. Cummings, S. Bruni, and P. J. Mitchell, "Human supervisory control challenges in network-centric operations," *Reviews of Human Factors and Ergonomics*, vol. 6, no. 1, pp. 34–78, 2010.

[111] A. Doan, R. Ramakrishnan, and A. Y. Halevy, "Crowdsourcing systems on the world-wide web," *Commun. ACM*, vol. 54, pp. 86–96, Apr. 2011.

[112] N. R. Prestopnik and K. Crowston, "Gaming for (citizen) science: Exploring motivation and data quality in the context of crowdsourced science through the design and evaluation of a social-computational system," *e-Science Workshops, IEEE International Conference on*, vol. 0, pp. 28–33, 2011.

[113] B. Woolford and F. Mount, *Handbook of Human Factors and Ergonomics*, ch. 34, pp. 929–944. Wiley, 3rd ed., 2006.

[114] S. Doll and P. Eckart, *Human Spaceflight Mission Analysis and Design*, ch. 17, pp. 539–573. McGraw-Hill Companies, 1999.

[115] R. W. Humble, *Human Spaceflight Mission Analysis and Design*, ch. 25, pp. 797–810. McGraw-Hill Companies, 1999.

[116] C. M. McCleskey, "Space shuttle operations and infrastructure: A systems analysis of design root causes and effects," tech. rep., National Aeronautics and Space Administration, John F. Kennedy Space Center, Florida, April 2005. NASA/TP-2005-211519.

[117] J. Wilson, "What's next for u.s. human spaceflight?," *Aerospace America*, vol. 50, pp. 24–31, January 2012.

[118] J. A. Rumerman, C. Gamble, and G. Okolski, eds., *Human spaceflight a record of achievement, 1961-2006*. Washington, DC: NASA History Division, Office of External Relations, 2007.

[119] M. Nelson, N. S. Pechurkin, J. P. Allen, L. A. Somova, and J. I. Gitelson, "Handbook of environmental engineering," in *Environmental Biotechnology* (L. K. Wang, ed.), vol. 10, ch. 11, pp. 517–565, Humana Press, 2009.

[120] D. R. Williams, *Isolation: NASA experiments in Closed Environment Living*, vol. 104 of *Science and Technology*, final report 1, pp. 1–5. San Diego, California: American Astronautical Society, 2002.

[121] M. B. Abney, L. A. Miller, and T. Williams, "Sabatier reactor system integration with microwave plasma methane pyrolysis post-processor for closed-loop hydrogen recovery," in *Proceedings of the 40th International Conference on Environmental Systems*, (Barcelona, Spain), AIAA, 11-15 July 2010.

[122] National Aeronautics and Space Administration, Huntsville, Alabama, *NASA Facts: International Space Station Environmental Control and Life Support System*, May 2008.

[123] A. L. Clements, R. G. Stinson, M. V. Wie, and E. Warren, "Development of the second generation international space station (iss) total organic carbon analyzer (toca)," in *Proceedings of the 39th International Conference on Environmental Systems*, (Savannah, Georgia), SAE, July 2009.

[124] G. Drayer and A. Howard, "Ecophysiological models in simulations of an aquatic habitat for closed-loop life support research," in *42nd International Conference on Environmental Systems*, (San Diego, CA), AIAA, July 2012.

[125] V. Blüm and F. Paris, "Possible applications of aquatic bioregenerative life support modules for food production in a martian base," *Advances in Space Research*, vol. 31, no. 1, pp. 77–86, 2003.

[126] V. Blüm and F. Paris, "Novel aquatic modules for bioregenerative life-support systems based on the closed equilibrated biological aquatic system (cebas)," *Acta Astronautica*, vol. 50, no. 12, pp. 775–785, 2002.

[127] V. Blüm, "Aquatic modules for bioregenerative life support systems: Developmental aspects based on the space flight results of the cebas mini-module," *Advances in Space Research*, vol. 31, no. 7, pp. 1683–1691, 2003.

[128] V. Blüm, "Aquatic modules for bioregenerative life support systems: Developmental aspects based on the space flight results of the c.e.b.a.s. mini-module," *Advances in Space Research*, vol. 31, pp. 1683–1691, 2003.

[129] K. Slenzka, M. Dünne, and B. Jastorff, "Biomonitoring and risk assessment on earth and during exploratory missions using aquahab," *Advances in Space Research*, vol. 42, no. 12, pp. 1944 – 1950, 2008.

[130] I. A. Stan, *Bioavailability and biological properties of several selected ionic liquids*. PhD thesis, Fachbereich Biologie/Chemie, Universität Bremen, September 2009.

[131] G. Wang, Y. Liu, G. Li, C. Hu, D. Zhang, and X. Li, "A simple closed aquatic ecosystem (caes) for space," *Advances in Space Research*, vol. 41, no. 5, pp. 684 – 690, 2008.

[132] G.-H. Wang, G.-B. Li, C.-X. Hu, Y.-D. Liu, L.-R. Song, G.-H. Tong, X.-M. Liu, and E.-T. Cheng, "Performance of a simple closed aquatic ecosystem (caes) in space," *Advances in Space Research*, vol. 34, no. 6, pp. 1455 – 1460, 2004.

[133] D. Bradshaw, *Vertebrate Ecophysiology: An Introduction to its Principles and Applications*. Cambridge University Press, June 2003.

[134] T. Watanabe-Asaka, C. Mukai, and H. Mitani, "Technologies and analyses using medaka to evaluate effects of space on health," *Biological Sciences in Space*, vol. 24, pp. 3–9, 2010.

[135] G. Drayer and A. Howard, "A granular approach to the automation of bioregenerative life support systems that enhances situation awareness," in *Proceedings of the 2nd IEEE Conference on Cognitive Methods in Situation Awareness and Decision Support*, IEEE Xplore, March 2012.

[136] G. Drayer and A. Howard, "Design, modeling and simulation of a reconfigurable aquatic habitat for life support control research," in *41st International Conference on Environmental Systems*, (Portland, Oregon), AIAA, July 2011.

[137] E. L. Cussler, *Diffusion: mass transfer in fluid systems*. Cambridge : Cambridge University Press, 1984.

[138] W. K. Lewis and W. G. Whitman, "Principles of gas absorption.," *Industrial & Engineering Chemistry*, vol. 16, pp. 1215–1220, Dec. 1924.

[139] M. Timmons and J. Ebeling, *Recirculating Aquaculture*. North Eastern Regional Aquaculture Center, 2007.

[140] B. J. Atwell, P. E. Kriedemann, and C. Turnbull, eds., *Plants in Action: Adaptation in Nature, Performance in Cultivation*. Macmillan Education Australia Pty. Ltd., 1999.

[141] W. Press, S. Teukolsky, W. Vetterling, and B. Flannery, *Numerical recipes 3rd edition: The art of scientific computing*. Cambridge University Press, 2007.

[142] P. C. Withers and C. E. Cooper, "Metabolic depression: A historical perspective," in *Aestivation* (C. Arturo Navas and J. E. Carvalho, eds.), vol. 49 of *Progress in Molecular and Subcellular Biology*, pp. 1–23, Springer Berlin Heidelberg, 2010.

[143] T. Ross, *Fuzzy Logic with Engineering Applications*. John Wiley & Sons, 3 ed., 2010.

[144] Y. Yao, "Granular computing: basic issues and possible solutions," in *Proceedings of the 5th Joint Conference on Information Sciences*, vol. I, pp. 186–189, 2000.

[145] Y. Yao, "The art of granular computing," in *Proceeding of the International Conference on Rough Sets and Emerging Intelligent Systems Paradigms*, pp. 101–112, 2007.

[146] L. Zadeh, "Fuzzy sets," *Information and Control*, vol. 8, no. 3, pp. 338 – 353, 1965.

[147] E. H. Ruspini, "A new approach to clustering," *Information and Control*, vol. 15, no. 1, pp. 22 – 32, 1969.

[148] R. C. Eberhart, J. Kennedy, and Y. Shi, *Swarm Intelligence*. Morgan Kaufmann, 2001.

[149] G. Drayer and A. Howard, "Human-expert data aggregation for situation-based automation of regenerative life support systems," in *42nd International Conference on Environmental Systems (ICES)*, AIAA, July 2012.

[150] G. Drayer and A. Howard, "A granular multi-sensor data fusion method for situation observability in life support systems," in *42nd International Conference on Environmental Systems (ICES)*, AIAA, July 2012.

[151] H. Taylor, B. Lee, J. Jhingory, G. Drayer, and A. Howard, "Development and evaluation of user interfaces for situation observability in life support systems," in *42nd International Conference on Environmental Systems (ICES)*, AIAA, July 2012.

[152] G. Drayer and A. Howard, "Modeling and simulation of an aquatic habitat for bioregenerative life support research," *Acta Astronautica*, vol. 93, pp. 138–147, January 2014.

[153] G. Grice, R. Nullmeyer, and V. Spiker, "Human reaction time: Toward a general theory," *Journal of Experimental Psychology*, vol. 111, pp. 135–153, March 1982.

[154] M. R. Khan and S. A. Naqvi, "Simulation study of reaction times at varying visual angles," *Computers & Industrial Engineering*, vol. 28, no. 3, pp. 467 – 472, 1995.

[155] G. J. Klir and B. Yuan, *Fuzzy sets and fuzzy logic: Theory and Applications*. Prentice Hall New Jersey, 1995.

[156] S. Ceri, A. Bozzon, M. Brambilla, E. D. Valle, P. Fraternali, and S. Quarteroni, *Web Information Retrieval*, ch. Human Computation and Crowdsearching, pp. 235–257. Data-Centric Systems and Applications, Springer, 2013.

[157] L. von Ahn, *Human computation*. PhD thesis, Carnegie Mellon University, Pittsburgh, PA 15213, December 7 2005. Doctoral dissertation.

[158] A. J. Quinn and B. B. Bederson, "Human computation: a survey and taxonomy of a growing field," in *Proceedings of the SIGCHI Conference on Human Factors in Computing Systems*, CHI '11, (New York, NY, USA), pp. 1403–1412, ACM, 2011.

[159] F. Wayland, *The Limitations Of Human Responsibility*. Applewood Books, 1838.

[160] A. M. Turing, *Computing Machinery and Intelligence*. Oxford University Press, 1950.

[161] J. Howe, "The rise of crowdsourcing," *Wired magazine*, vol. 14, no. 6, pp. 1–4, 2006.

[162] M.-C. Yuen, I. King, and K.-S. Leung, "A survey of crowdsourcing systems," in *Privacy, security, risk and trust (PASSAT), 2011 IEEE Third International Conference on and 2011 IEEE Third International Conference on Social Computing (SocialCom)*, pp. 766–773, IEEE Computer Society, 2011.

[163] M. B. Abney and J. M. Mansell, "Evaluation of bosch-based systems using non-traditional catalysts at reduced temperatures," in *Proceedings of the 41st International Conference on Environmental Systems*, (Portland, Oregon), AIAA, 17 - 21 July 2011.

[164] M. B. Abney, L. A. Miller, and K. Barton, "Evaluation of sorbents for acetylene separation in atmosphere revitalization loop closure," in *Proceedings of the 41st International Conference on Environmental Systems*, (Portland, Oregon), AIAA, 17 - 21 July 2011.

[165] M. Allahbakhsh, B. Benatallah, A. Ignjatovic, H. R. Motahari-Nezhad, E. Bertino, and S. Dustdar, "Quality control in crowdsourcing systems: Issues and directions," *Internet Computing, IEEE*, vol. 17, no. 2, pp. 76–81, 2013.

[166] A. Bechar, "Robotics in horticultural field production," *Stewart Postharvest Review*, vol. 6, pp. 1–11, September 2010.

[167] A. Bernstein, M. Klein, and T. W. Malone, "Programming the global brain," *Communications of the ACM*, vol. 55, no. 5, pp. 41–43, 2012.

[168] S. Breznitz, *Cry Wolf: The Psychology of False Alarms*. Lawrence Erlbaum Associates, 1983.

[169] D. L. Carter, "Status of the regenerative eclss water recovery system," in *Proceedings of the 39th International Conference On Environmental Systems*, (Savannah, Georgia), SAE, July 2009.

[170] L. Carter, L. L. Wilson, and N. Orozco, "Status of iss water management and recovery," in *Proceedings of the 41st International Conference on Environmental Systems*, (Portland, Oregon), AIAA, 17 - 21 July 2011.

[171] N. Correll, N. Arechiga, A. Bolger, M. Bollini, B. Charrow, A. Clayton, F. Dominguez, K. Donahue, S. Dyar, L. Johnson, H. Liu, A. Patrikalakis, T. Robertson, J. Smith, D. Soltero, M. Tanner, L. White, and D. Rus, "Indoor robot gardening: design and implementation," *Intelligent Service Robotics*, vol. 3, pp. 219–232, 2010.

[172] V. H. Dale and S. C. Beyeler, "Challenges in the development and use of ecological indicators," *Ecological Indicators*, vol. 1, pp. 3–10, 2001.

[173] D. David, M. Miclea, and A. Opre, "The information-processing approach to the human mind: Basics and beyond," *Journal of Clinical Psychology*, vol. 60, no. 4, pp. 353–368, 2004.

[174] G. DeGangi and S. Porges, *Neuroscience Foundations of Human Performance*. American Occupational Therapy Association Inc., 1990.

[175] S. Dow, A. Kulkarni, S. Klemmer, and B. Hartmann, "Shepherding the crowd yields better work," in *Proceedings of the ACM 2012 conference on Computer Supported Cooperative Work*, pp. 1013–1022, ACM, 2012.

[176] H. Durrant-Whyte and T. C. Henderson, *Springer Handbook of Robotics*, ch. 25, pp. 585–614. Springer-Verlag Berlin Heildelberg, 2008.

[177] H. Furukawa, *Autonomous Robots and Agents*, ch. 19, pp. 163–170. Studies in Computational Intelligence, Springer, 2007.

[178] D. Geiger, S. Seedorf, T. Schulze, R. C. Nickerson, and M. Schader, "Managing the crowd: Towards a taxonomy of crowdsourcing processes," in *Proceedings of the Seventeenth Americas Conference on Finformation Systems*, (Detroit, Michigan), August 4–7 2011.

[179] D. M. Green and J. A. Swets, *Signal Detection Theory and Psychophysics*. Wiley, 1988.

[180] P. A. Hancock, A. J. Masalonis, and R. Parasuraman, "On the theory of fuzzy signal detection: theoretical and practical considerations," *Theoretical Issues in Ergonomics Science*, vol. 1, no. 3, pp. 207–230, 2000.

[181] S. Hayashi, K. Shigematsu, S. Yamamoto, K. Kobayashi, Y. Kohno, J. Kamata, and M. Kurita, "Evaluation of a strawberry-harvesting robot in a field test," *Biosystems Engineering*, vol. 105, no. 2, pp. 160 – 171, 2010.

[182] C. Junaedi, K. Hawley, D. Walsh, S. Roychoudhury, M. B. Abney, and J. L. Perry, "Compact and lightweight sabatier reactor for carbon dioxide reduction," in *Proceedings of the 41st International Conference on Environmental Systems*, (Portland, Oregon), AIAA, 17 - 21 July 2011.

[183] D. B. Kaber, M. C. Wright, and M. A. Sheik-Nainar, "Investigation of multi-modal interface features for adaptive automation of a human-robot system," *International Journal of Human-Computer Studies*, vol. 64, pp. 527–540, 2006.

[184] J. Kohlas and P.-A. Monney, *A Mathematical Theory of Hints: An Approach to the Dempster-Shafer Theory of Evidence*. Springer-Verlag Berlin Heidelberg, 1995.

[185] M. A. Livingston, Z. Ai, K. Karsch, and G. O. Gibson, "User interface design for military ar applications," *Virtual Reality*, vol. 15, pp. 175–184, 2011.

[186] J. M. Mansell and M. B. Abney, "Influence of oxygenated compounds on reaction products in a microwave plasma methane pyrolysis assembly for post-processing of sabatier methane," in *Proceedings of the 40th International Conference on Environmental Systems*, (Portland, Oregon), AIAA, 17-21 July 2011.

[187] R. E. Mayer, *Multimedia Learning*. Cambridge University Press, 2001.

[188] G. Min, K. Li, and L. T. Yang, "Special issue: Advances in high-performance computing and communications," *Concurrency and Computation: Practice and Experience*, vol. 22, no. 4, pp. 395–397, 2010.

[189] D. O'Hare, M. Wiggins, R. Batt, and D. Morrison, "Cognitive failure analysis for aircraft accident investigation," *Ergonomics*, vol. 37, pp. 1855–1869, 2007.

[190] O. Olmos, C. D. Wickensand, and A. Chudy, "Tactical displays for combat awareness: An examination of dimensionality and frame of reference concepts and the application of cognitive engineering," *International Journal of Aviation Psychology*, vol. 10, no. 3, pp. 247–271, 2000.

[191] A. U. Paivio, *Mental representations: a dual coding approach*. Oxford University Press, 1986.

[192] J. Pedersen, D. Kocsis, A. Tripathi, A. Tarrell, A. Weerakoon, N. Tahmasbi, J. Xiong, W. Deng, O. Oh, and G.-J. de Vreede, "Conceptual foundations of crowdsourcing: A review of is research," in *System Sciences (HICSS), 2013 46th Hawaii International Conference on*, pp. 579–588, IEEE, 2013.

[193] M. I. Posner and S. E. Petersen, "The attention system of the human brain," *Annual Review of Neuroscience*, vol. 13, pp. 25–42, 1990.

[194] R. W. Proctor and K.-P. L. Vu, "The cognitive revolution at age 50: Has the promise of the human information-processing approach been fulfilled?," *International Journal of Human-Computer Interaction*, vol. 21, no. 3, pp. 253–284, 2006.

[195] J. Reason, *Human Error*. Cambridge University Press, 1990.

[196] H. Samaras, T. Giouvanakis, D. Bousiou, and K. Tarabanis, "Towards a new generation of multimedia learning research," *Association for the Advancement of Computing In Education Journal*, vol. 14, no. 1, pp. 3–30, 2004.

[197] T. Sawaragi, T. Shiose, and G. Akashi, "Foundations for designing an ecological interface for mobile robot teleoperation," *Robotics and Autonomous Systems*, vol. 31, pp. 193–207, 2000.

[198] G. Shafer, *A Mathematical Theory of Evidence*. Princeton University Press, 1976.

[199] C. E. Shannon, "A mathematical theory of communication," *Bell Systems Technical Journal*, vol. 27, pp. 379–423, 623–656, 1948.

[200] J. Sharit, *Handbook of Human Factors and Ergonomics*, ch. 27, pp. 708–760. John Wiley & Sons, Inc., 2006.

[201] S. Sternberg, "The discovery of processing stages: Extension of donders' method," *Acta Psychologica*, vol. 38, pp. 878–893, 1969.

[202] D. L. Strayer, C. D. Wickens, and R. Braune, "Adult age differences in the speed and capacity of information processing, ii: An electrophysiological approach," *Psychology and Aging*, vol. 2, pp. 99–110, 1987.

[203] W. P. Tanner and J. A. Swets, "A decision-making theory of visual detection," *Psychological Review*, vol. 61, pp. 401–409, 1954.

[204] C. D. Wickens and J. S. McCarley, *Applied Attention Theory*. CRC Press, 2008.

[205] D. A. Wiegmann and S. A. Shappell, "A human error analysis of commercial aviation accidents using the human factors analysis and classification system (hfacs)," tech. rep., 1. Institute of Aviation, University of Illinois at Urbana-Champaign 2. FAA Civil Aeromedical Institute, 2001.

[206] K. W. Williams, "Documentation of sensory information in the operation of unmanned aircraft systems," Tech. Rep. OK-09-0434, Department of Transportation, Federal Aviation Administration, Office of Aerospace Medicine, October 2008.

[207] J. Nin and D. Villatoro, eds., *Citizen in Sensor Networks*, vol. 7685 of *Lecture Notes in Computer Science*. Montpellier, France: Springer, 2013. ISBN: 978-3-642-36073-2 (Print) 978-3-642-36074-9 (Online).

[208] R. R. Yager and L. Liu, eds., *Classic Works of the Dempster-Shafer Theory of Belief Functions*. Springer-Verlag Berlin Heidelberg, 2008.

[209] National Aeronautics and Space Administration, *Reference guide to the International Space Station*, assembly complete ed., November 2010.